SOME STUDIES IN ELECTROCHEMICAL MACHINING

A Thesis submitted

to the University of Glasgow

for the Degree of Doctor of Philosophy

by

Joseph Anthony McGeough, B.Sc.

October 1966

ProQuest LLC.
789 East Eisenhower Parkway
P.O. Box 1346
Ann Arbor, MI 48106 – 1346

C O N T E N T S

A C K N O W L E D G E M E N T S

The author wishes to acknowledge with thanks the help of his Supervisor throughout the project, Professor G.D.S. MacLellan. He is also indebted to the Science Research Council for its interest and support through its Research Grant B/SR/466.

	NOTATION	DIMENSIONS
a	atomic weight	M
$a_{A,B}$	atomic weight of element A,B etc.	M
b	electrode width	L
c	cathode step size	L
c_e	solubility limit of neutral salt	ML^{-3}
c_o	concentration of ions next the electrode	ML^{-3}
c_b	bulk concentration of ions in solution	ML^{-3}
C	electrolyte specific heat	$Q^{2}L^{2}T^{-3}\theta^{-1}$
D	diffusion coefficient	$L^{2}T^{-1}$
E	chemical equivalent for metal	M
E_H	chemical equivalent for hydrogen	M
e	electrochemical equivalent	MQ^{-1}
f	volume fraction of hydrogen in electrolyte ($= V_H/Q$)	
F	Faraday's constant (96500 A.s)	Q
G	equivalent average value $\left(= \frac{E R T(x)}{F P(x)}\right)$	$L^{3}Q^{-1}$
h	inter electrode gap width	L
h_o	initial gap width, gap width at point $x = 0$	L
h_e	equilibrium gap width	L
$h(x)$	local gap width at point x along electrode length	L

NOTATION		DIMENSIONS
i	current density	$L^{-2}T^{-1}Q$
i_o	current density at x = 0 initial current density	$L^{-2}T^{-1}Q$
$i(x)$	local current density at point x	$L^{-2}T^{-1}Q$
K	electrolyte conductivity	$M^{-1}L^{-3}TQ^2$
K_o	initial electrolyte conductivity at point x = 0	$M^{-1}L^{-3}TQ^2$
$K(x)$	electrolyte conductivity at point x	$M^{-1}L^{-3}TQ^2$
L	electrode length	L
$\dot{m}$	mass removal rate per unit anode area	$MT^{-1}L^{-2}$
$(\dot{m})_{alloy}$	removal rate for alloy	$MT^{-1}L^{-2}$
$P(x)$	gas pressure at point x	ML^{-2}
Q	electrolyte volume flow rate	L^3T^{-1}
R	Gas constant	$ML^2T^2\theta^{-1}$
Re	Reynolds number (= flow rate per unit width/kinematic viscosity)	
Re_x	Reynolds number at point x	
s	anode step size	L
t	machining time	T
T	electrolyte temperature	θ
T_o	initial electrolyte temperature, temperature at flow entry	θ
$T(x)$	electrolyte temperature at point x	θ

NOTATION		DIMENSIONS
U	cathode feed rate	LT^{-1}
v	electrolyte velocity	LT^{-1}
$v(x)$	electrolyte velocity at point x	LT^{-1}
v_o	$\left(= \frac{5\upsilon}{\delta_o}\right)$ friction velocity	LT^{-1}
V	applied voltage	$ML^2T^{-2}Q$
V_o	decomposition voltage (constant = 2V) dependent on electrode potential and overpotentials	$ML^2T^{-2}Q$
V_H	volume production rate of hydrogen	L^3T^{-1}
W	molecular weight for hydrogen	M
x	distance along electrode length	L
$X_{A,B,C}$	% by weight in alloy of element A,B,C,	
y	deviation of gap from initial value	L
yf	final deviation of gap	L
z	valency of dissolving ions	
$z_{A,B,C,}$	valency of dissolving ions of element A,B,C,	

	NOTATION	DIMENSIONS
α	temperature coefficient of electrolyte conductivity	θ^{-1}
β	machining parameter $= \frac{E(V-V_o)K}{F\rho}$	L^2T^{-1}
γ	dimensionless factor ($\doteqdot$ 1) (Ch.2)	
δ	diffusion film thickness	L
δ_1	diffusion sub layer thickness	L
δ_o	laminar diffusion sub layer thickness	L
ρ	anode material density	ML^{-3}
ρ_e	electrolyte density	ML^{-3}
υ	kinematic viscosity	L^2T^{-1}

Chapter 1

General Introduction

The development of alloys resistant to high temperatures and stresses has made forming by established processes increasingly difficult. Electrochemical machining (E.C.M.) has been developed initially to form such metals, although any electrically conductive material can be so formed. The main features of the process have been described by Kleiner[1], Mountford[2], and Boothroyd[3]. The anode workpiece is dissolved at a rate roughly proportional to the product of its electrochemical equivalent and the current density (usually in the range 100 to 1000 A/in^2). Electrolyte is pumped through the inter-electrode gap (usually in the range 0.005 to 0.030 in), at velocities up to 200 ft/s to remove the products of machining.

Most electrochemical literature is concerned with low current densities (<1A/in^2) and electrolytes which are unstirred or in motion at low velocities. For example, Hoar and Rothwell[4][5] have investigated the electrolysis of copper, magnesium and nickel in an electrolyte flowing at velocities in the range 0 to 40 cm/s (1.5 ft/s) and with a maximum current density of about 2 A/in^2. Higgins[6] has studied the dissolution of nickel in an unstirred electrolyte with current densities up to 16 A/in^2. He has concluded that anodic dissolution is in certain circumstances governed by the existence of a boundary layer in which the ion concentration gradient determines the limiting current density on the basis of an ion diffusion process. Ord and Bartlett[7], amongst others, have studied the dissolution of

pure iron similarly with current densities up to about 1 A/in^2. Work of this kind has been stimulated by the industrially important processes of anodic polishing, following the earlier work of Jacquet[8] Edwards[9] and Elmore [10] on this subject. While these investigations throw increasing light on such features as the importance of ion diffusion boundary layers in limiting anode current densities for polishing conditions, they stop well short of the range of current densities important in E.C.M.

Little information on work at these current densities is available. Relevant literature on E.C.M. is given in a recent review by Cole[11].

He and his co-workers have investigated electrolytic grinding[12][13] in which metal is removed from the anode by a combination of mechanical and electrolytic action. Current densities up to 1150 A/in^2 were used. Negligible residual stress was induced on the metal by the process; the electrolyte flow rate had to be uniform to obtain uniform metal removal. A method for "jet polishing" of metals by anodic dissolution at high current densities (to 1750 A/in^2) has also been developed[14] in which any metal can be polished in ordinary salt solutions if the current density is sufficiently high.

Recently, Cuthbertson and Turner[15] have shown that Nimonic 80 can be machined satisfactorily in saturated sodium chloride solution, and from potentiostat studies have deduced that the machining reaction is diffusion controlled.

Tipton[16] has proposed a method for predicting the shape of the cathode required in the E.C.M. process to give a specified final form to the anodic workpiece. In the analysis he assumes that metal removal takes place in accordance with Faraday's Law and is independent of flow conditions. The usefulness of this kind of work is confirmed by the observations of Faust[17]: for a mild steel anode at current densities of the order of 100 A/in^2, the current efficiency (actual metal removal rate as a percentage of that predicted by Faraday's Law) was in the range 97 to 100% in a die-sinking process.

However there is little information available on either the relationship between the principal process variables, viz. current density, voltage, inter-electrode gap, flow rate, conductivity and temperature, or their effects on the machining action. Investigations of some of these problems are described in the following chapters.

In Chapter 2, the effect of electrolyte velocity upon current density is investigated in terms of the diffusion layer thickness next to the electrodes. At laminar flow rates, the current density is shown to be proportional to the square root of the velocity, but for sufficiently high turbulent flows, it is independent of flow rate and approaches the value given by Ohm's Law.

In Chapter 3 the products of machining are shown to have no effect on the conductivity and density of the bulk electrolyte, but increase slightly its viscosity.

The machining of metals under E.C.M. conditions of current density and flow rate is described in Chapter 4. Three methods for predicting alloy removal rates are outlined, and one, based on the

Law of Superposition of Charge shows good agreement with experimental results for Nimonic 75. For a given flow rate, current efficiency and surface roughness are observed to decrease with increase in current density. These, and other results, e.g. that metals like cast iron do not machine satisfactorily in 20% NaCℓ, are discussed in terms of Jacquet's theory of electropolishing.

The related use of the potentiostat as an instrument for selection of suitable electrolytes for different metals is considered in Chapter 5. Results from potentiostat experiments predicting appropriate electrolyte/metal combinations are shown to agree with E.C.M. tests.

Some aspects of the forming process are analysed in Chapter 6. For a cathode with a single step, the machining time required to impose a similar step on an initially flat anode is deduced in terms of the cathode feed rate and gap width. The time decreases as the gap is decreased. Experimental results agree with the theory and also show that definition of the anode step is better for the narrower gaps.

Chapter 7 deals with the effects of Joule heating and hydrogen evolution on the forming process. The former causes the gap to increase in the direction of flow whilst the gas causes an opposite effect, which is shown to be much greater. For both conditions, calculations have been made of flow rates required to maintain a certain accuracy of gap along the electrode length, and the machining time required to achieve an equilibrium state.

General conclusions and suggestions for further research are given in Chapter 8.

Chapter 2

The Effect of Electrolyte Velocity on Current Density

2.1 Introduction

In this chapter the effect of electrolyte velocity on current density is investigated both theoretically and experimentally, for a system with a constant potential difference applied across plane, parallel electrodes, between which the electrolyte flows.

The factors which affect current density have been considered by Higgins[6] in his study of the dissolution of nickel in unstirred hydrochloric acid. He obtained a limiting current density of 16 A/in^2 and suggests that such a reaction is diffusion controlled.

For a diffusion reaction, Fick's Law states the current density i is given by

$$i = Dz\mathcal{F}\frac{\partial c}{\partial y} \qquad (2.1)$$

where D = diffusion coefficient (cm^2/s), z is valency of dissolving ions, $\mathcal{F}$ = Faraday's constant (96500 C), and $\frac{\partial c}{\partial y}$ is the concentration gradient across the region where the ions diffuse.

Faust[17] also has considered the diffusion reaction as the controlling mechanism for ion transport. To machine nickel in HCl at 120 A/in^2, he estimates that the diffusion layer would have to be 0.0001 in. thick. This is an order of magnitude less than the thinnest film measured for diffusion controlled dissolution, even in stirred solutions. To achieve such high current densities, Faust concludes that high electrolyte flow rates must be used.

Diffusion reactions in moving electrolytes have been studied by Levich[18]. His studies form the basis of Section 2.2.

2.2 Theoretical Considerations

(i) Laminar Flow

For an electrolyte flowing past a flat plate the ion concentration distribution is similar to the velocity distribution. Thus Levich considers that in a layer next the electrodes (the layer being the equivalent of the hydrodynamic boundary layer) a concentration gradient exists.

In this region ions move under the influence of diffusion. The thickness of this diffusion layer δ is

$$\delta = 50 \left(\frac{D}{\nu}\right)^{1/3} \left(\frac{\nu x}{v}\right)^{1/2} \qquad (2.2)$$

where ν is the electrolyte kinematic viscosity, x is the distance along the electrode length and v is the electrolyte mainstream velocity.

Beyond the diffusion layer, the electrolyte concentration is assumed to be constant. In this regions ions should migrate under the influence of the electric field across the electrode gap.

From mass transfer considerations, the ion diffusion rate across the diffusion layer must equal the ion migration rate across the constant concentration zone.

Since the reaction commences next the electrodes, the diffusion mechanism will determine the quantity of current that can pass.

Using Fick's Law (2.1), Levich gives the diffusion current density as

$$i = \frac{D z F (c_b - c_o)}{\delta} \qquad (2.3)$$

where c_b is the bulk concentration of ions in the solution (g mole/ℓ), and c_o is the concentration next the electrodes.

For the limiting current density, $c_o = 0$. Using (2.1), the expression for i becomes:

$$i = \frac{D z F c_b}{5.0} \left(\frac{\nu}{D}\right)^{1/3} \left(\frac{v}{\sqrt{x}}\right)^{1/2} \qquad (2.4)$$

Thus i increases with $v^{1/2}$ but decreases with $x^{-1/2}$.

Current density i will not increase indefinitely as v is increased or as x is decreased. Ion migration across the constant concentration zone will impose an upper limit to the diffusion current densities given by (2.4). For a constant voltage gradient, the maximum current density (given by Ohm's Law) will be reached for flow conditions such that the migration path length approaches the electrode gap width, i.e. the diffusion boundary layer thickness is small. (Note that at $x = 0$, $\delta = 0$. The current density here is given by Ohm's Law).

(ii) Turbulent Flow

In many E.C.M. applications, the flow in the gap will be turbulent. For turbulent flow past a flat plate, Levich suggests that only in a very thin layer next the electrodes, the diffusion sub-layer, δ_1, is ion transfer controlled by diffusion. The limiting diffusion current density for turbulent flow, i_1, is again given from

Fick's Law (c.f. 2.3):

$$i = \frac{D\, z\, F(c_b - c_o)}{\delta_1} \qquad (2.5)$$

Levich calculates that

$$\delta_1 = \left(\frac{D\,\delta_o^3}{\gamma\, v_o}\right)^{1/4} \qquad (2.6)$$

where δ_o is the thickness of the laminar sub-layer, γ is a dimensionless quantity (of approximate value unity), v_o is the friction velocity (given by Schlichting[19] as $v_o = 5.0\nu/\delta_o$ (2.7))

(Levich does not pursue further the expression for i_1. To deduce i_1 in terms of measurable quantities (i.e ν and x) results from Schlichting have been used).

Schlichting also gives the magnitude of δ_o as:

$$\delta_o = 4.6\, x\, (Re_x)^{-0.9} \qquad (2.8)$$

where $Re_x = \frac{vx}{\nu}$ (2.9)

$$\therefore \quad \delta_1 = 4.6\, x \left(\frac{vx}{\nu}\right)^{-0.9} \left(\frac{D}{5\nu}\right)^{0.25} \qquad (2.10)$$

For high Prandtl numbers ($\nu/D \gg 1$), and for $\gamma \sim 1$, Levich writes:

$$i_1 = \frac{D\, c_b\, z\, F}{\frac{4}{3}\,\delta_1}$$

Thus, using Levich's and Schlichting's results, i_1 is deduced as:

$$i_1 = \frac{3.0\, D\, c_b\, z\, F}{184\, x} \left(\frac{vx}{\nu}\right)^{0.9} \left(\frac{D}{5\nu}\right)^{-0.25} \qquad (2.11)$$

Thus, it is postulated that, for turbulent flow, at any point x,

$$i_l \propto v^{0.9}$$

As before, ionic migration current density sets an upper limit (the Ohmic current density) to the current density for diffusion in turbulent flow.

While Levich and others have investigated diffusion experimentally at low flow rates and current densities (e.g. up to 18 in/s and 2 A/in^2 - Hoar and Rothwell[5]), no work has previously been done for E.C.M. conditions.

Experiments to investigate these effects of electrolyte velocity on current density for the conditions of E.C.M. have been performed and are reported below in Sections 2.3 to 2.7.

2.3 Apparatus and Procedure

A "Barmax" electrochemical machine, manufactured by Crow, Hamilton and Co. Ltd. under licence from Rolls Royce Ltd. was used. A constant voltage of 12V was supplied across two plane parallel electrodes of side 1 in., the anode being of mild steel and the cathode of brass. The associated pump system delivered electrolyte between the electrodes at flow rates in the range 0.2 to 60 in^3/s.

The Barmax machine and its associated equipment are described fully in Appendix 1.

Fig.2.1 shows details of the typical perspex jig used with the Barmax machine.

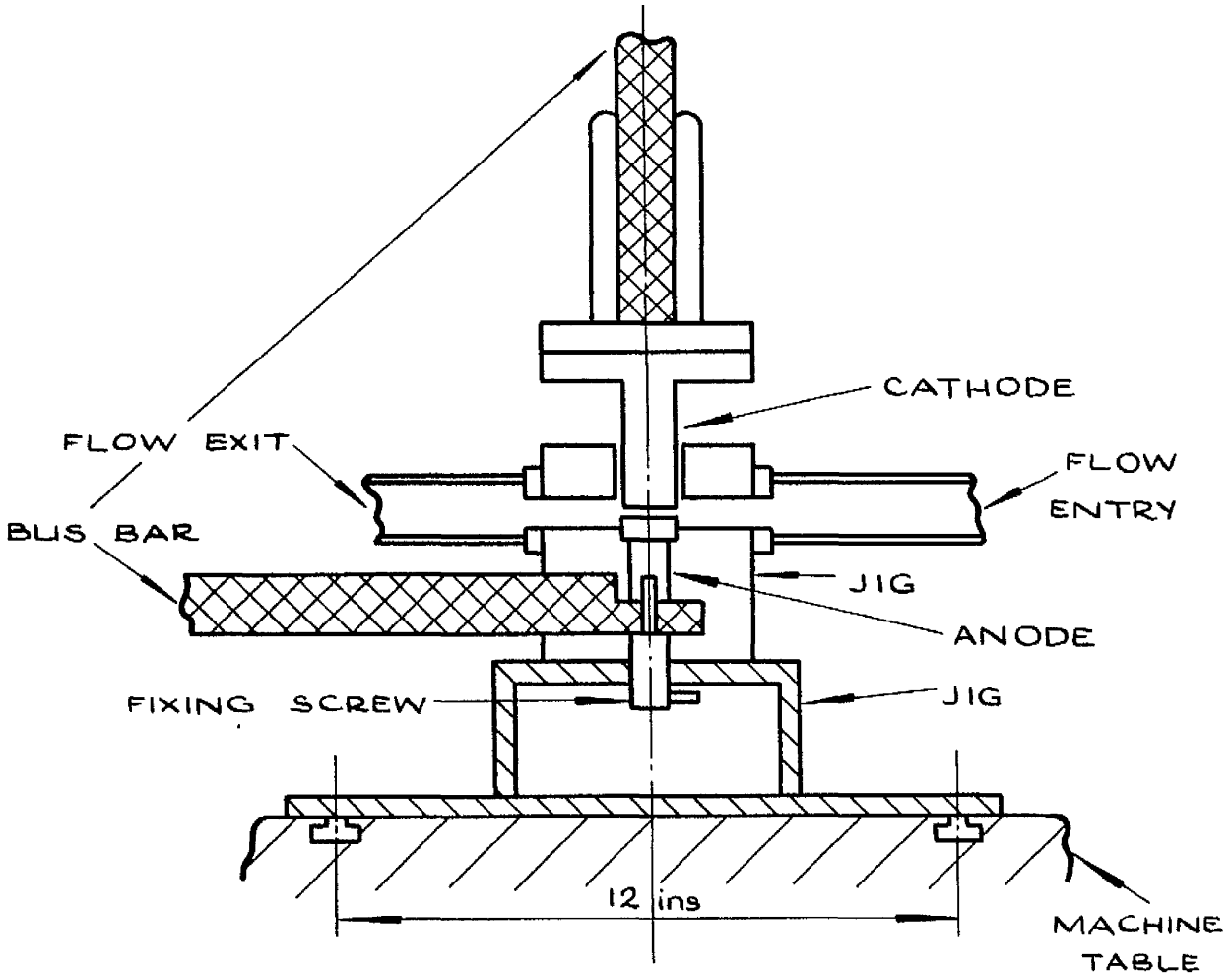

FIG. 2.1. DETAIL OF TYPICAL JIG USED WITH BARMAX MACHINE

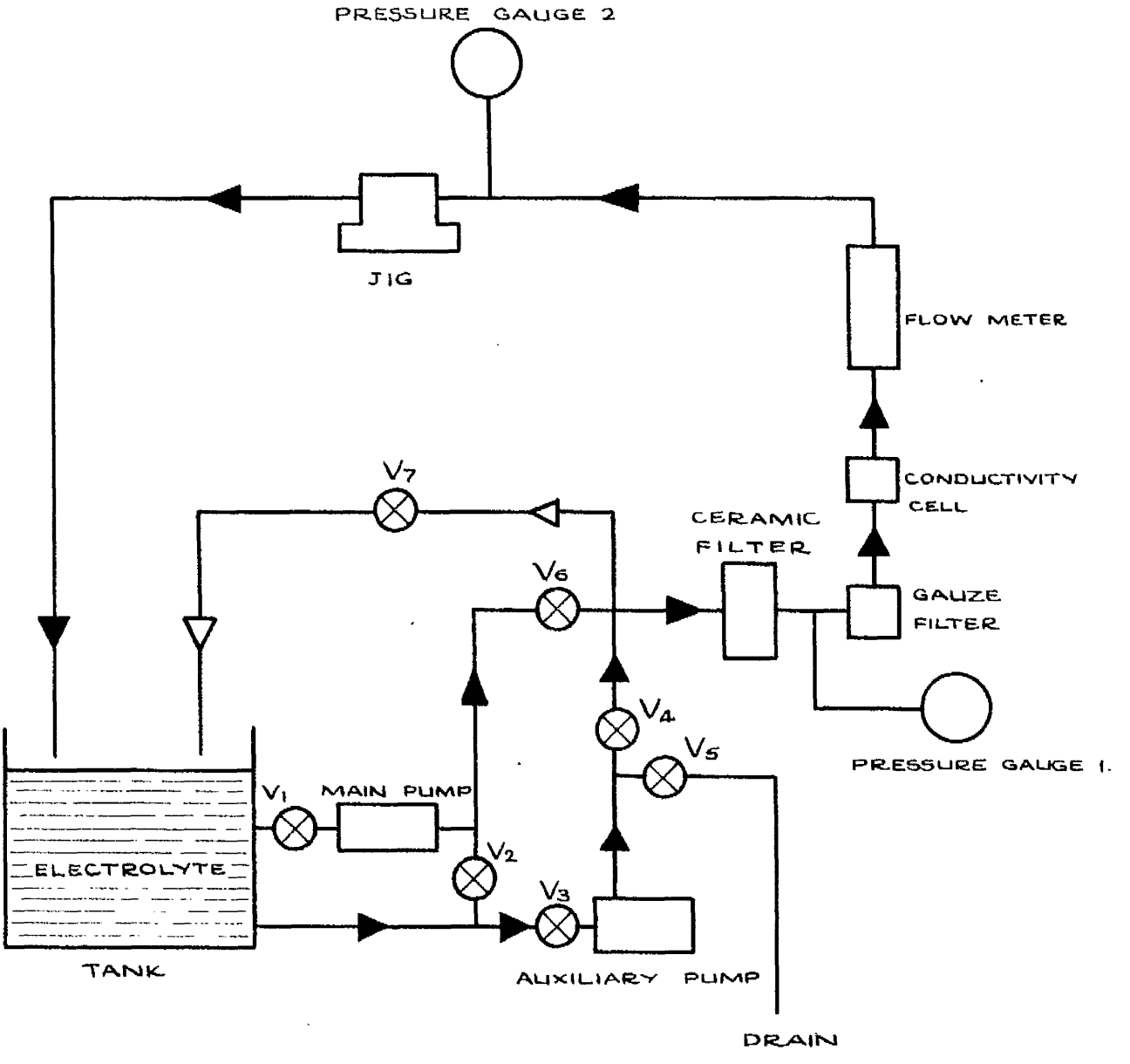

FIG 2.2. MODIFIED ELECTROLYTE FLOW SYSTEM

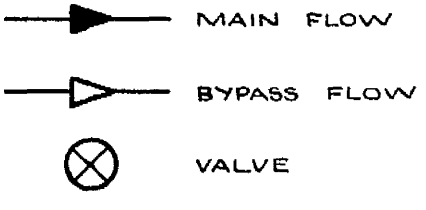

Flow System This is shown in Fig.2.2

(i) Flow rates between 23 in^3/s and 60 in^3/s.

A Saunders six stage centrifugal pump was used for these flow rates, which were measured with a Platon "Gapmeter" calibrated up to 92 in^3/s. The "main flow" system indicated in Fig.2.2 was used. The flow rates could be varied by adjustment of hand valve in the by-pass line.

(ii) Flow rates up to 23 in^3/s

The by-pass valve system proved inadequate in reducing the flow below 23 in^3/s. The main flow system, discussed in Appendix 1, was modified and an auxiliary pump, normally used for draining the tank, employed to give the required flow rates. A "Rotameter" flowmeter, calibrated for flows up to 23 in^3/s, replaced the "Gapmeter" for these tests.

Flow rates could again be varied by the use of the by-pass.

To ensure an exact gap, the electrode surfaces were ground before tests. A ground finish on the cathode also reduced the effect of hydrogen (which, by lowering the effective conductivity in the gap can lower the current density) as hydrogen bubbles are less likely to form on a polished surface than on a rough one.[20]

It is normal electrochemical practice to ensure that the electrolyt is "clean". This usually demands careful filtration before use. During the E.C.M. tests, the solution velocities were high compared with velocities hitherto used in electrochemistry .

flow rates Q, and gaps indicated in Fig.2.3 : $v = Q/bho$, where b is the electrode width, and h_o is the gap width.

(ii) Following Schlichting[19], regions of laminar and turbulent flow were determined from the Reynolds number, Re : $Re = \frac{2Q h_o}{bh_o\nu}$, where ν is the kinematic viscosity. For laminar flow, Re < 2500. For turbulent flow, Re > 2500

(iii) In Fig.2.5, the electrolyte velocity regions in which current density is constant, have not been included.

(iv) Ohmic current densities i were calculated from the equation $i = K (V - V_o) / h_o$ where K is the electrolyte conductivity, V is applied voltage, and V_o the decomposition voltage, (assumed constant).

(v) the theoretical lines in Fig.2.4 and 2.5 were calculated from equation (2.4) and (2.11) respectively. Previous work (6) (15) (17) has indicated that the diffusion layer has an almost constant thickness. Thus values of δ averaged with respect to x (i.e. $\frac{2}{3}\delta$ for laminar flow) were used. Theoretical current densities were calculated from these values.

(vi) For the electrolyte the following values were used:

$K_o = 0.105\,\Omega^{-1}\,cm^{-1}$ (extrapolated from Kaye and Laby's Tables[21]);

$V_o = 2V$ (constant)[34]; $c_b = 1.3$ g mole/ℓ., $D = 1.25 \times 10^{-5}$ cm^2/s, (from International Critical Tables[22]), $\nu = 1.1.10^{-2}$ in^2/s (by experiment)

Fresh electrolyte was presented to the electrodes every fraction of a second, so the electrolyte was "clean" without the usual precautions.

2.4 Procedure

An anode specimen was inserted in the perspex jig, and the cathode wound down until it touched the anode. A micrometer gauge measured the travel of the cathode. The latter was then wound back until the required gap was read on the gauge. The pump was switched on and the required flow obtained by valve adjustment. Inlet temperature and pressure were noted. The voltage was switched on and the instantaneous maximum current read. (This occurred after 0.5 to 1 s).

The voltage and flow were switched off, the cathode head raised and the test piece removed.

The procedure was repeated for different flows and gaps.

2.5 Results

Fig.2.3 shows for a voltage of 12V applied across gaps of 0.010 in to 0.040 in, the effect of electrolyte volume flow rate upon the mean current density. For each gap, the theoretical Ohmic current density is indicated.

In Fig.2.4, 2.5 and 2.5* the theoretical and observed effects of electrolyte velocity on current density for the above gaps and voltage are compared for laminar and turbulent flow respectively.

Notes: (i) Electrolyte velocities v were determined from the volume

GAP (in)	SYMBOL	THEORETICAL
·040	O	— — — —
·030	•	————
·020	×	——·——
·010	+	—·—·—

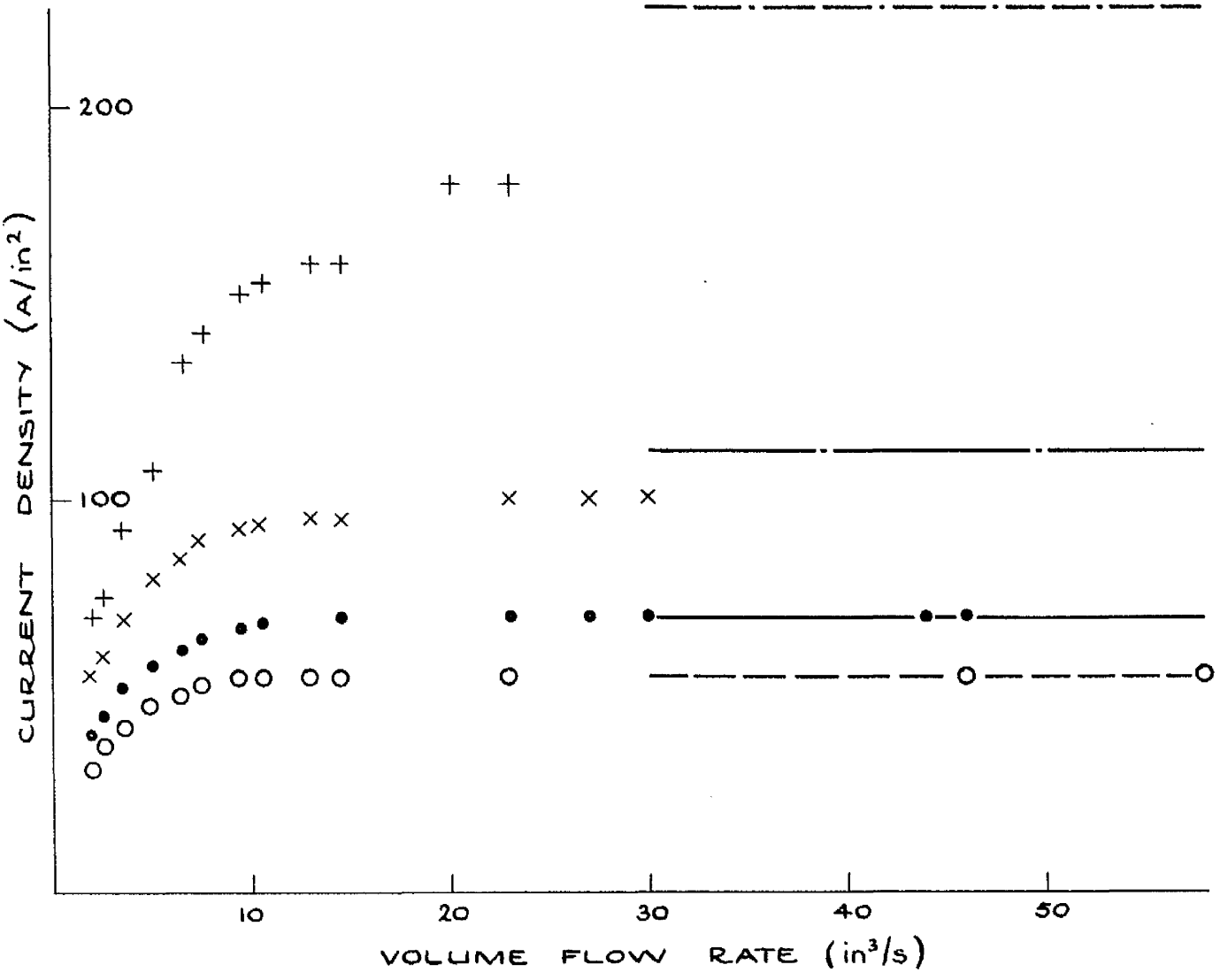

FIG 2.3. CURRENT DENSITY AS A FUNCTION OF VOLUME FLOW RATE AND GAP WIDTH

SYMBOL	FLOW (in^3/s)
O	2
×	2·5
+	3·5

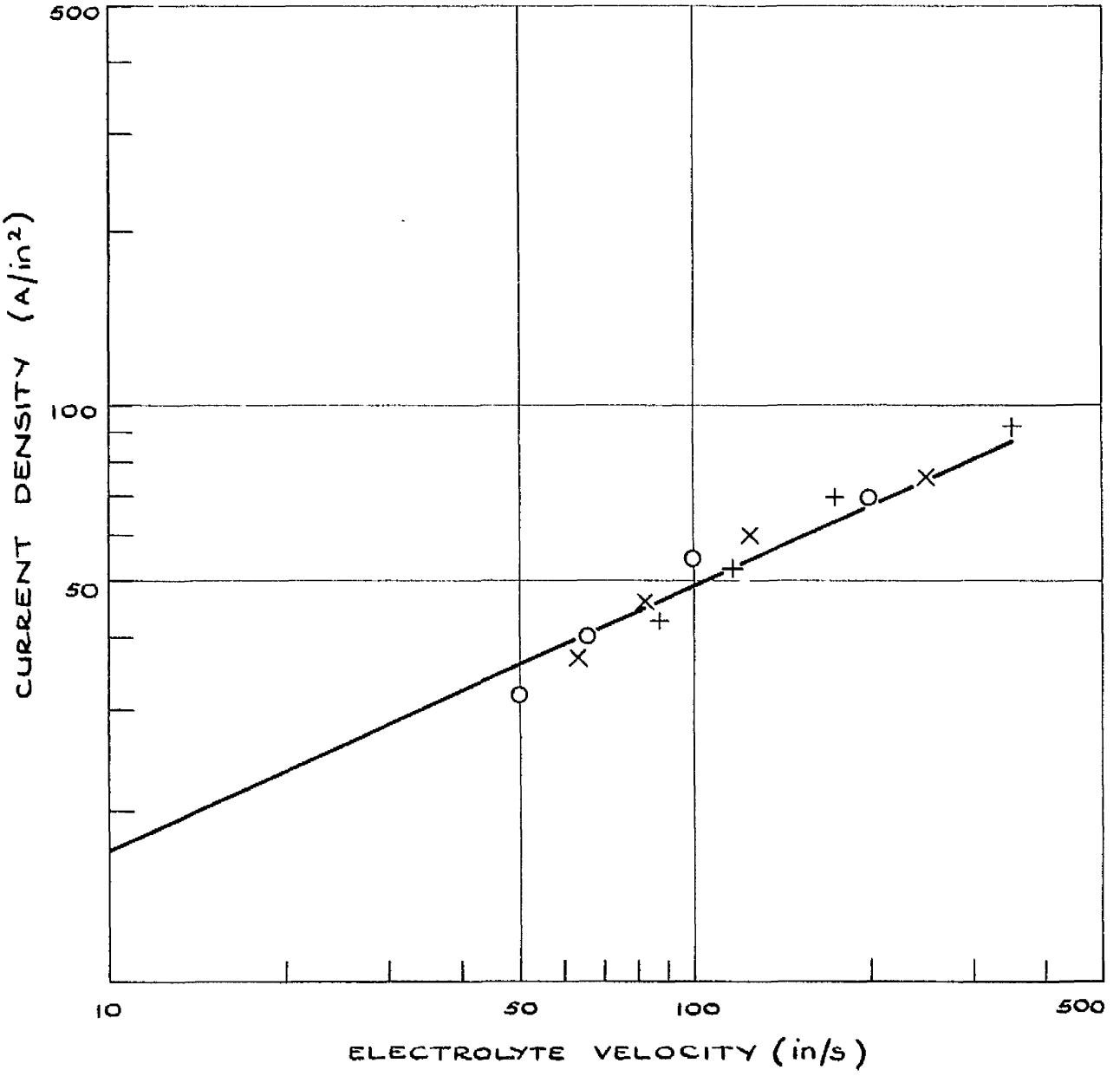

FIG 2.4. EFFECT OF ELECTROLYTE VELOCITY ON CURRENT DENSITY FOR LAMINAR FLOW

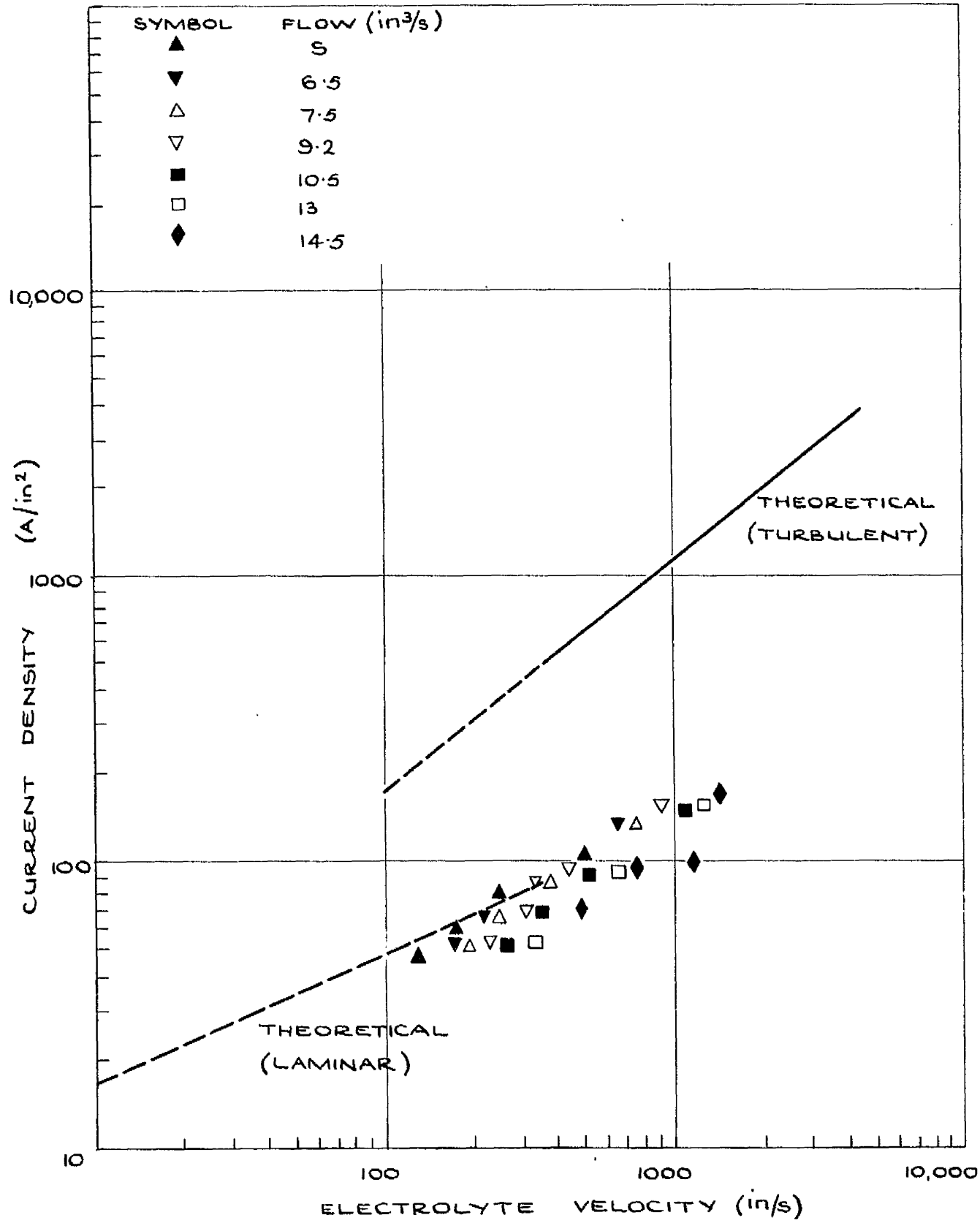

FIG. 2.5. EFFECT OF ELECTROLYTE VELOCITY ON CURRENT DENSITY FOR TURBULENT FLOW.

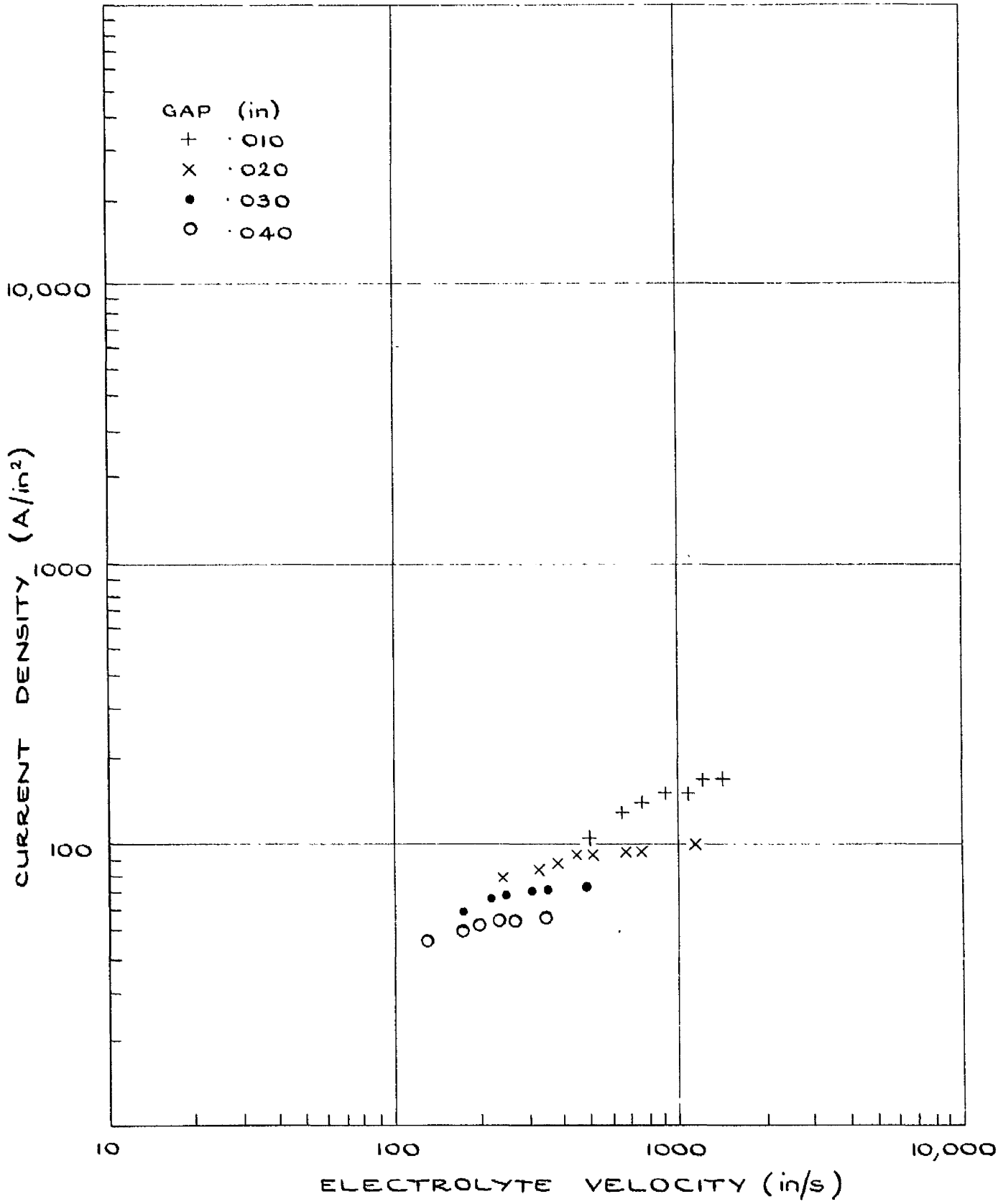

FIG. 2.5* CURRENT DENSITY AS A FUNCTION OF ELECTROLYTE VELOCITY AND GAP WIDTH FOR TURBULENT FLOW.

2.5 Discussion

From Fig.2.3, for each potential gradient current density increases with flow rate to a limiting value. As the potential gradient is increased, the flow rate for which the limiting current density is achieved also increases.

For the larger gaps, 0.040 in and 0.030 in, the limiting current density is near to the Ohmic value. This suggests that for the high velocities the transport of ions is migration controlled, and not diffusic controlled.

For the smaller gaps, 0.020 in and 0.010 in, the limiting current density is near to, but proportionately less than, the Ohmic value. However, values near the Ohmic values again indicate a migration controlled reaction. The observation that as the gap is decreased, the current density value becomes less than the Ohmic value, suggests that hydrogen evolution is indeed occurring at the cathode, and is increasing the effective resistivity of the solution and so reducing the observed current density. This effect is more marked at smaller gaps. It is discussed more fully in Chapter 7.

The regions where flow rate affects the current density can be divided into laminar and turbulent flow regions.

From the theoretical analysis for laminar flow, current density is proportional to the square root of velocity (Eqn. 2.4).

Fig.2.4 shows good agreement between the theoretical and experimental plots of current density as functions of electrolyte velocit

The current densities for each gap are less than the Ohmic value, and for each velocity there is no apparent effect of gap width. Thus the ionic diffusion rate is not yet being limited by the ionic migration rate, and the current density can be calculated from Levich's equation (2.4) and not from Ohm's Law.

For turbulent flow, it has been postulated that $i \propto v^{0.9}$ (Eqn.(2.16))

Fig.2.5 shows poor agreement between theory and experiment for turbulent flow. Current density nevertheless increases with velocity (up to the limiting value) and the current density values are still greater than those for laminar flow. Thus diffusion must still be influencing the ion movement, and the diffusion layer must be thinner.

However, the re-drawing of Fig.2.5 - Fig.2.5* - shows the effect of gap width on the current density-electrolyte velocity relationship. (For laminar flow there was no such effect). For a constant velocity, as the gap decreases, the current density increases. This suggests the additional influence of ionic migration.

Thus, for turbulent flow it is suggested that:

(i) at the electrodes, ions still diffuse across the diffusion layer.

(ii) the diffusion rate is greater than the rate for laminar flow.

(iii) the migration rate limits the diffusion rate.

(iv) the diffusion rate can be increased by increasing the electrolyte velocity. (The migration rate can be increased by decreasing the gap width. For a constant electrolyte velocity, the ion transfer rate can be increased only if the gap is decreased).

(v) the maximum current density is the Ohmic current density. (This is obtained when the path length for ion migration approximates to the gap width, and occurs when the diffusion layers are decreased by the high velocities to very thin regions).

2.6 Conclusions

(1) For laminar flow, ionic transport is diffusion controlled, the current density is approximately proportional to the square root of the electrolyte velocity.

(2) For turbulent flow, current density still increases with velocity but the ion migration rate limits the diffusion rate. For a given potential gradient, the maximum migration rate is given by Ohm's Law.

(3) For the smaller gaps, 0.020 in and 0.010 in hydrogen evolution appears to lower the maximum current density below the Ohmic value.

Chapter 3

Effects of the Products of Machining on Electrolyte Properties

3.1 Introduction

During machining the metal dissolved from the anode goes into basic solution as metal hydroxide. In most E.C.M. applications, the electrolyte with the hydroxide in suspension, will duly circulate back to the working area. If the metal particles affect the electrolyte properties the machining action may be affected, and calculations based on the original properties made erroneous.

The results below show the effects of machining products on the bulk electrolyte conductivity, density and viscosity.

3.2 Apparatus

Conductivity was measured at 18°C using a Wayne-Kerr Conductivity Bridge. Density was measured with a Griffin and George Hydrometer calibrated in 0.001 g/mℓ divisions from 1.000 to 1.500 g/mℓ. A Griffin and George U-tube viscometer was used to check the viscosity (at 16°C).

3.3 Results

Table 3.1 gives the measurements of electrolyte conductivity, density and viscosity for three samples of 20% NaCℓ solution: one fresh and uncontaminated, and two containing the products of approximately 6 hours and 9 hours machining respectively, at an average current of 80A, with a total electrolyte volume of 12 cu.ft.

	THEORETICAL (from Kaye and Laby's Tables[21])	FRESH SOLUTION	SOLUTION AFTER 6 hrs. MACHINING	SOLUTION AFTER 9 hrs. MACHINING
CONDUCTIVITY (Ω^{-1} cm^{-1})(18°C)	0.195	.200	.200	.200
DENSITY (g/mℓ)(18°C)	1.149	1.15	1.15	1.15
VISCOSITY (cP) (16°C)		0.97	1.01	1.03

Table 3.1: The effects of the products of machining on the conductivity, density and viscosity of a 20% NaCℓ solution.

3.4 Discussion

The conductivity and density are not altered by the metal hydroxide particles in suspension in the solution. The solution viscosity is however increased, but the change is small and would have little effect on the electrolyte motion.

Similar results have been found by Bayor[23].

3.5 Conclusion

The metal particles in solution should have virtually no effect on electrolyte motion and do not affect conductivity or density. Their effects on metal machining can then be disregarded.

This is assumed in subsequent discussions on machining experiments.

Chapter 4

The Machining of Metals

4.1 Introduction

There is little published work on the behaviour of metals in different electrolytes under E.C.M. conditions. This chapter describes experiments to investigate some effects of current density and Reynolds number on removal rates and surface finish for a range of metals, machined in a 20% sodium chloride electrolyte.

There appears to be no established method for predicting removal rates for an alloy from the electrochemical equivalent of its constituent metals. Three possible methods are first deduced. These have been tested with three alloys: Nimonic 75, Monel, and an aluminium-copper alloy.

4.2 Removal rates for alloys

In the methods below, an alloy is considered to consist of X_A % by weight of element A, with atomic weight a_A and with its ions dissolving in valency state z_A, of X_B % of element B, with atomic weight and valency a_B and z_B respectively, and of X_C % of element C etc.

Method 1: "% by weight" method

The sum of the chemical equivalents (C.E) of each element in the alloy, multiplied by its respective proportion by weight, gives a value for $\left(\frac{a}{z}\right)_{alloy}$, the C.E. of the alloy:

$$\left(\frac{a}{z}\right)_{alloy} = \frac{X_A}{100} \cdot \left(\frac{a_A}{z_A}\right) + \frac{X_B}{100}\left(\frac{a_B}{z_B}\right) + \frac{X_C}{100}\left(\frac{a_C}{z_C}\right)$$

The removal rate can then be found from Faraday's Law:

$$\dot{m} = \left(\frac{a}{z}\right)_{alloy} \cdot \frac{i}{F}$$

Method 2: "observed removal rate for elements" method

By this method, it is not necessary to know the C.E. values for each element, if the elements are individually machined at the required current density. The observed removal rates, multiplied as above, are then added to give a removal rate for the alloy:

$$\dot{m} = \frac{X_A}{100}(\dot{m})_A + \frac{X_B}{100}(\dot{m})_B + \frac{X_C}{100}(\dot{m})_C$$

Method 3: "Superposition by charge" method

From Faraday's Law, the addition of the coulombs required to liberate the mass contributions to the alloy of each element, gives the number of coulombs required to liberate 1_g of the alloy. From this, a value for the C.E. for the alloys is found:

For element A, the number of coulombs required to liberate the mass contribution = $\frac{X_A}{100} \cdot \frac{z_A}{a_A} \cdot F$

(Similarly for elements B,C)

For the alloy, the number of coulombs required to liberate $1g = \left(\frac{z}{a}\right)_{alloy} F$

$$\therefore \left(\frac{z}{a}\right)_{alloy} \cdot F = F\left(\frac{X_1}{100}\right)\left(\frac{z_1}{a_1}\right) + F\left(\frac{X_2}{100}\right)\left(\frac{z_2}{a_2}\right) + \ldots$$

$$\text{i.e.} \left(\frac{a}{z}\right)_{alloy} = \frac{100}{X_A\left/\left(\frac{a_A}{z_A}\right)\right. + X_B\left/\left(\frac{a_B}{z_B}\right)\right. + X_C\left/\left(\frac{a_C}{z_C}\right)\right.}$$

The removal rate for the alloy can then be found from Faraday's Law.

4.3 Apparatus and Procedure

The apparatus used with the Barmax machine is fully described in Appendix 1.

Two types of plane, parallel electrodes have been used:

(a) for current densities up to 525 A/in^2: cylindrical electrodes of diameter 1.3 in.

(b) for current densities between 500 and 1200 A/in^2: square electrodes of side 0.45 in.

A typical jig used with the Barmax machine is shown in Fig.2.1

A 20% sodium chloride solution was chosen as the electrolyte, on advice from industrial users of the process, because it was known to give satisfactory results in the machining of mild steel and Nimonic alloys under suitable conditions of current density and gap width.

The following metals have been investigated: nickel, Nimonic 75, mild steel, aluminium, monel, copper, cast iron, and an aluminium-copper alloy.

The experimental procedure required with the Barmax machine is

also given in Appendix 1.

4.4 Results - alloy removal rates

Removal rates for an aluminium-copper alloy, Nimonic 75 and Monel have been calculated by the first and third methods, and compared with experimental values.

The second method has been applied to the aluminium-copper alloy (with constituents copper and aluminium) and to Monel (with its main constituents, nickel, copper and iron).

The composition and assumed atomic weight and valency of each metal were:

Al-Cu alloy: 94% Al; 5% Cu; 0.5% Bi; 0.5% Fe

Cu : 99.9% Cu; 0.05% Bi; 0.05% Pb;

$a_{Cu} = 63.57 \quad z_{Cu} = 1$

Al : 99% Al; 0.1% Cu; 0.7% Fe; 0.1% Mn; 0.1% Zn.

$a_{Al} = 26.97 \quad z_{Al} = 3$

For the calculation the proportions assumed were:

Al-Cu alloy: 94% Al; 5% Cu (the other 1% was neglected)

Cu : 100%

Al : 100%

Nimonic 75 : 72.5% Ni; 19.5% Cr; 0.4% Ti; 5% Fe; 0.5% Cu; 0.1% Si; 0.1% Mn; 0.1% Cu.

Monel : 63.0% Ni; 31.7% Cu; 2.5% Fe; 2% Mn; 0.5: Si; 0.3% C.

Table 4.1: Evaluation of C.E. for Al - Cu alloy, Nimonic 75 and Monel by Method 1.

Alloy	Element	% by wt. X	Atomic wt. a	Valency z	C.E. (a/z)	C.E. x (prop. by wt)
Al - Cu Alloy	Al	94.0	26.97	3	8.99	8.45
	Cu	5.0	63.57	1	63.57	3.18
	Alloy					11.63
Nimonic 75	Ni	72.5	58.71	2	29.36	21.20
	Cr	19.5	52.01	3	17.34	3.37
	Fe	5.0	55.85	2	27.93	1.39
	Ti	0.4	47.9	2	23.95	0.09
	Si	1.0	28.09	4	7.02	0.07
	Mn	1.0	54.94	2	27.47	0.27
	Cu	0.5	63.57	1	63.57	0.31
	C (inert)	0.1	-	-	-	-
	Alloy	100				26.70
Monel	Ni	63	58.71	2	29.36	18.5
	Cu	31.7	63.57	1	63.57	20.2
	Fe	2.5	55.85	2	27.93	0.69
	Mn	2	54.94	2	27.47	0.55
	Si	0.5	28.09	4	7.02	0.04
	C (inert)	0.3	-	-	-	-
	Alloy	100				39.98

Table 4.2: Evaluation of C.E. for Aℓ - Cu alloy and Monel by Method 2. (This has been applied to Monel, using the three main elements of the latter).

Alloy	Element	% by wt. X	METAL REMOVAL RATE (g/(min.in^2) OBSERVED			X (OBSERVED)			ALLOY		
			30A/in^2	60A/in^2	90A/in^2	30A/in^2	60A/in^2	90A/in^2	30A/in^2	60A/in^2	90A/in^2
Aℓ-Cu	Aℓ	94	.195	.39	.59	.18	.36	.55			
Alloy	Cu	5	.95	2.2	3.45	.05	0.11	0.18			
	Alloy								.23	.47	.73
Monel			30	60	75	30	60	75	30	60	75
	Ni	63	0.55	1.10	1.38	.35	.69	.87			
	Cu	31.7	0.95	2.2	2.85	.31	.70	.91			
	Fe	2.5	.55	1.09	1.37	.01	.027	.03			
	Mn	2	-	-	-	-	-	-			
	Si	0.5	-	-	-	-	-	-			
	C	0.3	-	-	-	-	-	-			
	Alloy								.67	1.42	1.81

Table 4.3: Evaluation of C.E. for Al - Cu alloy, Nimonic 75 and Monel by Method 3.

Alloy	Element	% by wt X	C.E. a/z	$X/\frac{a}{z}$	(C.E.) alloy = $100/X/\frac{a}{z}$
Aluminium - Copper	Al	94	8.99	10.35	
	Cu	5	63.57	0.08	
	Alloy	100		10.43	9.63
Nimonic 75	Ni	72.5	29.36	2.47	
	Cr	19.5	17.34	1.12	
	Fe	5.0	27.93	0.179	
	Ti	0.4	23.95	0.017	
	Si	1.0	7.02	0.143	
	Mn	1.0	27.47	0.0364	
	Cu	0.5	63.57	0.008	
	C (inert)	0.1	-	-	
	Alloy	100		3.97	25.2
Monel	Ni	63	29.36	2.15	
	Cu	31.7	63.57	0.49	
	Fe	2.5	27.93	0.89	
	Mn	2	27.47	0.07	
	Si	0.5	7.02	0.07	
	C (inert)	0.3	-	-	
	Alloy	100		3.67	27.3

Table 4.4: Comparison of predicted and observed removal rates for each alloy

Current Density A/in^2	ALLOY REMOVAL RATES (c/(min.in^2))				
	PREDICTED			OBSERVED	ALLOY
	Method 1	Method 2	Method 3		
30	.22	.23	0.18	0.27	Al - Cu
	.495	-	0.47	-	Mim.75
	.74	.67	0.51	-	Monel
60	.43	.47	0.36	0.47	Al - Cu
	.99	-	0.94	0.95	Mim.75
	1.48	1.42	1.03	1.30	Monel
75	.54	-	0.45	-	Al - Cu
	1.24	-	1.18	1.15	Mim.75
	1.86	-	1.27	1.65	Monel
90	.65	.63	0.54	0.69	Al - Cu
	1.49	-	1.42	1.40	Mim.75
	2.24	1.81	1.53	1.9	Monel
150	1.08	-	0.90	-	Al - Cu
	2.48	-	2.35	2.3	Mim.75
	3.72	-	2.54	3.25	Monel

Tables 4.1, 4.2, 4.3 show the calculations of the C.E. for each alloy by each method.

Table 4.4 shows the comparison of the calculated removal rate for each method, and observed removal rates for each alloy.

4.5 Discussion

Low current densities were used, as at higher values other anodic reactions become appreciable and lower the current efficiency. (See later - 4.10).

The removal rates predicted by method 1 are lower than the observed rates for the Aℓ-Cu alloy, but higher for Nimonic 75 and Monel. There is no apparent theoretical basis for adding the respective mass contributions for each alloy in this way, and the method can only be regarded as giving an empirical value.

In Method 2, the necessary knowledge of ion valencies is avoided by adding known removal rates for the alloy constituents. In general, the theoretical rates are less than the observed. However, the use of the method is limited, as all the alloy constituents may not be readily available for machining. This was the case with Nimonic 75.

The Law of Superposition of Charge was used as the physical basis for the third method. There is good agreement between the predicted and observed removal rates for Nimonic 75, but poor agreement for the other alloys.

For alloys with a large number of constituents the third method is possibly the most suitable as it does have the theoretical grounding

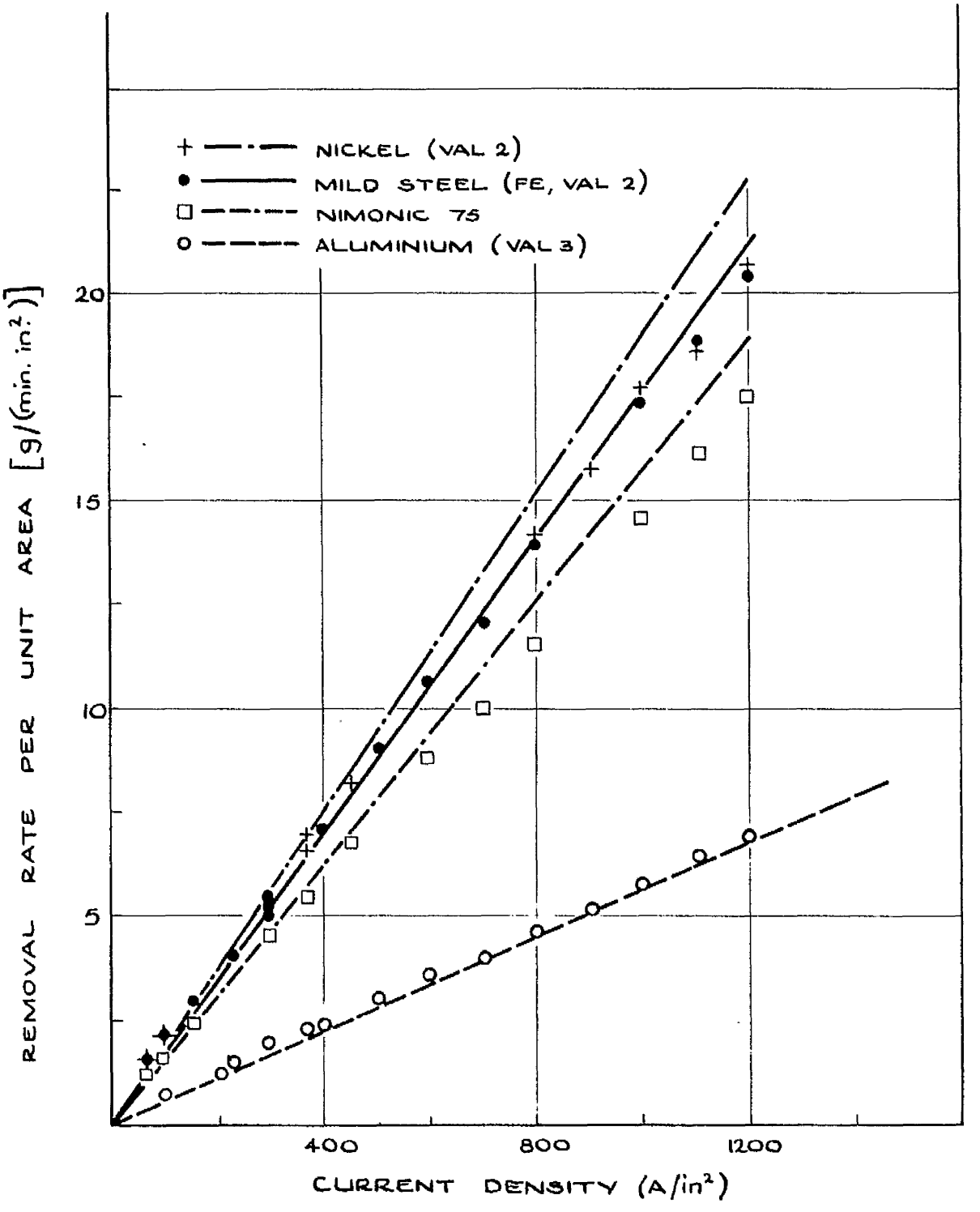

FIG. 4. 1. REMOVAL RATE AS A FUNCTION OF AVERAGE CURRENT DENSITY FOR NICKEL, MILD STEEL, NIMONIC 75 AND ALUMINIUM.

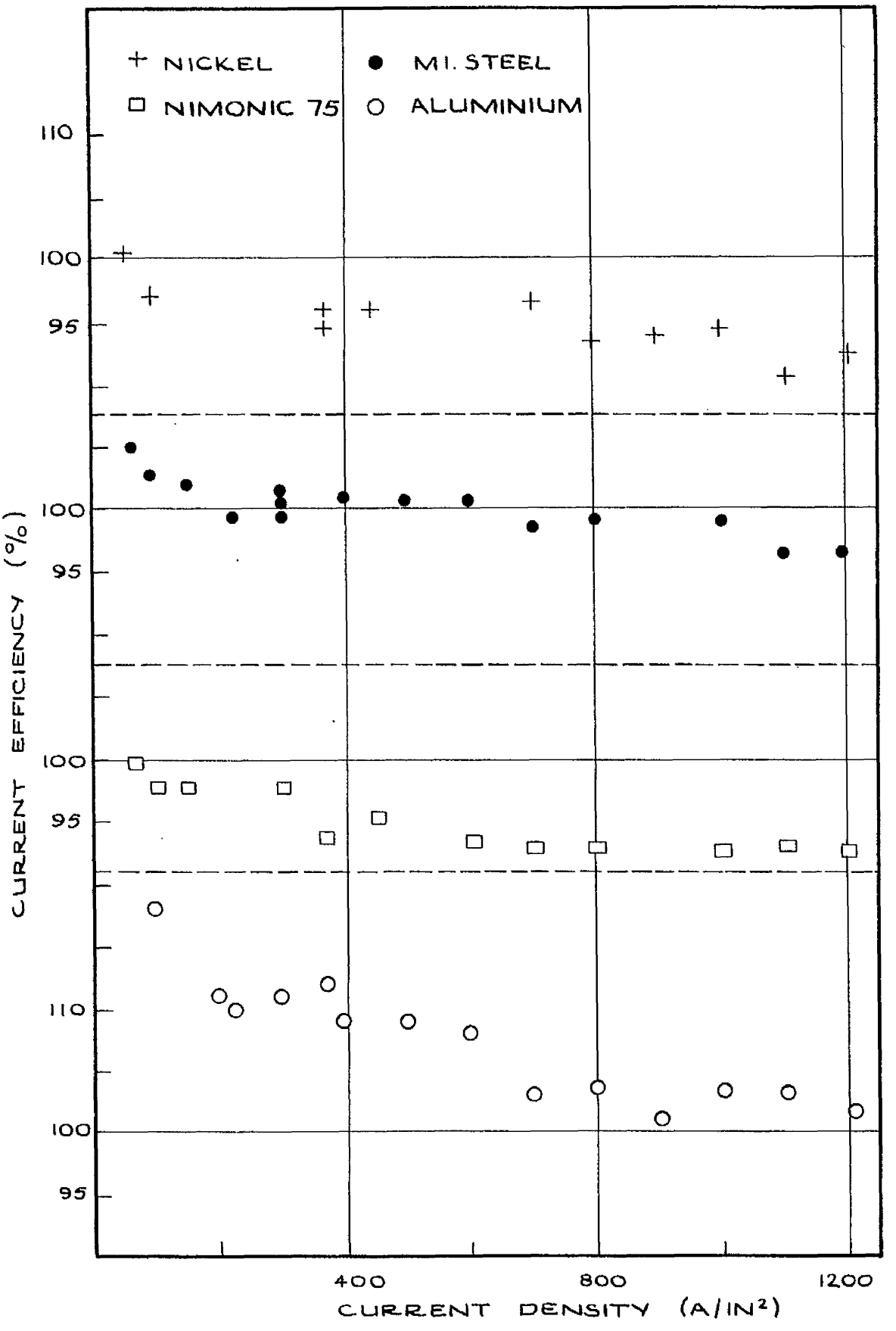

FIG. 4.2. CURRENT EFFICIENCY AS A FUNCTION OF CURRENT DENSITY FOR NICKEL, MILD STEEL, NIMONIC 75 AND ALUMINIUM.

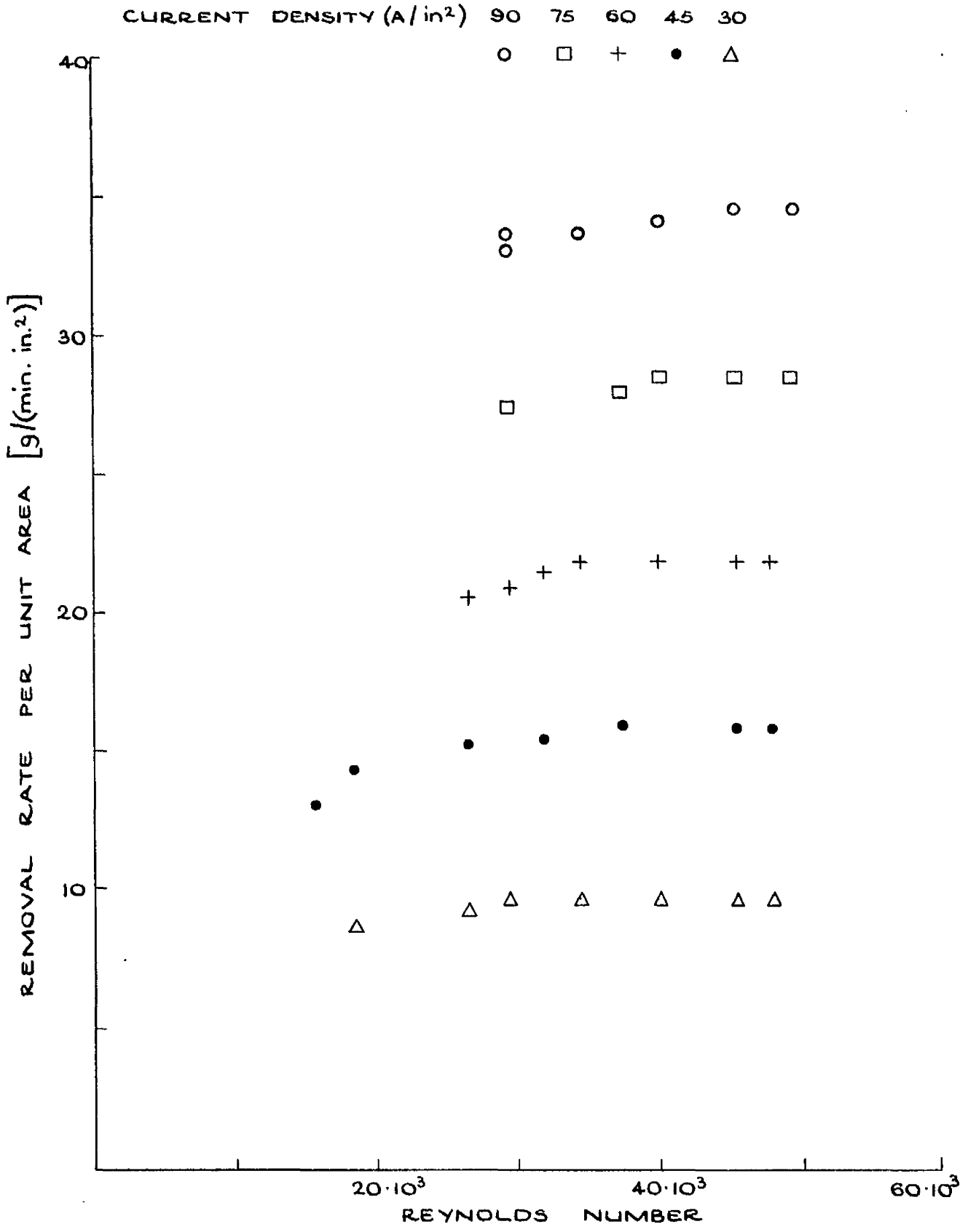

FIG.4.3. REMOVAL RATE FOR COPPER AS A FUNCTION OF CURRENT DENSITY AND REYNOLDS NUMBER.

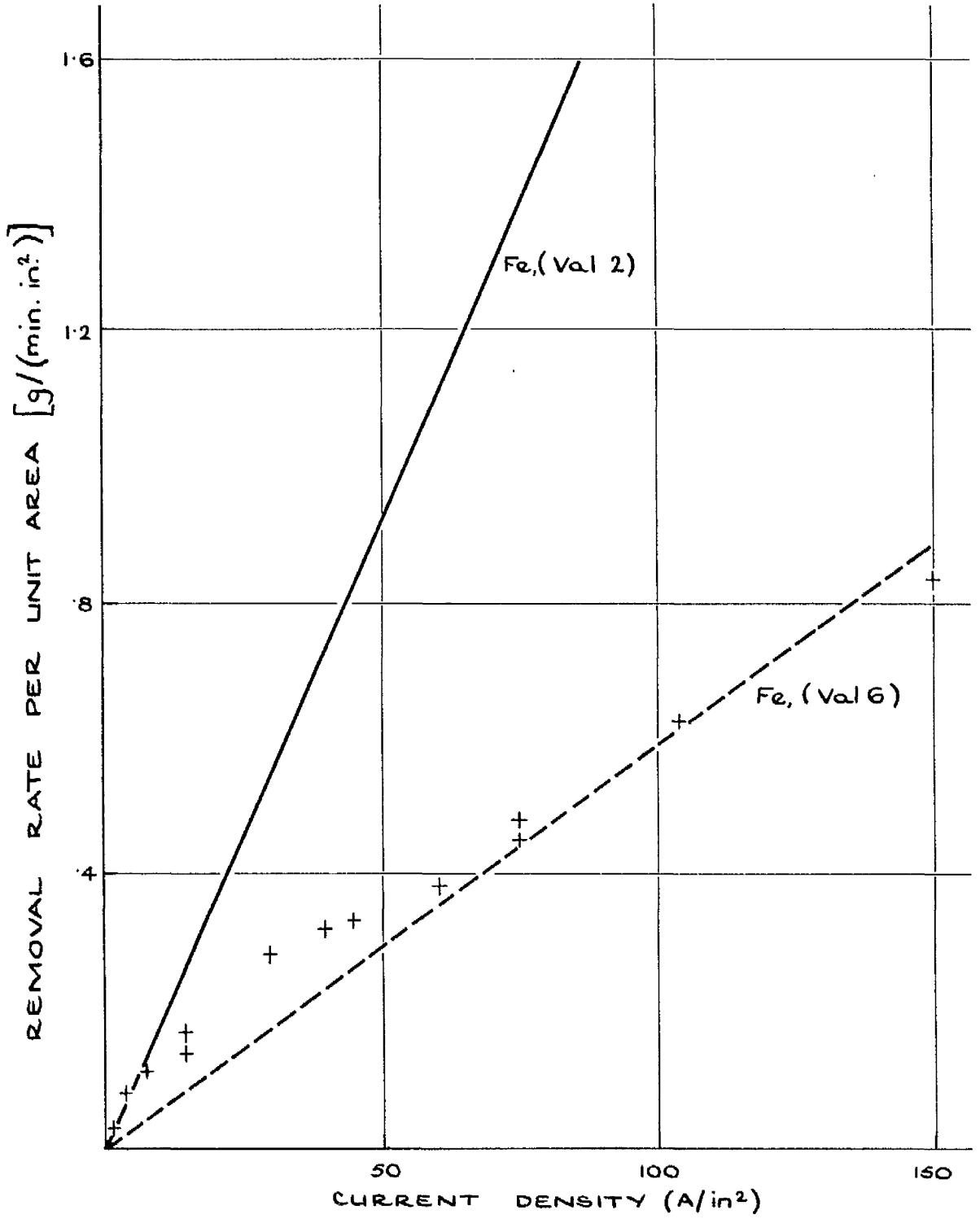

FIG.4.4. REMOVAL RATE AS A FUNCTION OF CURRENT DENSITY FOR CAST IRON.

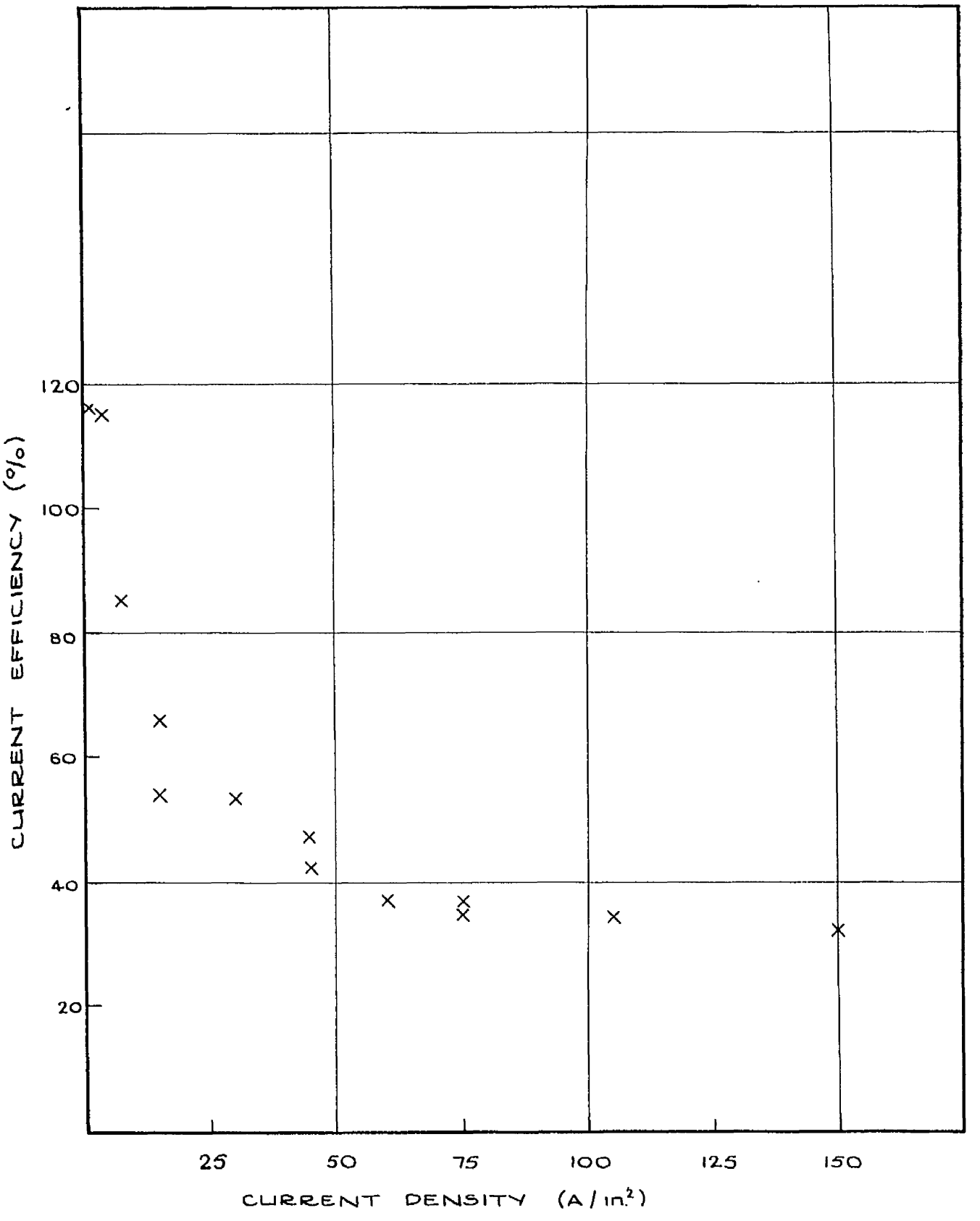

FIG. 4. 5. CURRENT EFFICIENCY AS A FUNCTION OF CURRENT DENSITY FOR CAST IRON.

that the others lack.

4.6 Results - The Machining of metals

Fig.4.1 shows the effect of current densities ranging from 75 A/in^2 to 1200 A/in^2 on the theoretical (Faraday) and experimental removal rates for nickel, mild steel, Nimonic 75 and aluminium.

For these metals, and the range of current densities 75 to 1200 A/in^2, Reynolds numbers ranging from 10000 to 48000 have no effect on removal rate.

Fig.4.2 shows the corresponding effects of current density on current efficiency.

Fig.4.3 shows the effect of Reynolds numbers ranging from 10000 to 48000 on the removal rates for copper, machined at current densities from 30 to 90 A/in^2.

Fig.4.4 and 4.5 show the dependence of removal rate and current efficiency, respectively, on current densities ranging from 1 A/in^2 to 150 A/in^2 for cast iron.

4.7 Discussion

4.7.1 The machining of nickel, mild steel, Nimonic 75 and aluminium.

From Figs. 4.1 and 4.2 the following characteristics of the individual metals have been established:

(i) Nickel

Nickel appears to dissolve in the divalent state. The current efficiency decreases with current density from about 102% at 75 A/in^2 to 97% at 12000 A/in^2

(ii) Mild Steel

Regarded from an electrochemical viewpoint as divalent pure iron, mild steel has a current efficiency which decreases with current density from about 105% at 75 A/in^2 to 96% at 1200 A/in^2.

(iii) Nimonic 75

Theoretical removal rates, shown in Fig.4.1 were calculated by the third method for calculation of alloy removal rates described above. From Fig.4.2 current efficiency decreases with current density from about 100% at 75 A/in^2 to about 92% at 1200 A/in^2.

(iv) Aluminium

The observed removal rates are greater than the theoretical for the metal in its normal trivalent state. This may be due, either to the sodium chloride electrolyte which has a strong affinity for aluminium (see, for example, Mellor's "Modern Inorganic Chemistry"[24]) assisting the electrolytic action by dissolving the metal whose ionic bonds have been loosened by the electric field, or to the metal ions going into solution in a lower valency than normal (see, for example, "Encyclopaedia of Electrochemistry"[25]), or to the metal ions dissolving in several different valency forms: these ions may then react with the hydrogen present, or with the water in the electrolyte, to form ions of normal valency. For example, for Al ions dissolving in the divalent state, a possible reaction might be:

$$Al^{++} + H^{+} = Al^{+++} + \tfrac{1}{2} H_2$$

The current efficiency decreases with current density from about 118% at 75 A/in^2 to about 102% at 1200 A/in^2.

This general decrease of current efficiency with increase in current density is discussed later in relation to surface finish.

4.7.2 The machining of copper

From Fig.4.3, removal rate increases with Reynolds numbers up to about 40000 after which the latter has no effect. Within the range 60 to 90 A/in^2, machining at Reynolds numbers less than 20000 was not possible due to shorting across the electrode gap. This limiting current density for a given Reynolds number suggests that the dissolution of copper in sodium chloride is diffusion controlled. The diffusion of copper in sodium chloride has also been noted by Hurlen[26].

Copper appears to dissolve from the anode in the monovalent state. This has also been observed by Hurlen who shows that in some solutions (e.g. chlorides and bromides) copper dissolves monovalently, whilst in others (e.g. sulphates) it dissolves divalently.

In Fig.4.3 for the removal rates independent of Reynolds number, the current efficiency was estimated as about 102%. That the efficiency was greater than 100% was possibly due to the detachment of actual grains from the anode by electrolytic grain boundary attack. The granular surface finish of the copper described below corroborates this explanation. Another possible reason - corrosion by the sodium chloride which, in Hurlen's work, is stated to cause efficiencies in excess of 100% - is dismissed because:

(i) the duration of each test (10 min.) was insuffiqiently long for corrosion to take place, and

(ii) in checks with the electrodes 0.060 in. apart with the electrolyte flowing (Re = 48000) but no current, there was no weight loss from the anode.

Effects of Reynolds number and current density on surface finish are described below.

4.7.3 The Machining of cast iron

Fig.4.4 shows that the experimental and theoretical removal rates (assuming, as before, that the metal is divalent pure iron) are almost coincident only up to about 10 A/in^2 above which the observed rate falls away from the theoretical.

This effect is due to partial passivation (a phenomenon described fully by Evans[27], and Uhlig[28]). It can be attributed to a protective oxide layer on the metal surface produced possibly by direct oxidation of the silicon in the metal with moisture, the reaction being

$$Si + 2\ H_2O = Si(OH)_2 + H_2$$

and to chlorine forming on the inert carbon in the metal (The chlorine was easily smelled at the end of each test).

Attempts were made to reduce the passivation effect (and so increase the removal rate) by

(i) increasing the Reynolds number to mechanically remove the passive layer,

(ii) scraping the surface to remove the initial oxide film, and

(iii) smearing the surface with concentrated HCℓ acid to dissolve the layer. They were all unsuccessful - at the end of each test, the metal surface was still covered with a thick, black oxide layer.

A possible explanation for passivity has been given by Uhlig. He suggests that metals which passivate are usually incomplete in the d-energy levels in the shell below that of the valency electrons, and thus have an incomplete filling of the d-band in the crystalline structure, i.e. metals in the electrochemical "transition group". Passivation will correspond to incomplete bands, and adsorption to filled bands. The adsorption of oxygen atoms onto the metal surface induces passivity since they behave as electron absorbers with no tendency to supply electrons to surface atoms of the metal.

Fig.4.5 shows that the corresponding current efficiency decreases with current density from about 118% at 25 A/in^2 to about 32% at 150 A/in^2. At the former current density, efficiency greater than 100% is probably due to differential erosion of the other elements in the metal, causing the grains of inert carbon to drop out, and thus increasing the observed removal rate.

4.8 Dependence of surface finish on machining parameters

Surface roughness measurements (using a Talysurf instrument) were made for current densities ranging from 75 A/in^2 to 1200 A/in^2, and for a constant Reynolds number (13000) and temperature (16°C).

4.9 Results

Table 4.5 shows the effect of current density on surface roughness

Metal		CURRENT DENSITY (A/in^2)														
		75	100	150	200	225	300	375	400	450	500	600	700	800	900	1000-1200
Nickel	Roughness (micro-in)	50	48	46		45	36									
	Comments	Matt, pitted						Fine, polished cusps, fineness increasing with increasing current density.								
Nimonic 75	Roughness (micro-in)	180		86	55	43	43	42	39	33	33					
	Comments	Coarse matt, pitted										Fine, polished cusps				
Mild Steel	Roughness (micro-in)	60		47		34	30				22	26		53	55	
	Comments	Smooth, matt, pitted										Increased pitting				Extreme pitting
Aluminium	Roughness (micro-in)	18		16			14									
	Comments	Smooth, etched							Fine, polished cusps							
Monel	Roughness (micro-in)			60			42	36								
	Comments	Alternate bands							Fine, polished cusps							

Table 4.5: Surface Roughness (micro-in) as a function of current density A/in^2, for nickel, Nimonic 75, mild steel, aluminium and monel (Re = 13,000, T = 16°C)

Re	13,000	21,000	27,000	37,000	45,000
Roughness at ($150\ A/in^2$)	47	38	28	26	23

Table 4.6: Surface roughness (micro-in) as a function of Reynolds number for mild steel.

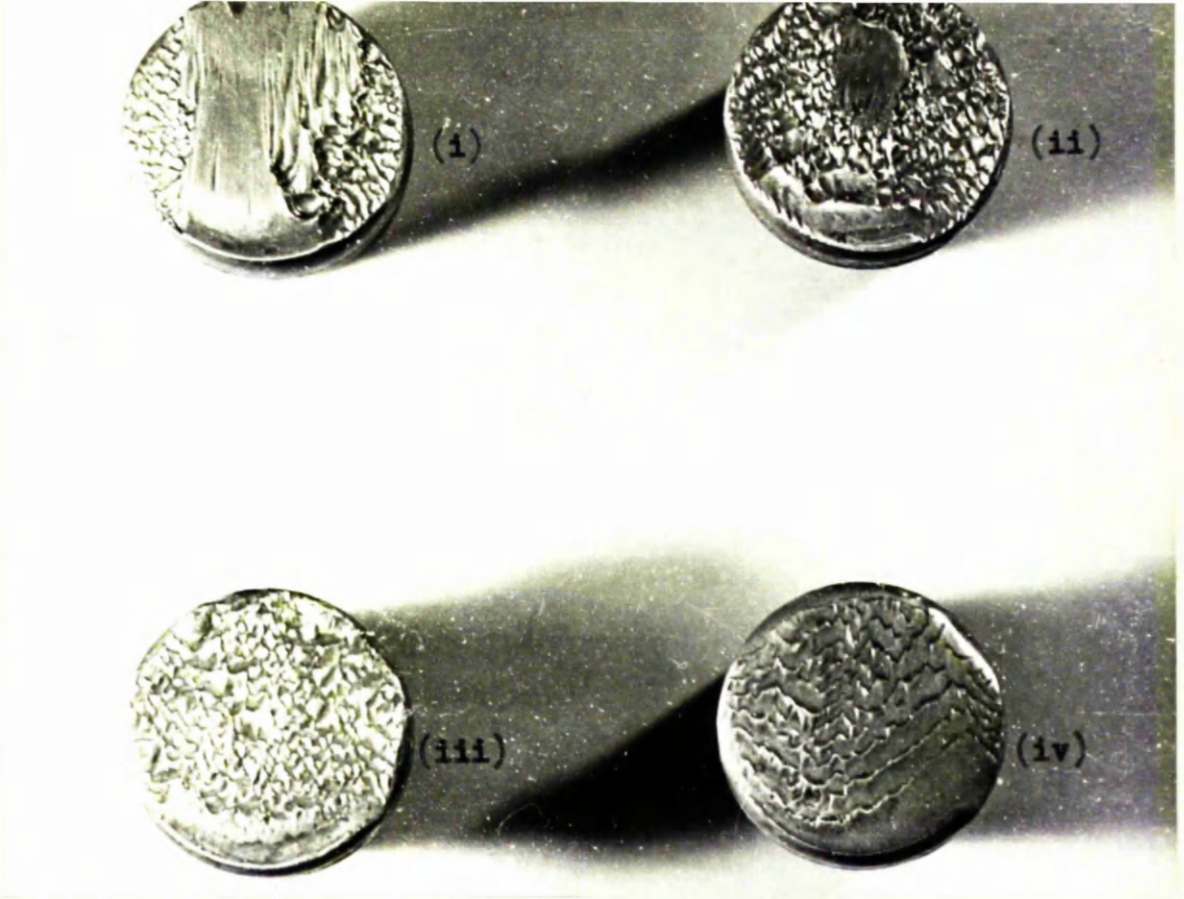

Fig 4.7 : Typical finishes for copper at 60 A/in^2

(i) (Re = 10000) : (ii) (Re = 20000)

(iii)(Re = 36000) : (iv) (Re = 48000)

Fig 4.6 : Typical finishes:

Monel : A(75 A/in^2) , B (225 A/in^2) (Re = 24000)

C(375 A/in^2) (Re = 16000)

Nickel : D (375 A/in^2)

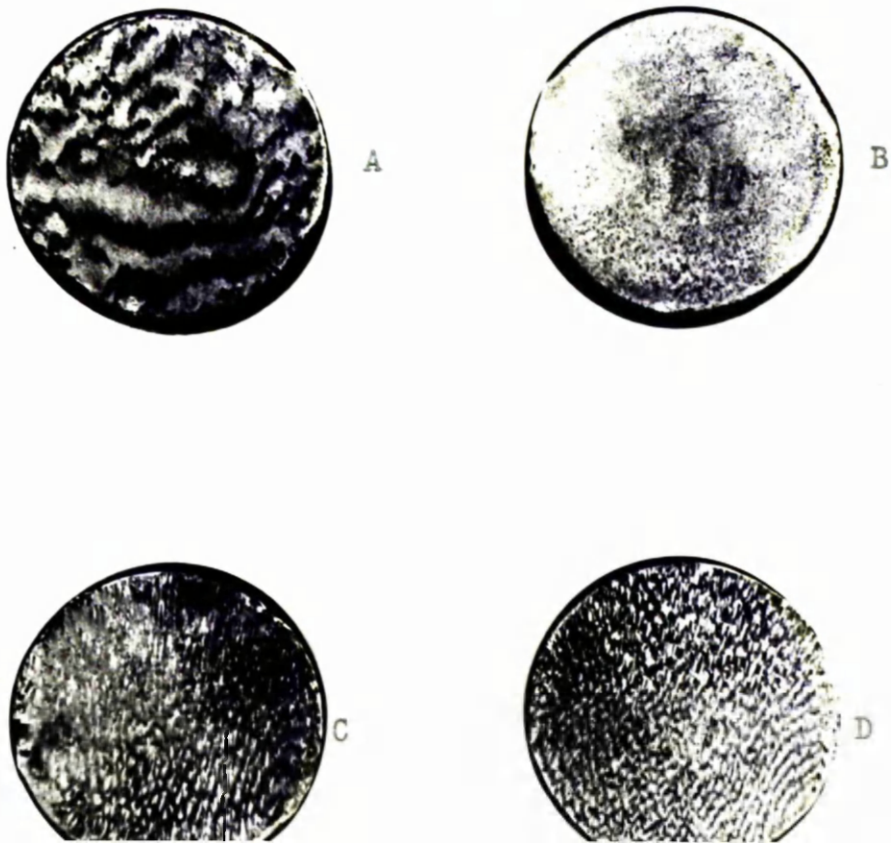

(measured in micro-in) for nickel, Nimonic 75, mild steel, aluminium and Monel.

Table 4.6 for mild steel shows the dependence of surface roughness on Reynolds numbers ranging from 13000 to 64000, for a current density of 150 A/in^2.

Fig.4.6 illustrates three Monel specimens machined at 75 A/in^2 and 225 A/in^2 (Re = 24000) and 375 A/in^2 (Re = 16000) and one nickel specimen machined at 375 A/in^2 (Re = 16000).

Fig.4.7 illustrates four copper specimens each machined at 60 A/in^2 but at different Reynolds numbers (10,000, 20,000, 36,000, 48,000).

4.10 Discussion

(i) Nickel, Nimonic 75, Monel, mild steel and aluminium

From Table 4.5 for current densities ranging from 75 to about 300 A/in^2 for nickel and aluminium, and from 75 to 500 A/in^2 for Nimonic 75 and mild steel a smooth finish is obtained; for aluminium the finish is smooth but etched.

For Nimonic 75, for current densities from 75 to 150 A/in^2 the surface roughness values are greater than those for nickel and mild steel. At higher current densities, the effect is less marked and a smoother finish obtained. This is possibly due to differential erosion of the alloy constituents: the constituent with the lowest decomposition potential will dissolve first. (This potential depends on the alloy, the electrolyte and on the current density). For a grain of metal at the anode surface which has a greater decomposition

voltage than the surrounding material, less current will flow to that grain. This will then dissolve at a lower rate than the surrounding metal, and will protrude from the surface increasing the overall roughness.

(Note: for any voltage gradient across the gap, dissolution of the protruding grain will only commence when its potential reaches the decomposition potential. At higher current densities the voltage gradient increases, the decomposition potential will be achieved more quickly and the surface will become smoother).

A similar effect is observed for Monel. In Fig.4.7 differential erosion at 75A/in^2 has separated the copper (dark) and the nickel (light). At a higher current density (225 A/in^2) the separation is not obvious: the differential erosion effect is decreased and the surface is smoother.

Table 4.5 also shows a general increase of smoothness with current density. This has also been noted by Edwards[9], but for low current densities (to 1 A/in^2).

At higher current densities (above 300-500 A/in^2), for nickel, aluminium and Nimonic 75, a polished, cusped finish is obtained. (see, e.g. Fig.4.6 - Nickel specimen).

For mild steel there is increased pitting at these current densities causing a rougher surface.

Smoothing and Polishing

For a given Reynolds number, smoothness depends on current density (Hoar and Rothwell[4][5]). The smoothing and polishing action is

controlled by the ion diffusion layer next to the anode; it is discussed more fully in the next chapter:

Briefly, in the 'Jacquet' theory for the polishing of a metal in an electrolyte, the plot of current potential against anode potential is an 'inverted S' shaped curve, with a plateau region parallel to the potential axis indicating the maximum smoothing (i.e. polishing) conditions. The curve then rises: this section corresponds to gas evolution at the anode causing pitting of the polished surface. Less current will be available for metal dissolution and the current efficiency will be reduced. The current density and potential at which polishing and gas evolution occur respectively can be increased by raising the flow rate(4)(5).

Current Efficiency and Gas Evolution

For the above metals, the decrease in current efficiency as the current density is increased may be linked to the pitting effect and hence to the evolution of gas (possibly oxygen) at the anode.

At the lower current densities (75 to 300-500 A/in^2) the effect of gas evolution may not be great, and the surfaces become smoother.

The polished, cusped finish at the higher current densities may signify that in the polarisation curve, the region favouring gas evolution with polishing has been entered, and that the Reynolds number is too low for overall polishing. Gas at the anode may then disrupt the polishing film and hinder the polishing action.

For mild steel there is no evidence of polishing, although at the

lower current densities, smoothness increases with current density. For this metal the Jacquet plateau current density region may be short, causing early onset of gas evolution. This effect would be more marked at higher current densities. The observed extreme pitting provides some evidence for this.

The effect of pitting on surface smoothness can be reduced if the gas is swept away before it can affect the polishing film. In Table 4.6 for mild steel, machined at 150 A/in^2 the roughness is reduced as the Reynolds number is increased. It is inferred that the effect of pitting on the surface roughness can be reduced if the gas is swept away before it can affect the diffusion layer.

(ii) Copper

A rough, uneven but polished finish is obtained in sodium chloride. From Fig.4.7, at low Reynolds numbers (10,000 to 20,000) there is greater erosion at the edges of the specimens. This is presumably due to higher flow at the sides allowing a local increase in conductivity by reducing the effect of hydrogen gas. (The effect of hydrogen is discussed in Chapter 7). As the Reynolds number is increased (to 48,000) the surface while still uneven becomes more uniform, possibly as a result of a more uniform flow.

Whilst it does not seem possible to obtain a smooth finish, the surface texture does become finer as the current density is increased.

(iii) Cast iron

After removal of the black, oxide layer a coarse, black finish was revealed. The roughness exceeded 200 micro-in for the range of current densities.

4.11 Conclusions

The following conclusions can be made:

1. The method for predicting alloy removal rates which is based on the Law of Superposition of Change gives good results for Nimonic 75.
2. Current efficiency decreases as the current density increases.
3. Nickel, Nimonic 75, mild steel and aluminium machine well in 20% sodium chloride solution and for appropriate values of the machining parameters produce a satisfactory surface finish.
4. For these metals, for current densities to about 300 A/in^2, surface roughness decreases as the current density increases.
5. Overall polishing at high current densities can deteriorate into polished "cusping" if copious gas evolution occurs at the anode and if the Reynolds number is insufficiently high to wash away the gas before it can disrupt the ion diffusion layer.
6. For mild steel, gas evolution at the anode causes pitting.
7. Copper and cast iron do not produce a smooth surface finish in sodium chloride; also, cast iron partially passivates in the solution.
8. For copper the limiting current density for a given Reynolds number may be increased if the gap width is increased.
9. A study of the current density-anode potential curve for a metal in an electrolyte may be useful as an indicator of the suitability of that solution for the metal.

Chapter 5

The Potentiostat as an Aid to Electrolyte Selection

5.1 Introduction

The results from Chapter 4 demonstrate that 20% sodium chloride is not a suitable electrolyte for all metals.

For particular metals, electrolyte selection has been pragmatic: e.g. Kleiner[1] has found that sodium chloride is suitable for the machining of nickel and iron alloys but not for tungsten. By experiment he has shown that this metal will machine in sodium hydroxide. Appropriate electrolytes for aluminium and copper alloys are still being sought[29].

Testing empirically by machining for each electrolyte and metal could be costly and cumbersome. (With the Barman experimental machine about 100 gallons of each electrolyte would have to be used).

If surface finish is the criterion for suitability then Jacquet's work on electro-polishing suggests a possible method of procedure. From characteristic curves of current density against anode potential Jacquet determined whether a metal would polish in a particular solution. Larsson[30] has applied Jacquet's findings to the problem of electrolyte selection in E.C.M. He has suggested that metals which can be electropolished in unstirred electrolytes can be satisfactorily machined under E.C.M. conditions. In the light of his observations, the method has been further investigated for flowing solutions.

Results from potentiostat experiments using flowing electrolytes are discussed in relation to Jacquet's theory of electropolishing. Corresponding tests under N.C.M. conditions of current density and flow rate have also been performed. The results from these tests are discussed in terms of the findings from the potentiostat work.

5.2 Theory of Electropolishing

Electropolishing is an anodic dissolution process. It can be achieved by applying across the electrodes in an electrolyte a potential difference, which is increased at a constant rate.

The electropolishing action is not yet completely understood. According to Jacquet[8] and more recently Tegart[31], it consists of:
(i) "smoothing" by the removal of relatively large scale irregularities (above about 10^{-6}in). This process is influenced by the diffusion of reaction products from the anode surface into the bulk of the electrolyte. The smoothing rate is faster at peaks and slower at valleys.
(ii) "brightening" by the removal of smaller defects (about 10^{-8}in). This is effected by a thin solid film on the anode surface which accepts cations from the metal lattice and releases them at its outer surface to the region of reaction products so that a state of equilibrium is achieved.

Jacquet showed that the plot of current density against anode potential has a characteristic shape, illustrated in Fig.5.1. For anode potentials in the region AB the "smoothing" process takes place

and the region usually has an etched appearance; along BC the current density is constant. (The constant value is usually termed "the limiting current density"). A thin film is formed on the anode surface with which is associated "brightening". As the potential is increased from C to D gas is evolved at the anode at a rate which is greater the greater the slope of the curve. The gas disrupts the brightening action causing pitting.

Polarisation curves of this form show that the anode reaction is diffusion controlled and that the metal can be polished.

A study of such curves for different metal/electrolyte systems should determine the anode reactions and whether the combinations are compatible for polishing. A potentiostat is usually used for these studies.

5.3 The Potentiostat

The potentiostat compares the potential difference between the working (anode) electrode and a stable, but adjustable, reference voltage. Any voltage difference is amplified and fed back into the circuit as a controlled output current which flows through the electrolytic cell, minimising the error signal, and maintaining the anode potential at the predetermined value.

The use of the instrument has been fully described by Ord and Bartlett[7] in their paper on the action of unstirred sulphuric acid on iron.

Many workers have used the potentiostat to study particular anode

reactions: Higgins[3] has shown that the polishing of nickel (at 16A/in^2) in HCl acid is a diffusion controlled reaction. For copper in O-phosphoric acid, Hoar and Rothwell[4] have observed that current density increases with flow rate (for the approximate ranges .97A/in^2 to 1.44A/in^2 and 0.4in/s to 2in/s) and have deduced that such a reaction is diffusion controlled.

These considerations indicate that potentiostat studies can help in deciding proper metal/electrolyte combinations for electropolishing. Although the current densities in E.C.M. are much greater than those in potentiostat work, useful information concerning electrolyte suitability for E.C.M. work may be obtained from potentiostat studies. Such experiments for flowing electrolytes are described below. The results are discussed in relation to deciding suitable metal/electrolyte combinations for E.C.M.

5.4 Apparatus

5.4.1 Flow System

The flow system is illustrated schematically in Fig.5.2.

A perspex flow cell, shown in Fig.5.3 was used. Its design is based on that of Hoar and Rothwell but with certain modifications.

A "Glen Creston" variable speed peristaltic pump capable of flows up to 9in^3/s was preferred to the normal centrifugal impellor to avoid possible detrimental effects due to acids and salt solutions.

The solution was circulated between the electrodes from a perspex tank, filled with about 1/3 gallon of electrolyte. A "Rotameter"

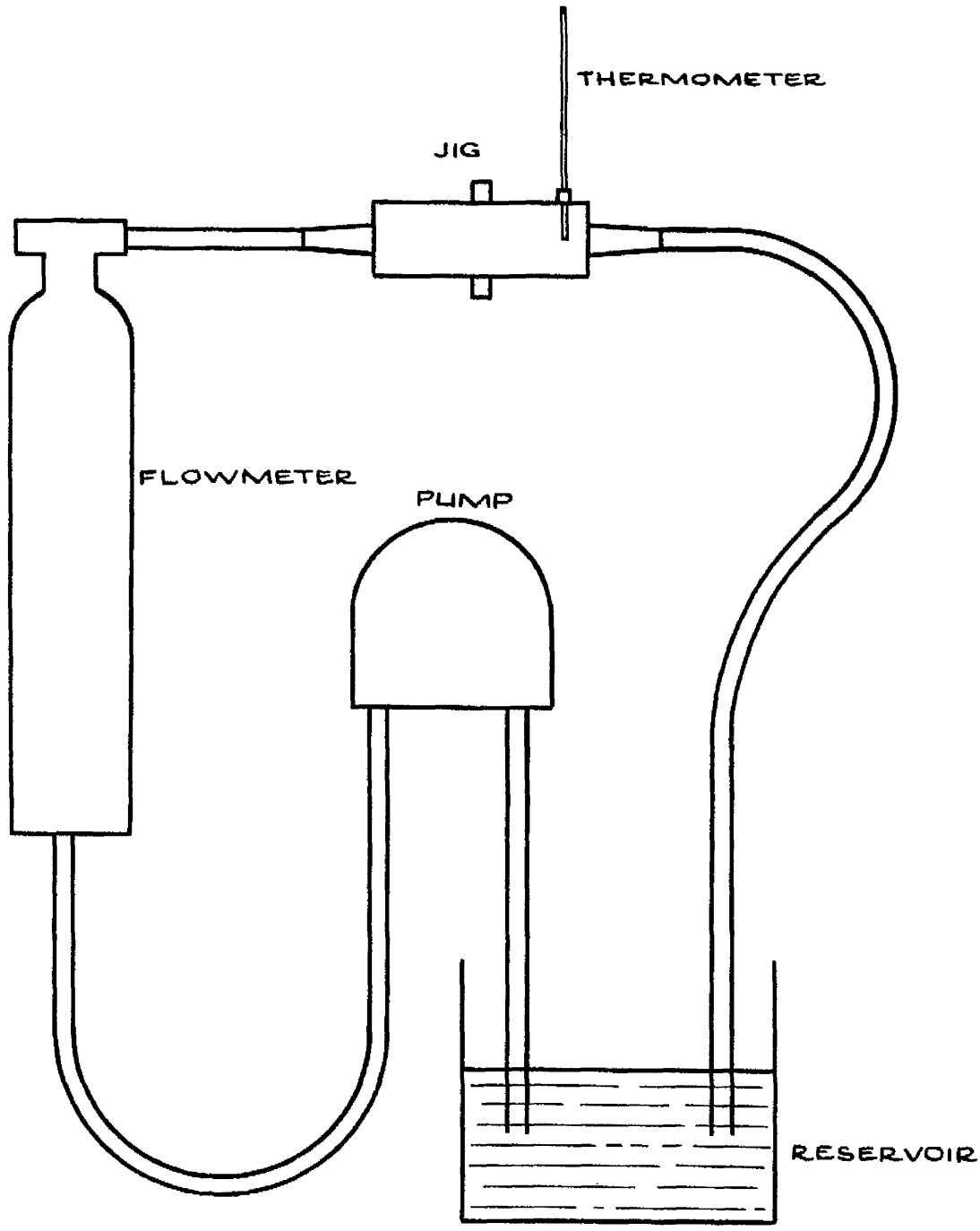

FIG. 5.2. SCHEMATIC DIAGRAM FOR POTENTIOSTAT FLOW SYSTEM

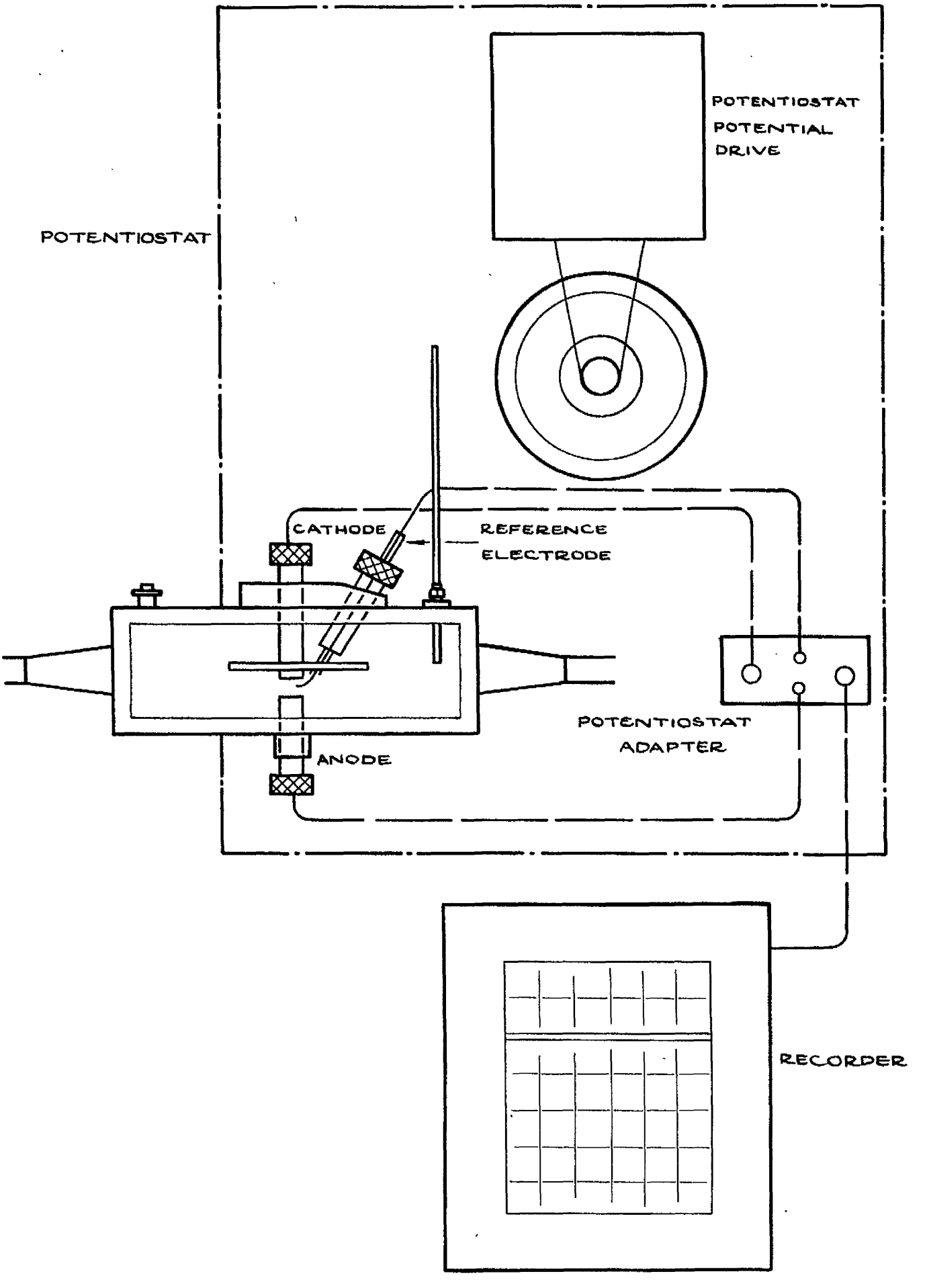

FIG. 5.3. SCHEMATIC DIAGRAM OF POTENTIOSTAT APPARATUS

flowmeter on the delivery line measured the flow rate. A thermometer graduated in ^{o}C was inserted in the cell.

5.4.2 Electrodes

The stainless steel cathode and anodes of diameter 0.43in were surface ground with "Lunis" grinding paper from grade "320" to grade "600". They were insulated along their lengths with "Laconit" varnish. The electrodes fitted into brass bushes. The assembly was screwed vertically into perspex mountings in the flow chamber. Rubber seals in each mounting prevented leaking.

The reference electrode was a $\frac{1}{16}$in diameter silver rod coated with silver chloride. This was mounted in a glass tube, which fitted obliquely through the top of the cell, so that the electrode tip was $\frac{1}{16}$in from the anode surface.

Larsson[30] has shown that good results are obtained when the electrode gap is about $\frac{1}{8}$ to $\frac{1}{4}$in. Initial tests showed that consistent results were achieved when the electrode gap was $\frac{1}{8}$in. The electrodes could be adjusted in their mounts to give this gap.

5.4.3 Potentiostat

An "Amel" '555' 10A potentiostat was used. The instrument is equipped with a dial for manual adjustment of the anode potential between 0 and 5V. As it is important that this drive rate should be constant, a chain drive was fitted to the dial which gave automatic potential scanning at a constant rate of 250mV/min. Rates of this

order have been shown to give satisfactory results (Larsson[30]). An adapter was added to the potentiostat to allow direct plotting on a recorder of the anode current as a function of the potential.

The complete apparatus for the potentiostat work is shown in Fig.5.3.

5.4.4 Solutions and anodes

Distilled water was used for all solutions. Four electrolytes have been investigated: 20% NaCl (to study further the effects reported in the previous chapter), 5% HCl and 5% H_2SO_4, (electrolytes frequently used in electrochemical drilling) and 5% H_3PO_4 (ortho phosphoric acid)(which at low current densities - 2A/in^2 - has been observed to give a good finish with copper[4]).

Anode materials were nickel, aluminium, nimonic 75, copper, cast iron and mild steel.

5.5. Procedure

The prepared anode specimen was mounted in the cell and the solution poured into the electrolyte tank. The appropriate connections were then made between the electrodes and the potentiostat.

The pump was switched on and its speed adjusted to give the required flow rate. To achieve a constant flow rate for all the electrolytes the volume flow rate for each electrolyte was adjusted to compensate for the different densities.

The initial temperature and flow rate were then noted. The recorder drive, the potential drive for the potentiostat and the

cell voltage were switched on and the current density-anode potential curve plotted.

At the end of each test the potential drive cut out automatically, and the cell voltage and recorder drive were switched off. The anode was then removed for examination.

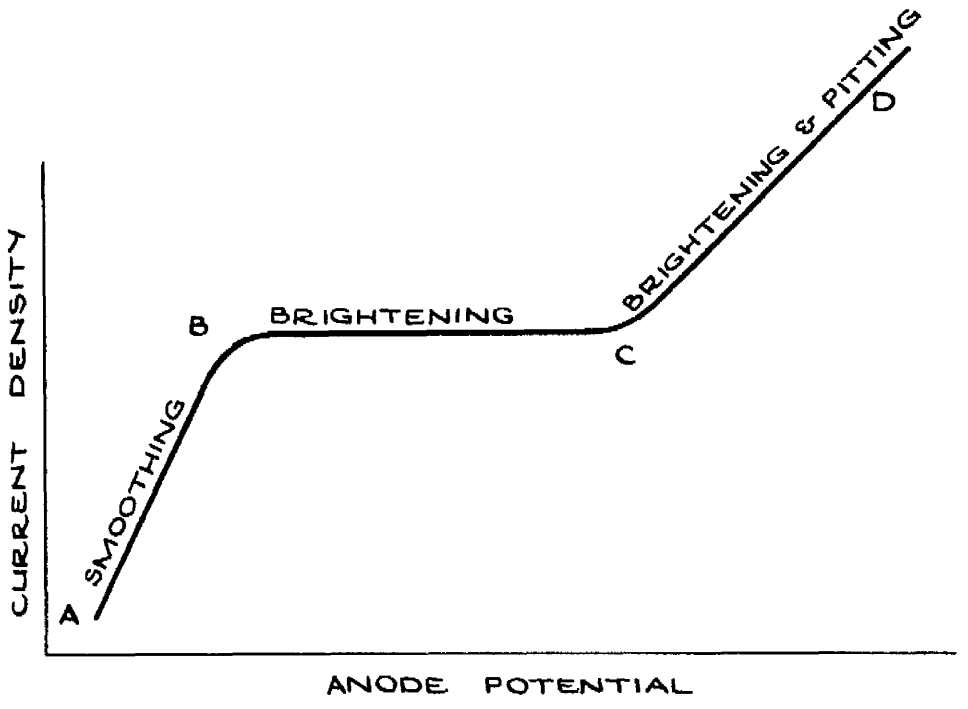

FIG. 5.1. CHARACTERISTIC POLARISATION CURVE FOR ELECTROPOLISHING

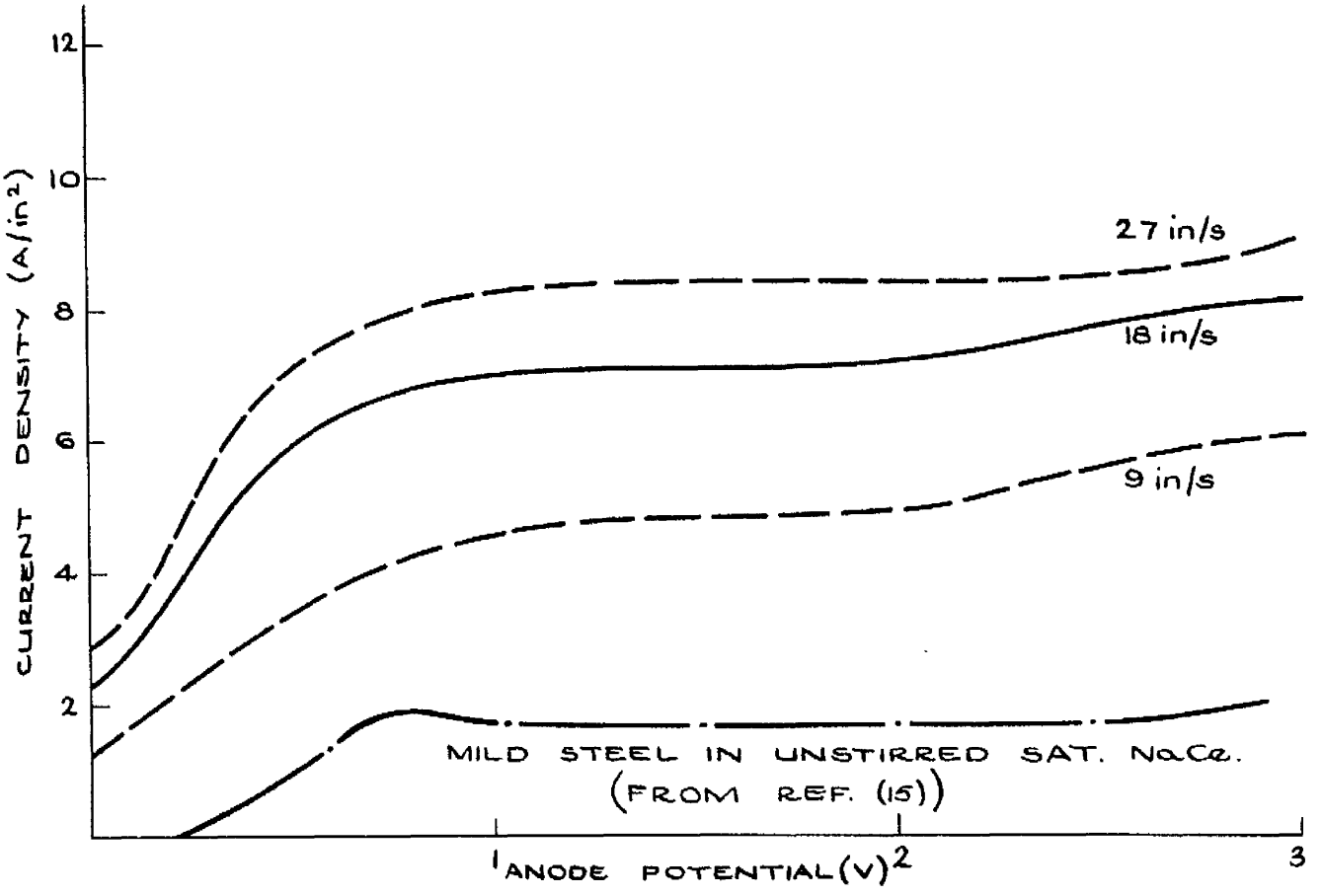

FIG. 5.4. TYPICAL POLARISATION CURVES FOR MILD STEEL IN 5% HCe - EFFECT OF ELECTROLYTE VELOCITY

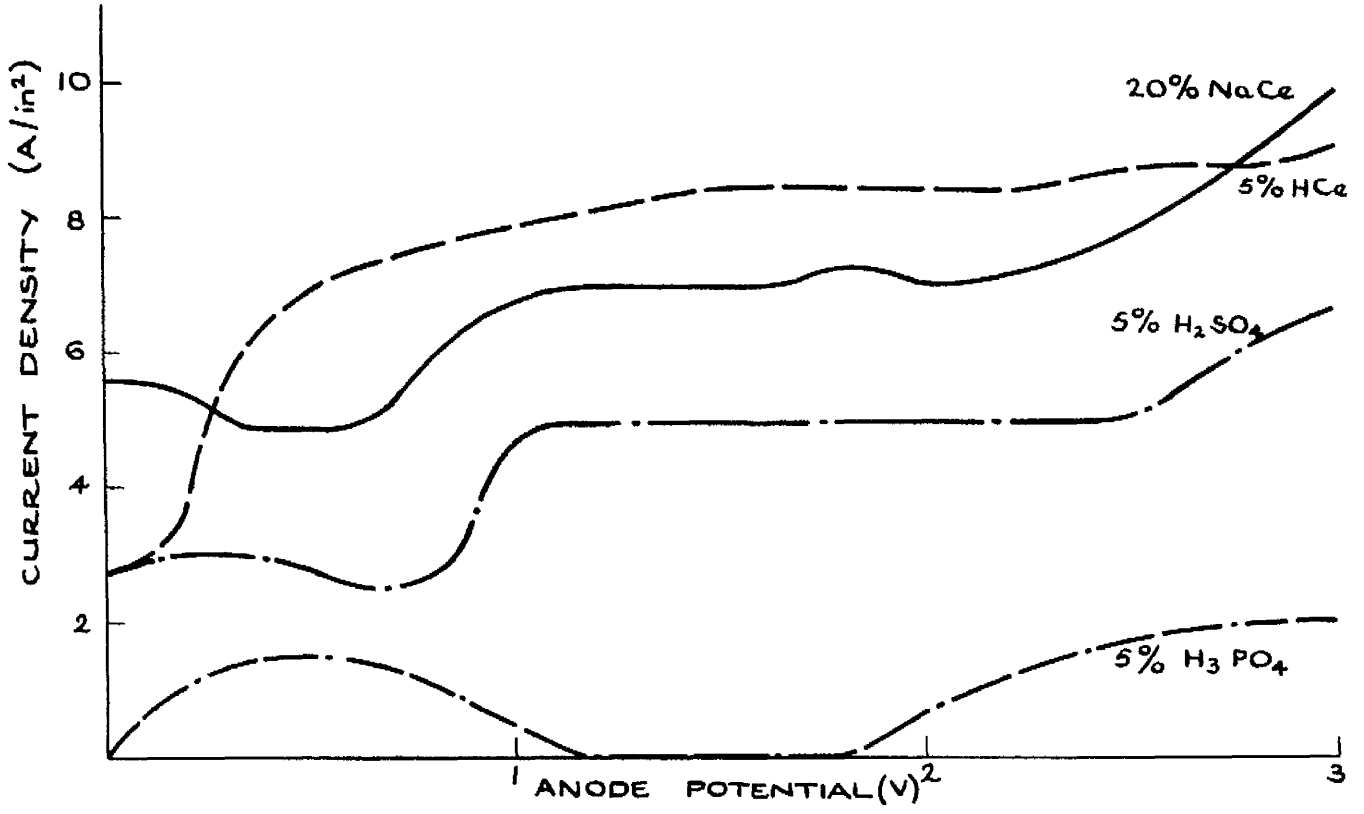

FIG. 5.5. POLARISATION CURVES FOR MILD STEEL IN 20% NaCe, 5% H_2SO_4, 5% HCe, 5% H_3PO_4

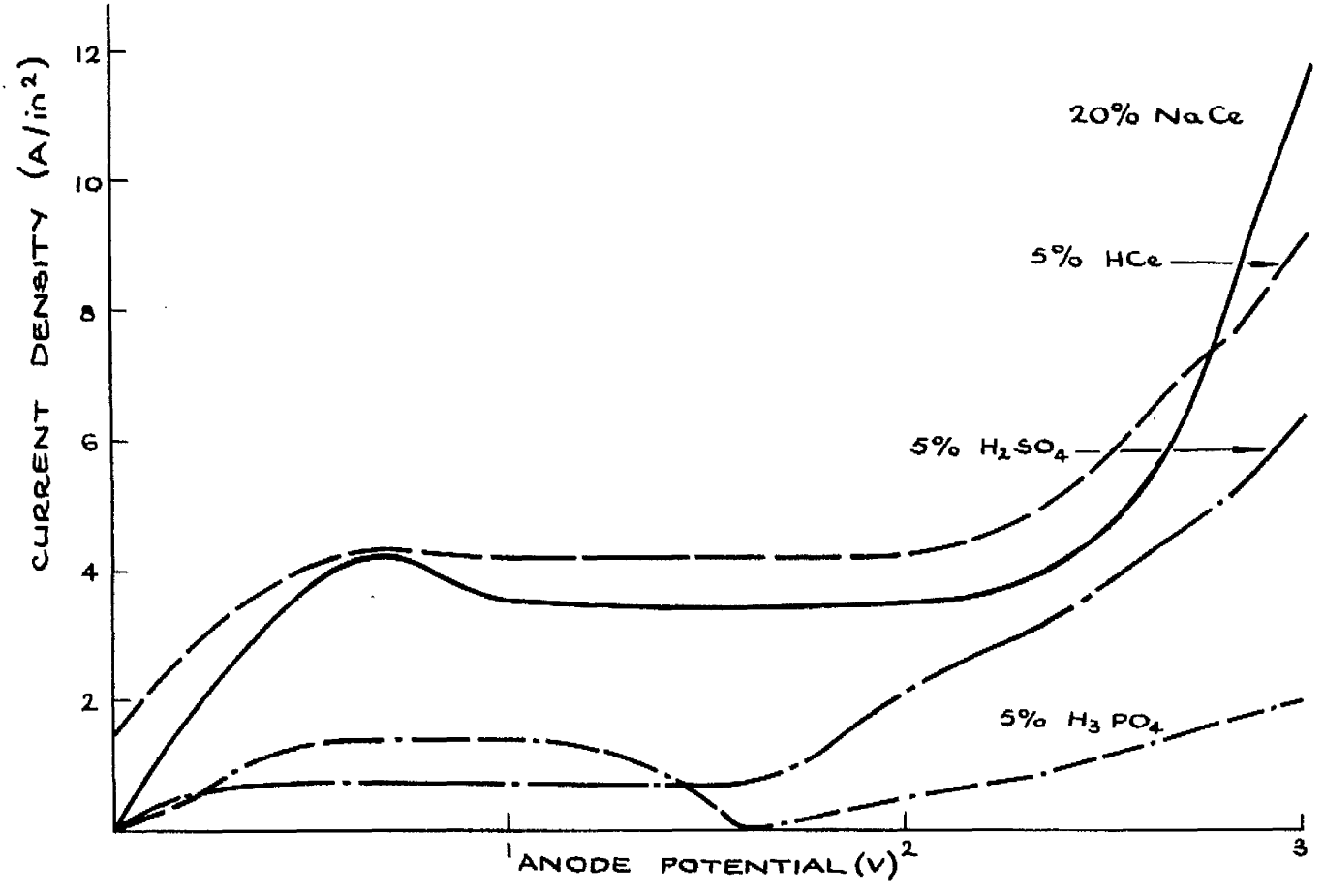

FIG. 5.6. POLARISATION CURVES FOR CAST IRON IN 20% NaCe, 5% H_2SO_4, 5% HCe, 5% H_3PO_4

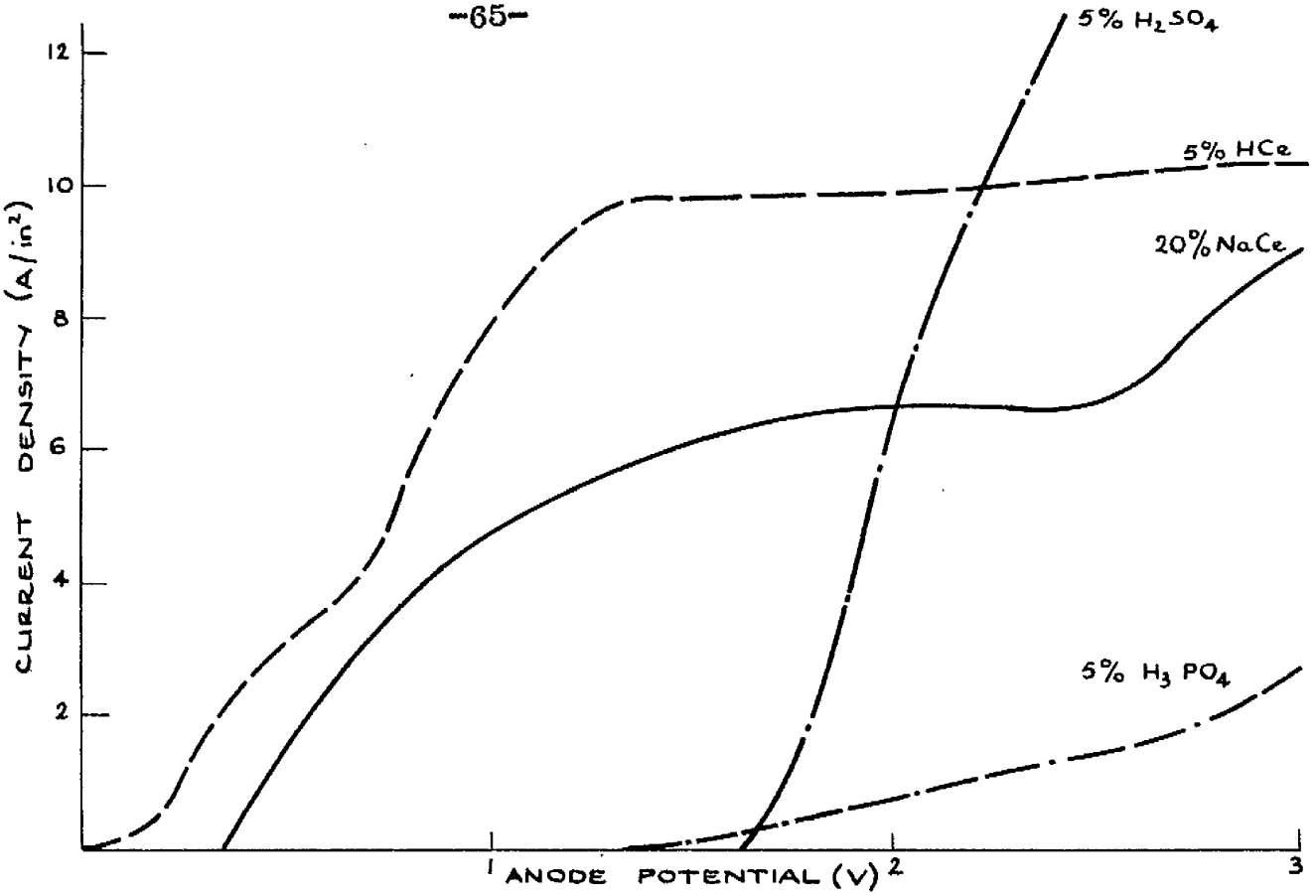

FIG. 5.7. POLARISATION CURVES FOR NICKEL IN 20% NaCe, 5% H_2SO_4, 5% HCe, 5% H_3PO_4

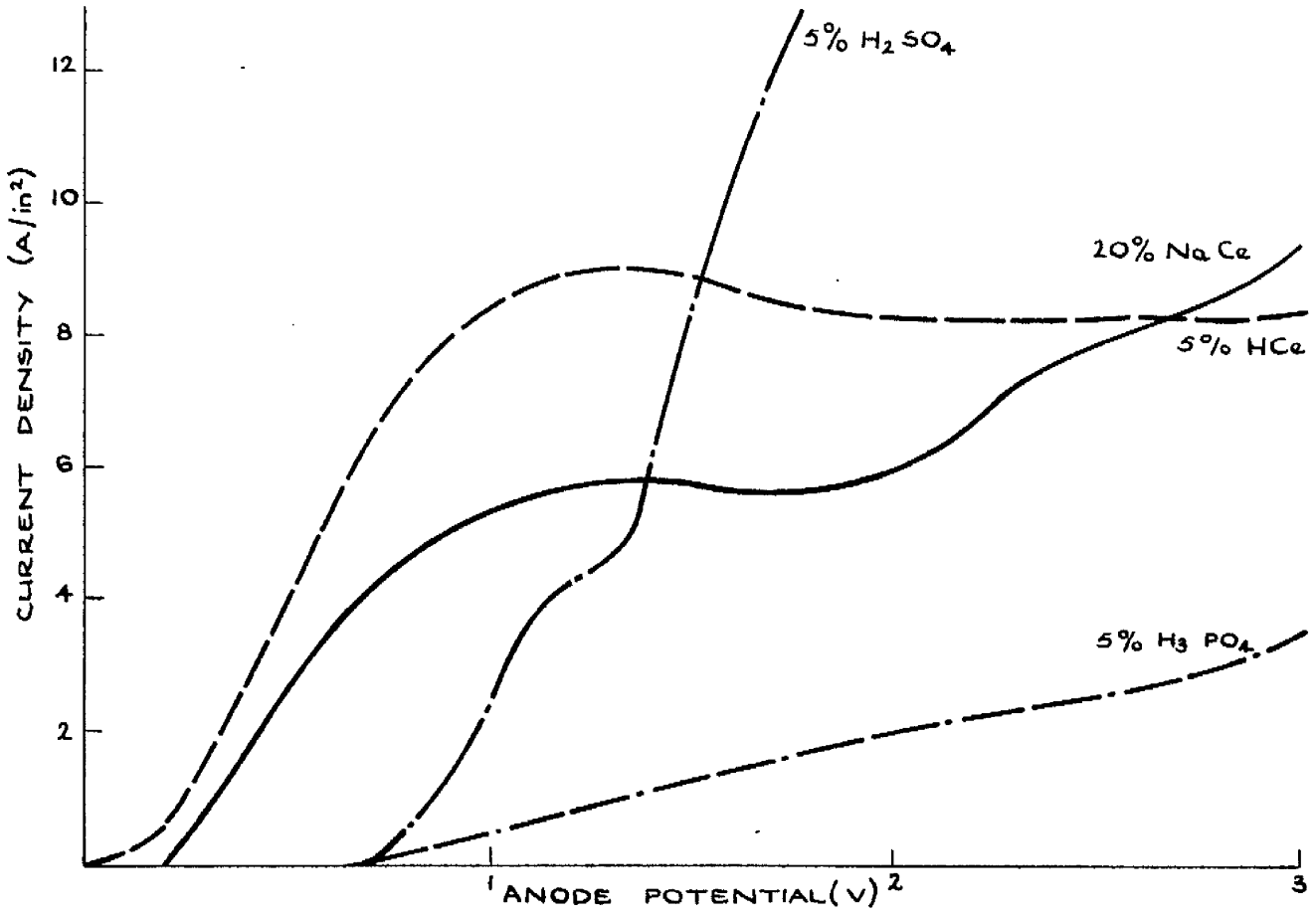

FIG. 5.8. POLARISATION CURVES FOR NIMONIC 75 IN 20% Na Ce, 5% H_2SO_4, 5% HCe, 5% H_3PO_4

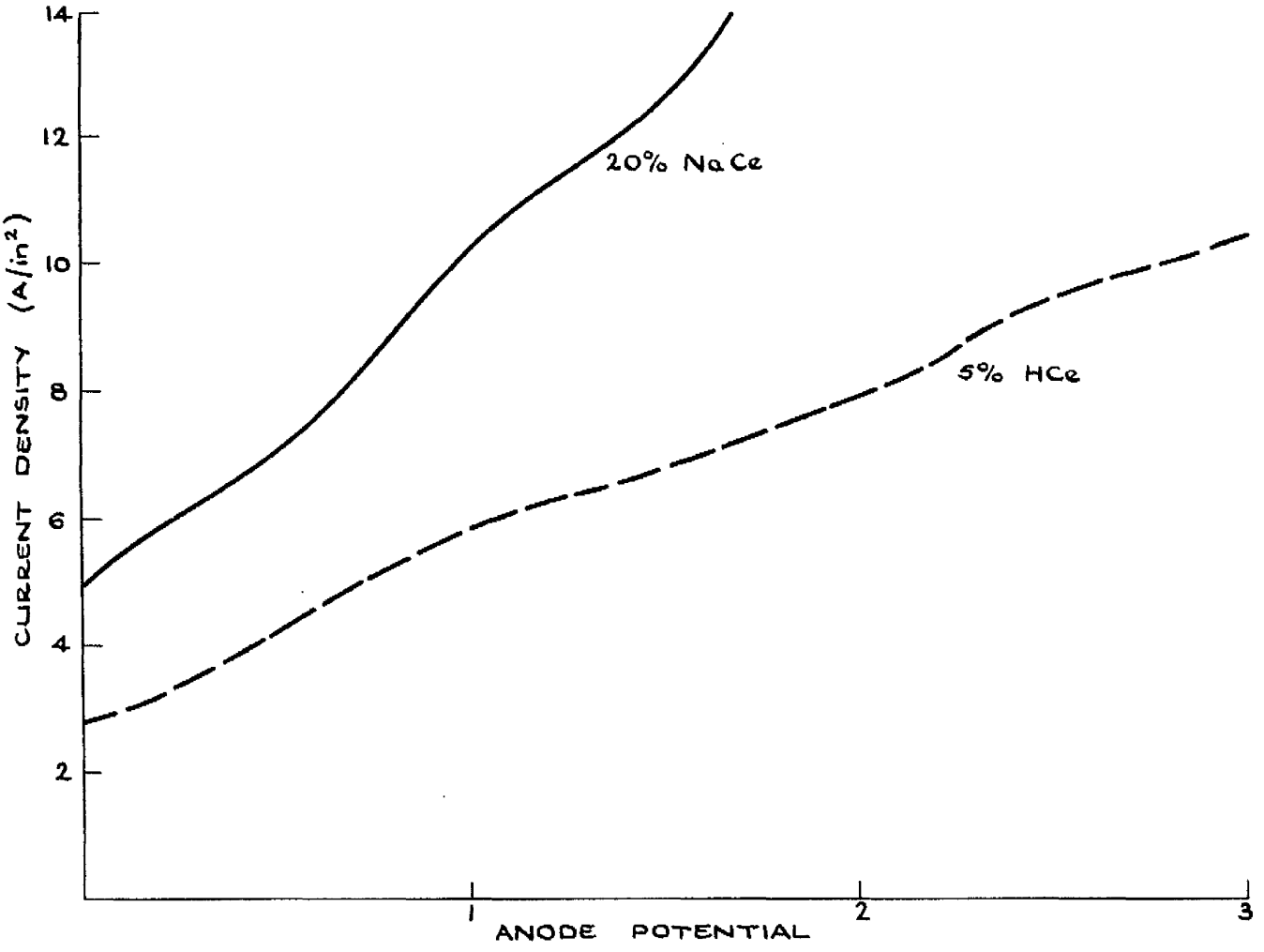

FIG.5.9. POLARISATION CURVES FOR ALUMINIUM IN 20% NaCe and 5% HCe

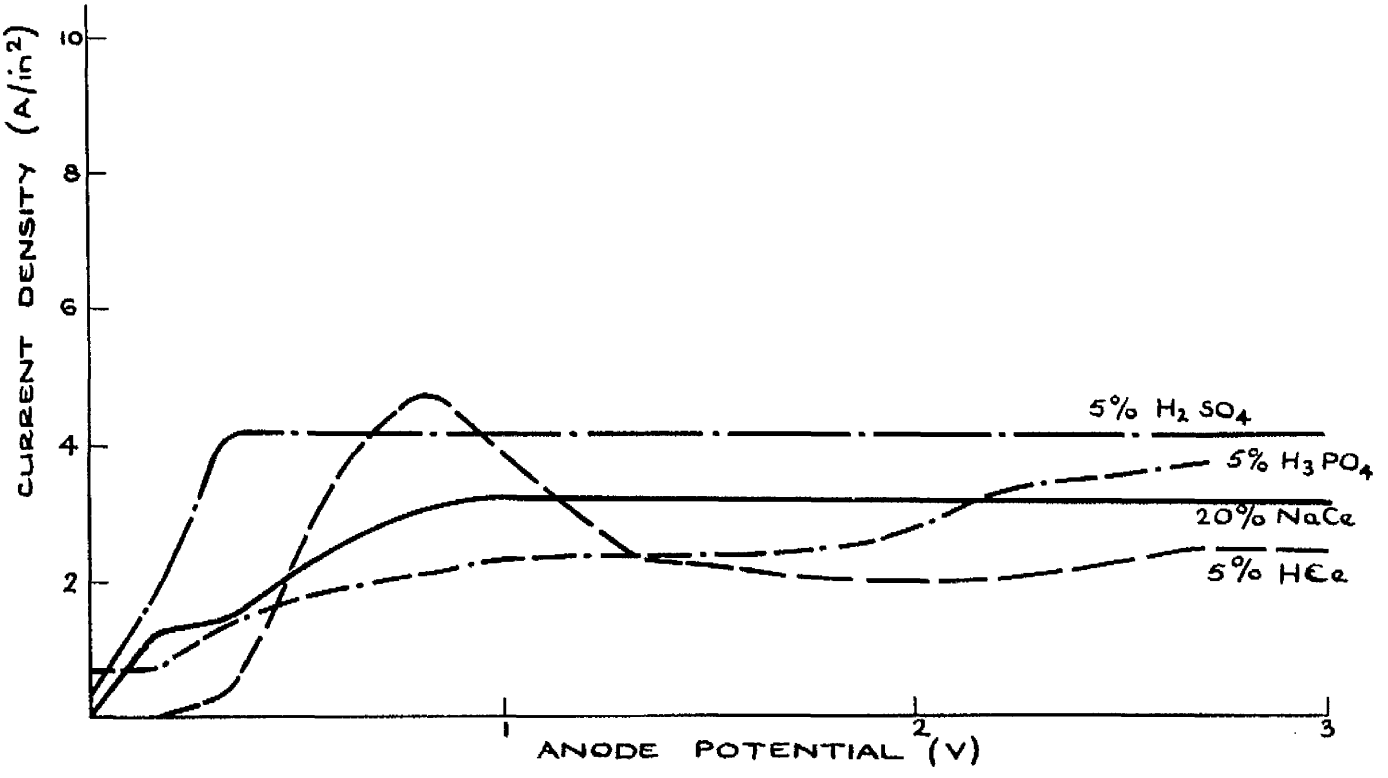

FIG.5.10. POLARISATION CURVES FOR COPPER IN 20% NaCe, 5% H_2SO_4, 5% HCe, 5% H_3PO_4

5.6 Results

Fig.5.4 shows the effects of electrolyte velocities from 9in/s on the polarisation curves for mild steel in 5% HCl. To compare these results with other typical results, the curve for mild steel in an unagitated solution of saturated NaCl is included. (from the paper by Cuthbertson and Turner[15]).

Figs.5.5 to 5.10 show typical polarisation curves for the metals, mild steel, cast iron, nickel, Nimonic 75, aluminium and copper respectively in two or more of the solutions 20% NaCl, 5% H_2SO_4, 5% HCl and 5% H_3PO_4. In these figures, only the effects of the highest flow rate - 27 in/s - are given.

(Note: the electrolyte velocities at the diameter have been used. Velocity $= \frac{Q}{hd}$ where Q is the observed volume flow rate, h is the electrode gap and d the electrode diameter).

5.7 Discussion

For metal/electrolyte combinations where plateau regions occurred - indicating that the reaction was diffusion controlled and that the particular electrolyte was suitable for E.C.M. - the limiting current density could be increased by increasing the electrolyte velocity. Fig.5.4 shows such behaviour for mild steel in 5% HCl. An increase of electrolyte velocity from 9 in/s to 27 in/s increases the current density from about 4.9 A/in^2 to about 8.4 A/in^2.

Cuthbertson and Turner[15] have recently reported a similar effect

for mild steel in saturated NaCℓ. At zero flow rate they observed a limiting current density of about 1.85A/in^2. This is indicated in Fig.5.4. By raising the flow rate to 24in/s they increased the limiting current density to about 5.8A/in^2.

Mild Steel

Fig.5.5 shows that plateau regions occur in 20% NaCℓ, 5% HCℓ and 5% H_2SO_4. In the last named solution the limiting current density is comparatively low. These solutions will then be suitable for the machining of the metal. As the potential is increased above about 2V, in each case the current density rises. Gas evolution and surface pitting are associated with this increase. When mild steel is electrochemically machined the anode potential is usually above 3V. From the potentiostat results surface pitting will then be expected. This effect has already been observed for mild steel machined in 20% NaCℓ (Chapter 4).

In 5% H_3PO_4, the current rises to a peak at about 0.3V then falls to nearly zero at about 1.2V. Dissolution recommences at about 1.7V. This is evidence of anodic passivation, which has been discussed in Chapter 4 for cast iron in 20% NaCℓ. It occurs when the normal metal dissolution process ($M = M^+ + e^-$) is replaced, or curbed, by the onset of another reaction (e.g. $2\,H_2O \rightleftharpoons O_2 + 4H^+ + e^-$). The efficiency of the process is then reduced.

Thus, from Fig.5.5 efficient machining is only possible to about 0.6V. From about 1.2 to 1.7V complete passivation is encountered,

and above 1.7V, partial passivation occurs. Under E.C.M. conditions dissolution at a low current efficiency will be expected.

Cast Iron

From Fig.5.6 the presence of plateau regions for current density for all four solutions indicates that the metal should machine satisfactorily in these electrolytes. Paradoxically, from Chapter 4, cast iron appears to partially passivate in 20% NaCℓ.

Comparison of the polarisation curves for mild steel (Fig.5.5) and cast iron shows that for cast iron the limiting current density values are lower for each electrolyte and that the rise in current density associated with gas evolution is steeper. Unlike the mild steel, the metal was always covered with a thick black film at the end of each test. Increase in flow rate had no effect on removing this film or on raising the current density.

If from an electrochemical viewpoint mild steel and cast iron are assumed to be pure iron, then anode reactions should be similar. The observation that the limiting current density is lower for cast iron in each electrolyte indicates that the reactions are not the same, and that for this metal partial passivation is occurring. Thus from Fig.5.6 efficient machining of cast iron in either NaCℓ or HCℓ solutions is only possible up to about 0.5V. Above this potential, partial passivation takes place with subsequent loss in efficiency. Above about 2V, the large slope suggests copious gas evolution and consequent extreme pitting. Low current efficiency together with a pitted surface

finish has been reported in Chapter 4 for cast iron electrochemically machined in 20% NaCl.

Nickel

Fig.5.7 shows a limiting current density in 20% NaCl, confirming the results reported in Chapter 4 that the solution is suitable for the machining of nickel. A plateau region is also obtained in 5% HCl, indicating that this is also a satisfactory electrolyte.

In 5% H_2SO_4 and 5% H_3PO_4 solutions, dissolution does not commence until the potential is above 1.5V. (Flow rate had negligible effect on altering this value). No limiting current density is obtained. (The film usually observed in the presence of the polishing action was absent). The surfaces obtained were dull in each test. Diffusion cannot therefore be the controlling mechanism. Thus, the potentiostate results indicate that the electrochemical machining of nickel in these electrolytes should be possible, but that a smooth, bright surface may not be obtained.

Nimonic 75

Fig.5.8 shows that similar results are also obtained for this metal: i.e. NaCl and HCl solutions are satisfactory; H_2SO_4 and H_3PO_4 solutions will give dissolution without polishing.

Aluminium

Fig.5.9 shows that in 20% NaCl and in 5% HCl dissolution occurs without any diffusion reaction. The finishes obtained were smooth and

etched. In Chapter 4 it was noted that similar finishes were obtained for aluminium electrochemically machined in 20% NaCl at current densities up to about 300 A/in^2. However at higher current densities, a cusped polished finish was obtained. This effect is not predicted by the potentiostat results which simply indicate anodic dissolution is possible.

The polishing in 20% NaCl may be due to the high current density conditions of E.C.M. Cole and Hopenfeld[14] have also found that aluminium can be polished if the current density is sufficiently high (above about 200 A/in^2). They suggest that in E.C.M. anodic products form a viscous layer at the anode. At low current densities (hence low machining rates) they show that ion transfer rate depends on both the ion concentration and the resistance of the solution to the ion motion. If the metal crystal planes at the surface are differently orientated, there will be a variation in specific surface energies and thus a variation in metal ion concentrations at the surface. Non-uniform metal dissolution should then occur causing surface etching. At high current densities (and high machining rates) the ion transfer rate is shown to depend solely on the solution resistance. Metal dissolution will be independent of crystal orientation and will be uniform. Polishing will then be obtained.

This would explain the polishing of aluminium in NaCl solution. The cusped finish may be due to the disruption of the polishing layer by gas evolved at the anode.

In 5% H_2SO_4 and 5% H_3PO_4 no reaction occurred. This is possibly due to the formation of a passive oxide layer on the surface of the metal. These electrolytes will not be suitable for machining.

Copper

Except for 5% HCl solution plateau regions are obtained in the polarisation plots for all the solutions (Fig.5.10). The surfaces obtained were bright and smooth. In 20% NaCl, electrochemically machined copper produced a bright, but granular finish (Chapter 4). The former effect is predicted by the potentiostat results; the granular finish is possibly a result of grain boundary attack due to the high current density conditions of E.C.M.

From Fig.5.10, it appears that efficient machining in 5% HCl is only possible up to about 0.8V; above this voltage, partial passivation occurs. Thus the potentiostat results predict that satisfactory machining is not possible with this electrolyte.

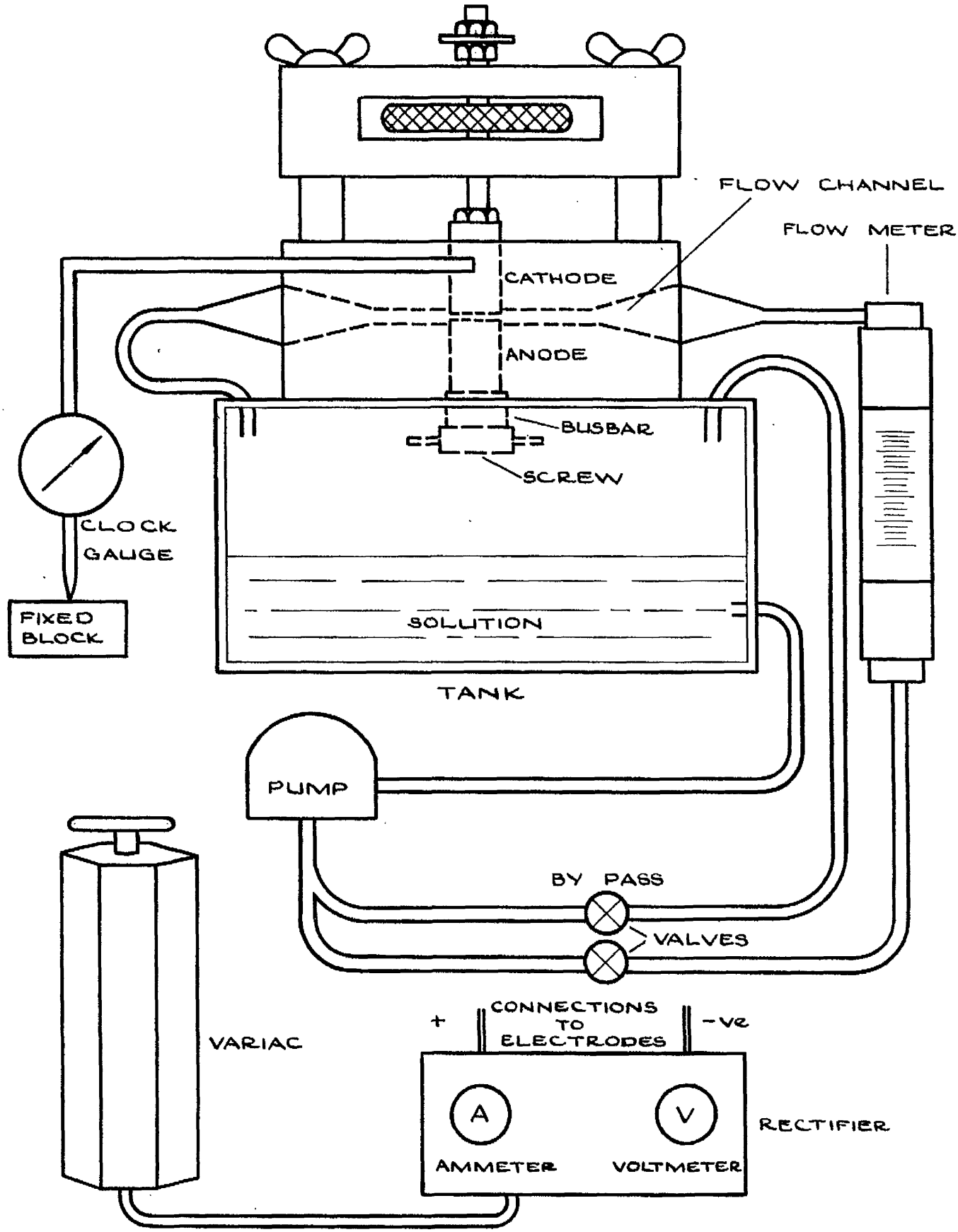

FIG. 5.11. RIG FOR E.C.M. TESTS ASSOCIATED WITH POTENTIOSTAT WORK.

5.8 Machining tests

5.8.1 Introduction

For 20% NaCl solution the predictions concerning electrolyte suitability from the potentiostat experiments show good agreement with the results of the machining tests reported in Chapter 4.

To investigate the validity of the predictions for the other solutions, further machining tests were carried out, using the small rig shown in Fig.5.11.

5.8.2 Apparatus

A perspex tank was filled with about 2 gallons of each electrolyte. A fixed speed centrifugal pump, capable of flows up to 9 in^3/s was used to circulate the solution between the electrodes from the tank. The flow rate, which could be varied by hand valve, was measured with a "Rotameter" flowmeter fitted in the delivery line. Electrolyte temperature in the tank was measured with a mercury thermometer.

Square electrodes of side 0.45 in were used. The anode was inserted in the flow box (the channel of which had the same width as the electrodes). The electrode was secured by a screw on the copper busbar. A stainless steel cathode was then placed in position. The electrode gap could be varied by adjustment of the cathode position. The movement of the cathode, and hence the gap width, were measured with a clock gauge.

The electrodes were fixed during machining. The gap thus increased with machining time.

Current was kept constant by adjustment of a variac in circuit with a 50A rectifier. Current and voltage were measured with a 25A ammeter and 20V voltmeter respectively. Machining times were taken with a stop watch.

5.8.3 Procedure

The electrolyte was poured into the tank. A weighed anode was fitted into the flow box, and the cathode position adjusted for a gap of 0.030 in. The pump was switched on, and the valves adjusted to give a flow rate of 7 in^3/s. (As with the procedure for the potentiostat (5.5) the volume flow rate for each electrolyte was adjusted to compensate for the different densities). The electrolyte temperature was noted. The power was then switched on, and the variac adjusted to give 10A. During machining the valves were adjusted to maintain a constant flow rate. After 5 min., the current and pump were switched off and the anode removed for examination and reweighing.

The procedure was repeated for each metal and electrolyte.

5.8.4 Results

Tables 5.1, 5.2, 5.3 show the comparison of the potentiostat results and predictions, and the results of the machining tests for the above metals in the (respective) solutions, 5% HCℓ, 5% H_2SO_4, 5% H_3PO_4.

5.8.5 Discussion

With the exception of copper and aluminium, tables 5.1, 5.2 and 5.3 confirm that when the potentiostat results show a diffusion reaction

Machining Tests

Metal	Potentiostat results and predictions	Current Efficiency %	Surface Finish	Comments
Mild Steel	Diffusion reaction Satisfactory electrolyte Smooth finish	104	Bright Smooth	
Cast Iron	Diffusion reaction Partial passivation Low current efficiency Poor finish	45	Dull grey Coarse Badly pitted	Surface covered with thick black layer
Nickel	Diffusion reaction Satisfactory electrolyte Smooth finish	94	Bright Smooth	
Nimonic 75	Diffusion reaction Satisfactory electrolyte Smooth finish	89	Bright Smooth	
Copper	Diffusion reaction Partial passivation above 0.8V Very low current densities	No machining possible		Unsatisfactory electrolyte
Aluminium	Reaction not established Machining possible Etched finish	90	Dull grey Smooth etched	

Table 5.1: Comparison of potentiostat and machining results for 5% NaCl

Metal	Potentiostat results and predictions	Machining Tests: Current Efficiency %	Surface Finish	Comments
Mild Steel	Diffusion Reaction Comparatively low limiting current density	48	Dull grey Matt	
Cast Iron	Diffusion reaction Partial passivation Low current efficiency and poor finish	45	Dull grey Coarse	
Nickel	Reaction not established Machining possible	66	Matt Grey	
Nimonic 75	Reaction not established Machining possible	56	Dull grey Coarse	
Copper	Diffusion reaction Satisfactory electrolyte Bright finish	100 (divalent) (reaction)	Bright Surface deeply grooved	Grooving possibly due to flow and c.d. conditions at [illegible]
Aluminium	No reaction Unsatisfactory electrolyte	No machining possible		

Table 5.2: Comparison of potentiostat and machining results for 5% H_2SO_4 solution

Machining Tests

Metal	Potentiostat results and predictions	Current Efficiency %	Surface Finish	Comments
Mild Steel	Diffusion reaction Partial passivation Low current efficiency	47	Black finish Smooth	Black film on surface - indicative of partial passivation
Cast Iron	Diffusion reaction Partial passivation Low current efficiency	45	Dull grey Coarse	As above
Nickel	Reaction not established Machining possible (above 1.5V)	35	Bright	
Nimonic 75	As nickel	42	Dull grey Matt	
Copper	Diffusion reaction Satisfactory electrolyte Bright finish	100 (divalent) (reaction)	Bright Smooth	
Aluminium	No reaction Unsatisfactory electrolyte	No machining possible		Unsatisfactory electrolyte

Table 5.3: Comparison of potentiostat and machining tests for 5% H_3PO_4

with no passivation, in the corresponding machining a good surface finish and a high current efficiency are achieved.

For copper in 5% H_2SO_4 the potentiostat results indicate that satisfactory machining is possible. Whilst a current efficiency of 100% and a bright finish were obtained, the surface was deeply grooved (c.f. the granular texture for copper in 20% NaCℓ - Chapter 4). The effect is possibly due to a combination of E.C.M. conditions and the characteristics of the metal. It is probably caused by local conductivity variations along the electrode surface. There is no apparent reason though why this should only occur for copper.

For this metal in 5% HCℓ the potentiostat results indicate partial passivation above about 0.8V. Under machining conditions complete passivation is obtained: it was not possible to machine at current densities from 10 to 50 A/in^2 and voltages from 5 to 20V.

For combinations where partial passivation is obtained in the potentiostat work, the corresponding machining produces a non-bright finish and a low current efficiency (e.g. 45% for cast iron).

For groups where the reaction is not established (e.g. nickel in 5% H_2SO_4) a grey matt finish and intermediate current efficiency (e.g. about 66% - Ni in H_2SO_4) are generally obtained.
(Note: from Table 5.3 for nickel in 5% H_3PO_4 the surface finish is bright. There is no apparent reason for this; paradoxically, a dull grey finish is produced with Nimonic 75 (which contains about 72% Ni))

Aluminium in 5% HCl is the exception. Although the reaction is not established in the potentiostat experiments, a high current efficiency (90%) is achieved. The effect may be due to the affinity of chlorine for aluminium discussed in Chapter 4.

For aluminium in 5% H_2SO_4 and 5% H_3PO_4 no reaction occurred in either the potentiostat or the E.C.M. experiments. Complete passivation causes this effect. It may be due to the formation of a passive oxide skin on the metal's surface in these solutions. (see, for example, Mellor[24]).

5.9 Conclusions

1. Potentiostat studies for flowing electrolytes give a good indication of the results to be obtained under E.C.M. conditions.

2. In addition to the results from Chapter 4, the following satisfactory metal/electrolyte combinations have been established (i.e. high current efficiency and good surface finish): Mild steel, nickel, Nimonic 75 in 5% HCl, copper in 5% H_3PO_4.

3. Machining with the following combinations is also possible, but with less satisfactory results (i.e. lower current efficiency and/or a dull surface finish):
mild steel, nickel, Nimonic 75 in 5% H_2SO_4 and 5% H_3PO_4.

4. Cast iron partially passivates in 20% NaCl, 5% HCl, 5% H_2SO_4 and 5% H_3PO_4.

5. The dissolution of aluminium in 20% NaCl, 5% HCl, 5% H_2SO_4 and 5% H_3PO_4 is not diffusion controlled. However, the metal can be machined at high current efficiency in 20% NaCl and 5% HCl.

Chapter 6

Some Aspects of the Forming Process

6.1 Introduction

In electrochemical forming, the anode tends to assume the inverse shape of the cathode. For a given cathode feed rate and inter-electrode gap, it is necessary to know the time of machining required to produce a given shape.

A theory is developed below for a cathode with a single step, based on the well known simple analysis described by Kleiner[1], Foertmeyer[32], Bayer[23] and Tipton[16], in which it is assumed that (i) an Ohm's Law relationship applies across the gap and (ii) current travels only normally between the electrodes. This gives the height of step formed on an initially flat anode as a function of machining time, cathode feed rate and minimum gap width. The concept of the equilibrium gap is introduced, and the general theory is applied for a case where the initial minimum gap is equal to the equilibrium gap.

Using cathodes with steps of 0.028 in and 0.125 in, experiments have been carried out to test the sections of the theory which deal with shaping. For a flat cathode, the theory of the equilibrium gap has been tested. The equipotential distribution between the electrodes has also been investigated using electrode models on conducting paper.

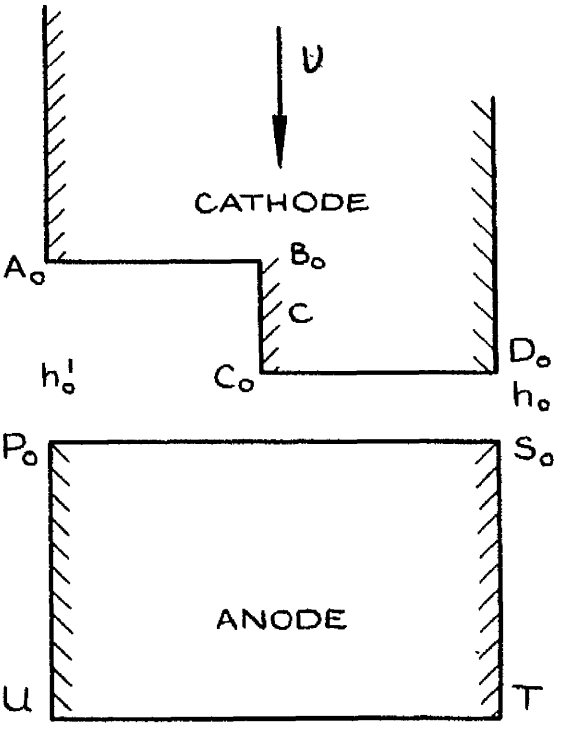

TIME $t = 0$

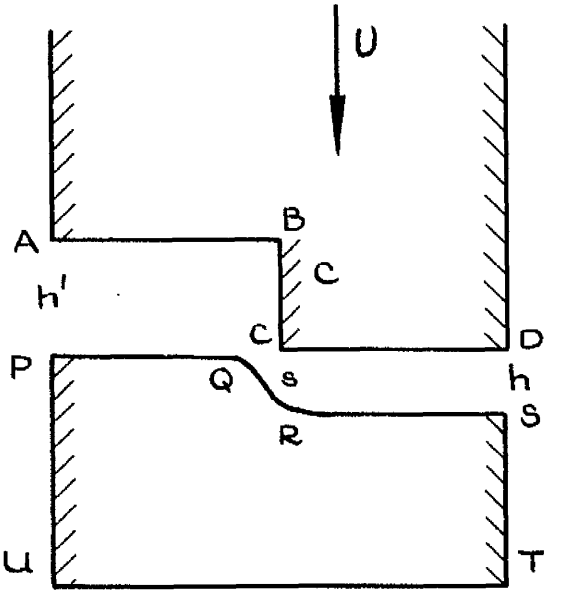

TIME t

FIG.6.1. ELECTRODE PROFILES: INITIALLY, AND AFTER TIME t.

6.2 Theory

Consider a cathode having a step of height c with an insulated surface as shown in Fig.6.1. Let the initial gap width be h_o between the initially flat anode surface P_oS_o and the surface CD of the cathode in its position C_oD_o. After time t, suppose that the cathode has advanced, at rate u to position ABCD, and that the anode surface is then defined by P'QRS. Let the gap between CD and RS be h, and let the step produced on the anode be of height s.

If 100% current efficiency is assumed, the rate of change of gap relative to the tool surface is given from Faraday's Law:

$$\frac{dh}{dt} = \frac{Ei}{F\rho} - U \qquad (6.1)$$

where E = chemical equivalent (g) of the anode, F = Faraday's Constant(C), ρ = anode density (g/in^3), U = cathode feed rate (in/s), i = current density (A/in^2).

Assuming no Joule heating, and no hydrogen effect, (see Chapter 7), Ohm's Law gives:

$$i = \frac{(V - V_o)K}{h} \qquad (6.2)$$

where V = applied voltage, V_o = decomposition voltage (assumed constant), K = conductivity ($\Omega^{-1}in^{-1}$), h = gap width (in)

$$\therefore \quad \frac{dh}{dt} = \frac{\beta}{h} - U \qquad (6.3)$$

where $\beta = \frac{E(V - V_o)K}{F\rho}$, an operating parameter which is determined by

the electrolyte conductivity the anode characteristics and the applied voltage.

If the current travels only normally between the electrodes (i.e. no stray current effects), the time taken for the gap between surfaces CD and RS to grow from h_o to h, (and for the gap between AB and PQ to grow from (h_o+c) to $(h+c-s)$ is

$$t = \int_{h_o}^{h} \frac{h\,dh}{\beta - Uh} = \int_{h_o+c}^{h+c-s} \left(\frac{h\,dh}{\beta - Uh}\right) \tag{6.4}$$

Case 1: Zero cathode feed rate, $U=0$

(6.4) becomes

$$t = \int_{h_o}^{h} \frac{h\,dh}{\beta} = \int_{h_o+c}^{h+c-s} \frac{h\,dh}{\beta} \tag{6.5}$$

$$= \frac{1}{2\beta}(h^2-h_o^2) = \frac{1}{2\beta}\left\{(h+c-s)^2-(h_o+c)^2\right\} \tag{6.6}$$

It follows that

$$h^2 = h_o^2+2\beta t \tag{6.7}$$

and $$s^2-2s(h+c)+2c(h-h_o) = 0 \tag{6.8}$$

or $$s = (h+c)\pm\sqrt{\left\{(h+c)^2-(2hc-2h_oc)\right\}}$$

$$= \left[\left\{(h_o^2+2\beta t)^{\frac{1}{2}}+c\right\}-\sqrt{\left\{(h_o+c)^2+2\beta t\right\}}\right] \tag{6.9}$$

only the negative sign being applicable here.

Solution of (6.9) for large t

(6.9) can be written

$$s = \sqrt{2\beta t}\left\{\left(1 + \frac{h_o^2}{2\beta t}\right)^{\frac{1}{2}} + \frac{c}{\sqrt{2\beta t}} - \left(1 + \frac{(h_o+c)^2}{2\beta t}\right)^{\frac{1}{2}}\right\}$$

Expanding for large values of t gives:

$$s = c\left\{1 - \frac{2h_o+c}{2(2\beta t)^{\frac{1}{2}}}\right\} \qquad (6.10)$$

i.e. for large t, s approaches c.

Case 2: Constant cathode feed rate, U

From the first integral of equation (6.4):

$$t = \frac{1}{U}\left\{(h_o-h) + \frac{\beta}{U}\,\ell n\left(\frac{\beta - Uh_o}{\beta - Uh}\right)\right\} \qquad (6.11)$$

This is of the form $t = h + A + B\ell n\,(h-D)$ which is solvable for h for specified A,B,D, and t. A method for solution is outlined in Appendix 2.

Also, from (6.4):

$$t = \frac{1}{U}\left\{(h_o-h) + s + \frac{\beta}{U}\,\ell n\left(\frac{\beta - Uc - Uh_o}{\beta + Us - Uc - Uh}\right)\right\} \qquad (6.12)$$

The times t in (6.11) and (6.12 are the same, so:

$$(h - h_o) + \frac{\beta}{U}\ell n\left(\frac{\beta - Uh}{\beta - Uh_o}\right) = h - h_o - s + \frac{\beta}{U}\ell n\left(\frac{\beta + Us - Uc - Uh}{\beta - Uc - Uh_o}\right)$$

$$\text{i.e.} \quad s = \frac{\beta}{U} \ell n \left\{ \frac{(\beta + Us - Uc - Uh)\ (\beta - Uh_o)}{(\beta - Uc - Uh_o)\ (\beta - Uh)} \right\} \qquad (6.13)$$

This is of the form $s = P\ell nQ\,(R-s)$, and is solvable for s for specified P,Q,R, where Q and R involve h, which is given by (6.11).

Equilibrium Gap

For a constant feed rate U, and voltage V, the gap h tends to an equilibrium value h_e given by

$$h_e = \beta/U \qquad (6.14)$$

This follows from equation (6.3):

for $\beta/h > U$, and for initial conditions,

$$\frac{dh}{dt} \text{ is +ve, and } \frac{d^2h}{dt^2} = \frac{-\beta}{h^2}\left(\frac{\beta}{U} - h\right) < 0$$

h then increases asymptotically to a value which corresponds to $\frac{dh}{dt} = 0$

i.e. $h_e = \beta/U$

Similarly, for $\beta/h < U$, h decreases asymptotically to the value, $h_e = \beta/U$

From (6.11), h_e is only achieved after an infinite time; in effect, h values near h_e can be obtained after finite times.

Special case (1): $h \to h_e$ after short time t

In many applications of the process, values of U and h_o are chosen such that h approaches t after a very short time t.

In this case let $h = \tau h_e$ (where $\tau \geq 1$) and let $h_o = mh_e (m \geq \tau)$. Then for required t, from (6.11)

$$t = \frac{h_e}{U}\left\{ (m-\tau) + \ell n\left(\frac{m-1}{\tau-1}\right)\right\} \qquad (6.15)$$

Thus from defined t, h_e, m and τ, the required U can be found.

Special case (2): $h_o \gg h_e$

In other uses, the initial gap h_o is much greater than the equilibrium gap h_e.

In this case, from (6.11):

$$\ell n\left(\frac{h_o - h_e}{h - h_e}\right) = \ell n\left(\frac{h_o - h_e}{(h_o-h_e)-(h_o-h)}\right) \qquad (6.16)$$

$$= \ell n \frac{1}{\left(1 - \frac{h_o-h}{h_o-h_e}\right)}$$

$$= \left(\frac{h_o-h}{h_o-h_e}\right) - \frac{1}{2}\left(\frac{h_o-h}{h_o-h_e}\right)^2 + \frac{1}{3}\left(\frac{h_o-h}{h_o-h_e}\right)^3 + \ldots \qquad (6.17)$$

For the condition $h \simeq 0$ (h_o):

$$\ell n\left(\frac{h_o-h_e}{h-h_e}\right) \simeq \left(\frac{h_o-h}{h_o-h_e}\right) \qquad (6.18)$$

(6.11) then becomes:

$$t = \frac{1}{U}\left\{ (h_o-h) + h_e\left(\frac{h_o-h}{h_o-h_e}\right)\right\}$$

$$= \frac{1}{U}\left\{\frac{h_o(h_o-h)}{(h_o-h_e)}\right\} \qquad (6.19)$$

i.e. the gap width h, initially varies linearly with time t. Thus for given U, h_o, and h_e, the approximate time for $h \to h_e$ can be estimated.

Note: for $h \to h_e$, the term $'\ell n\left(\frac{\beta - Uh_o}{\beta - Uh}\right)' \to \ell n \infty$

$$\therefore \quad t \simeq \frac{1}{U}\left\{\frac{\beta}{U}\,\ell n\left(\frac{\beta - Uh_o}{\beta - Uh}\right)\right\}$$

This can be written:

$$(h - h_e) = (h_o - h_e)e^{-tU^2/\beta} \tag{6.20}$$

Thus $h \to h_e$ only after large t.

Special Case (3): Gap, h_o, constant during machining

In this case $h_o = h_e = \beta/U$ (6.21)

Expression for s, for constant h_o

In equation (6.4), using (6.21):

$$t = \int_{h_o+c}^{h_o+c-s} \frac{h\,dh}{\beta - Uh}$$

$$= \frac{1}{U}\left\{ s + \frac{\beta}{U}\,\ell n\left(\frac{1}{1 - s/c}\right)\right\} \tag{6.22}$$

Thus for given c, s can be found in terms of t.

6.3 Apparatus

The perspex jig shown in Fig.2.1 was again used with the Barmax machine. The mild steel anodes and brass cathodes were of side 1 in. Three cathodes were used. One was flat; the other two had vertical steps of 0.030 in and 0.125 in. respectively halfway along their lengths. To reduce side current travel the electrodes were insulated along their vertical sides with varnish.

For the experiments with stationary cathodes, a 20% NaCℓ electrolyte was used. For constant gap machining tests, the solution was changed to 8% NaCℓ. The only significant effect of this weaker solution is a lowering of the conductivity (from $0.195\Omega^{-1}cm^{-1}$ for 20% NaCℓ to $0.105\Omega^{-1}cm^{-1}$ for 8% NaCℓ at 18°C).

Thus with the same power supply which has a fixed voltage/current characteristic, the electrode gap can be reduced.

6.4 Experimental Technique and Procedure

6.4.1 Tests with stationary cathodes (U = 0)

(a) Initial gap width - determination: the initial gap width, of 0.030 in., was set by:

(i) winding down the cathode until it touched the anode.

(ii) noting the reading on a clock gauge which registered the travel of the cathode.

(iii) winding back the cathode 0.030 in.

(b) Gap width h, and step height s: See Fig.6.1. The head was wound

down until CD touched RS. The difference in the gauge readings plus h_o gave the final gap width, h.

The final gap width between AB and PQ, h^1, was given by $h^1 = h+c-s$. The step S was found by taking the average difference in anode heights PU and ST, measured at several places along the length with a micrometer.

Procedure

The gap width was set as above and the electrolyte circulated between the electrodes. To reduce the effects of temperature and hydrogen on conductivity (see Chapter 7) a high volume flow rate ($60 in^3/s$),(see Chapter 2) was used. For such conditions the Ohm's Law was assumed valid (Eqn.6.2). The electrolyte temperature at inlet was measured with a mercury thermometer.

A constant voltage was applied across the electrodes. The machining time t was measured with a stop watch. At the end of each test the voltage and flow were cut off, and the gap widths h and h^1, and step heights s measured.

The procedure was repeated for different machining times and for each cathode.

6.4.2 Tests with constant gap (h_o) and feed rate (U)

The modified Barmax control system (described in Appendix 1) was used to maintain a constant minimum gap h_o during machining. The controls were adjusted so that this gap was attained almost immediately after the start of machining.

Determination of feed rate U, final gap h^1, step s

The average feed rate U was found by dividing the difference in final and initial clock gauge readings by the time of machining.

The step s and gap h^1 were found as above ($h^1 = h_o + c - s_1$ since $h_o = h$).

Procedure

A procedure similar to (6.4.1) was used, except for the maintenance of the constant gap h_o during machining. With the cathode in its uppermost position the pump and voltage were switched on. The cathode was made to descend at a fast approach speed ($\frac{1}{2}$in/s) until the pre-set gap h_o was achieved. At this stage the stop watch was started.

At the end of each experiment the cathode was halted. The pump and voltage were then switched off. The gap h_o was checked. After removal of the specimen the step height s was measured.

The procedure was again repeated for different machining times and for each cathode.

6.5 Results

Table 6.1 gives, for fixed cathodes with steps of 0.028 in and 0.125 in and for initial gaps of 0.010 to 0.030 in the machining times required for the anode step s to approach 0.9c (from equation 6.10). For these times, the exact step size (calculated from equation 6.9) are tabulated.

Fig.6.2 shows for the fixed, 0.028 in. stepped cathode, and for an initial gap of 0.030 in., the comparison of the theoretical and experimental anode steps as functions of machining time.

C (in.)	h_o (in.)	t for $(s = 0.9c)_{approx.}$	S_{exact} (in.)
0.028	0.040	1270	0.0195
	0.030	840	.0195
	.020	500	0.0196
0.125	0.040	4560	0.0878
	.030	3720	0.0880
	.020	2960	0.088

Table 6.1: Dependence of machining time for $s \to 0.9c$ on initial gap width and cathode step size. (For these times, the exact s values, calculated from equation 6.9 are also given).

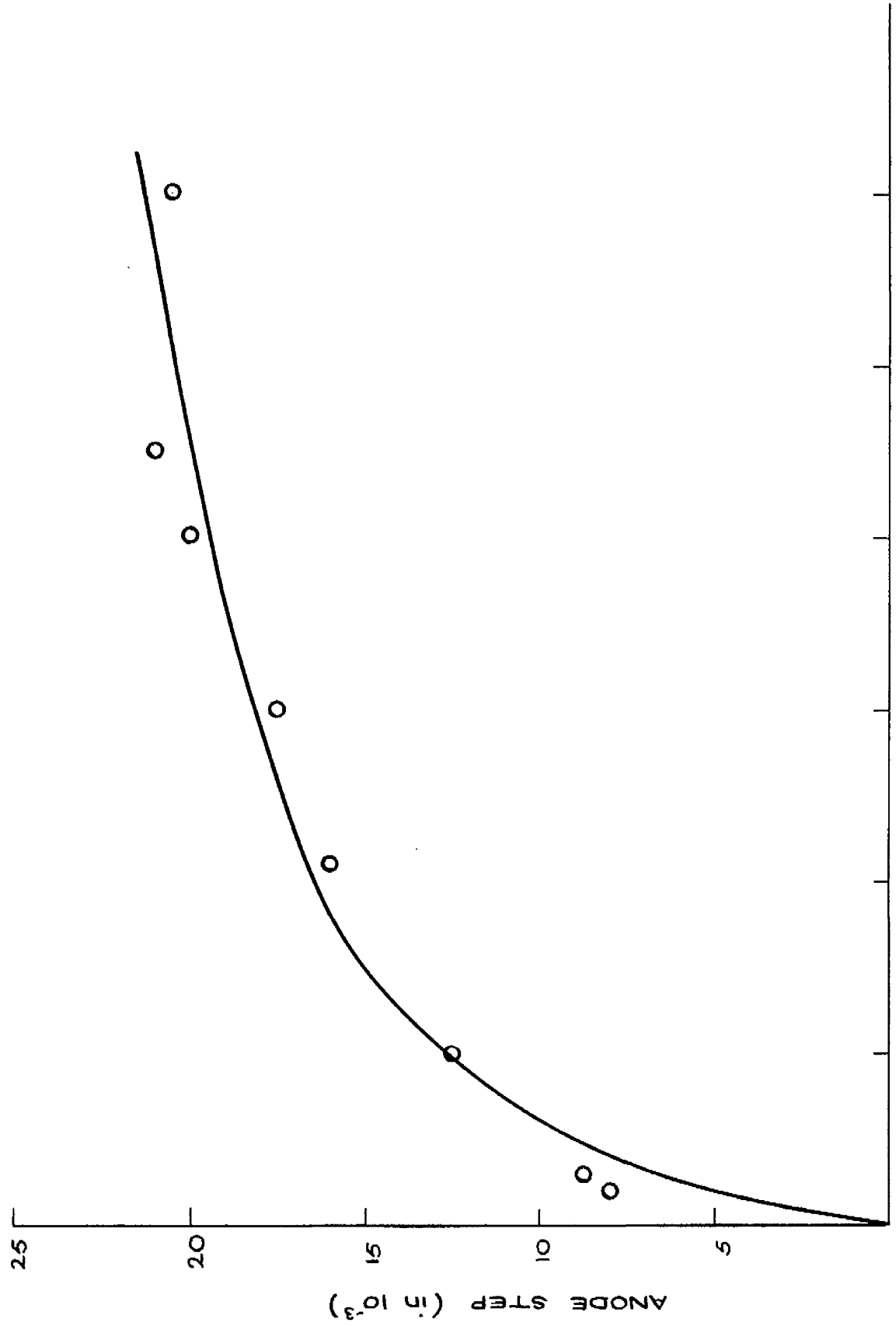

FIG. 6.2. ANODE STEP AS A FUNCTION OF MACHINING TIME.
(FIXED CATHODE WITH STEP 0·028 in)

Fig.6.3 shows, for a flat cathode with a fixed feed rate of 8.8×10^{-4} in/s, and for initial gap widths of 0.030, 0.060 and 0.098 in, the subsequent gap widths as functions of machining time. The theoretical relationships - gap width at the start of machining, as a linear function of time (equation 6.19) and final equilibrium gap width - are also indicated.

In Fig.6.4, for plane parallel electrodes, are compared the theoretical (from eqn.6.16) and experimental dependences of cathode feed rate on the equilibrium gap, for gaps from 0.010 in to 0.050 in.

Figs.6.5 and 6.6 give, for the 0.028 in and 0.125 in stepped cathodes respectively, the comparison of the theoretical (from eqn.6.22) and observed anode steps as functions of machining time and minimum equilibrium gap.

Fig.6.7 shows the initial equipotential distribution between the 0.028 in stepped cathode and a flat anode for minimum equilibrium gaps ranging from 0.010 in. to 0.042 in.

Fig.6.8 gives the equipotential distribution between the 0.028 in. stepped cathode and the anode, the latter having steps of 0.014 in. and 0.028 in. The equilibrium gaps h_o are 0.010 in. and 0.014 in. respectively.

(Note: four 1 ft. long brass plates were constructed so that when plated on conducting paper they simulated the electrodes in their machining positions. A scale of 1 in = 0.014 in. was used. This allowed the plotting of equipotentials for distances of 0.17 in. on either side

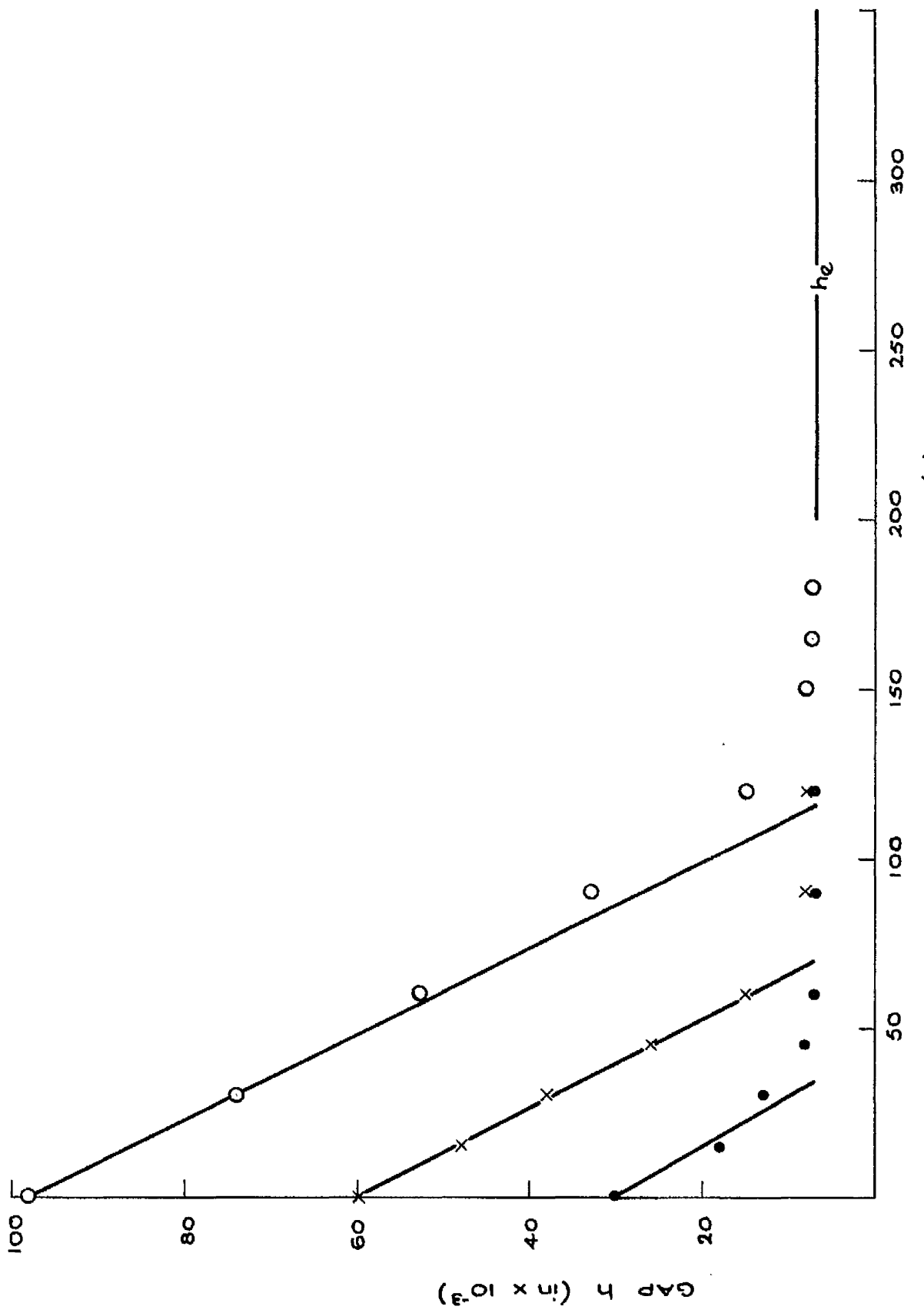

FIG.6.3. GAP WIDTH AS A FUNCTION OF MACHINING (CONSTANT CATHODE FEED RATE)

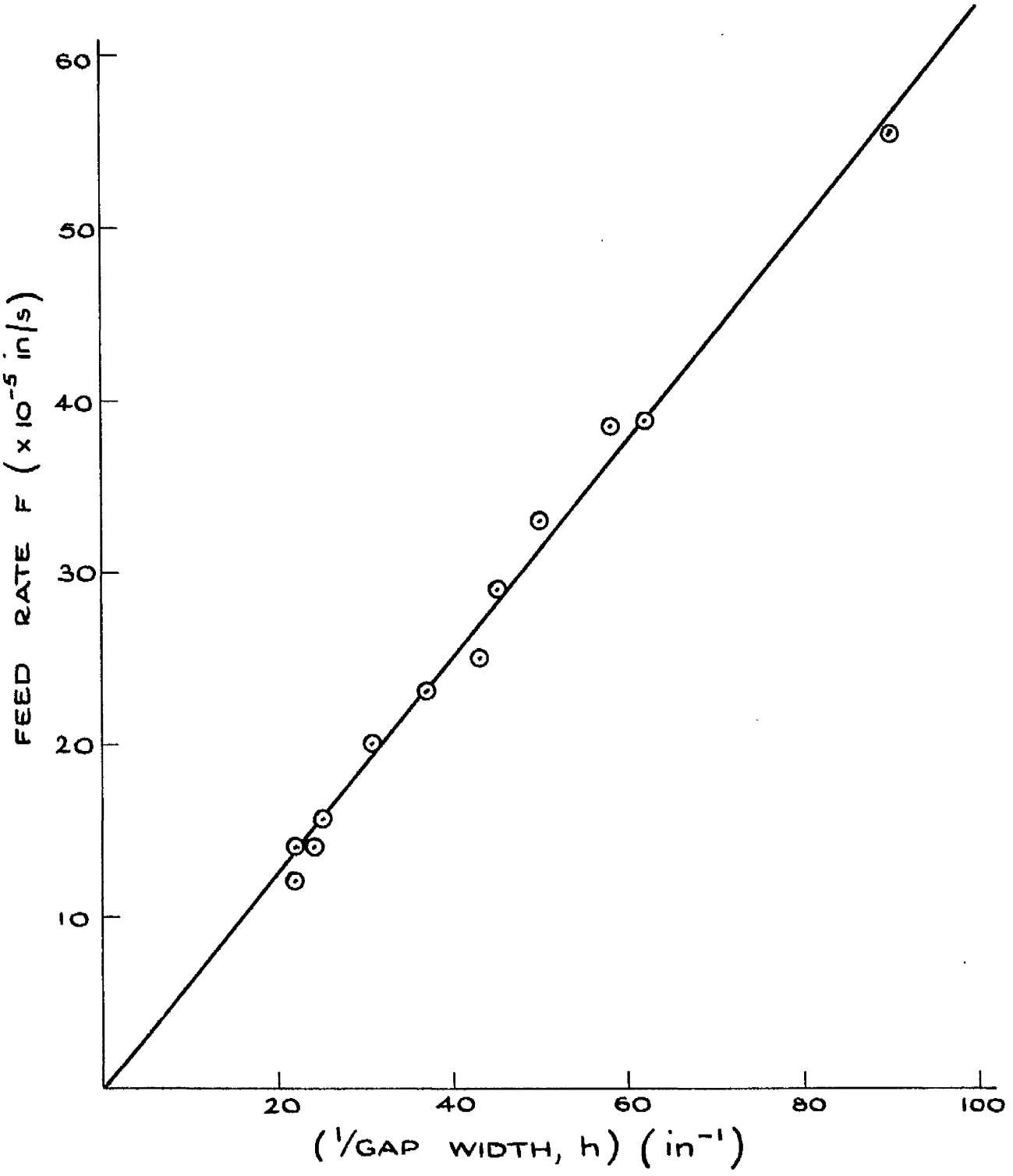

FIG. 6.4. FEED RATE AS A FUNCTION OF 1/(GAP WIDTH) (T = 18°C)

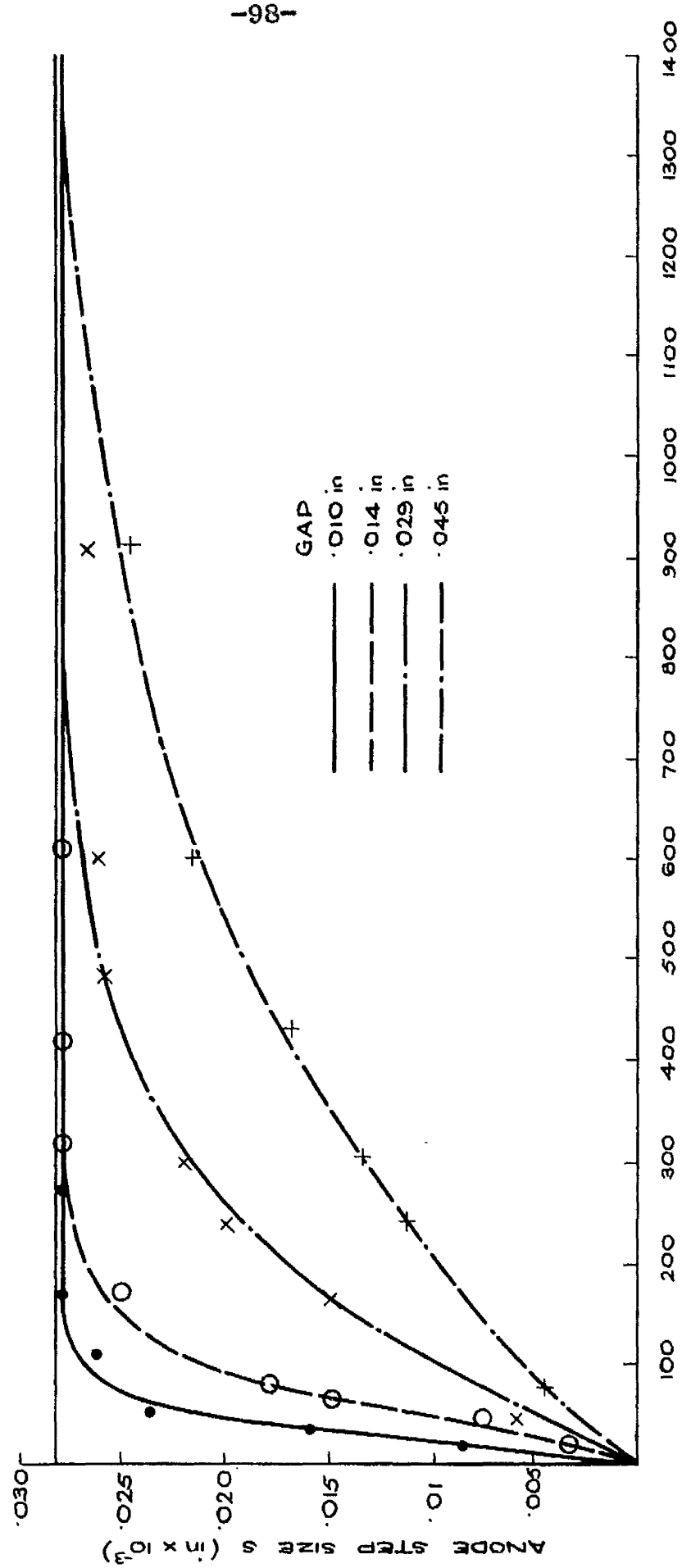

FIG. 6.5. ANODE STEP SIZE AS A FUNCTION OF GAP WIDTH AND MACHING TIME
(CATHODE STEP = 0·028 in)

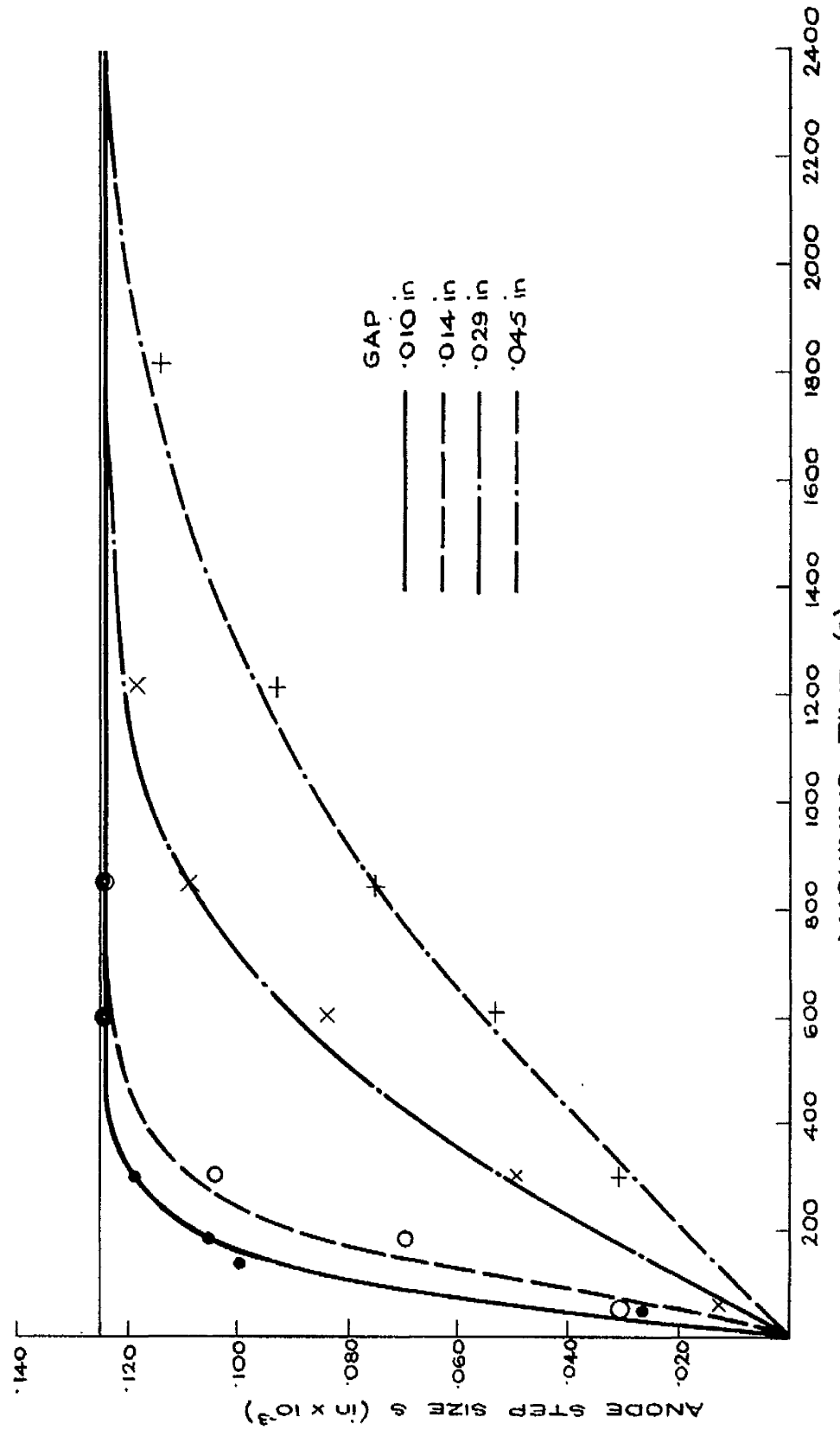

FIG. 6. 6. ANODE STEP AS A FUNCTION OF GAP WIDTH AND MACHINING TIME

(CATHODE STEP = 0·125 in)

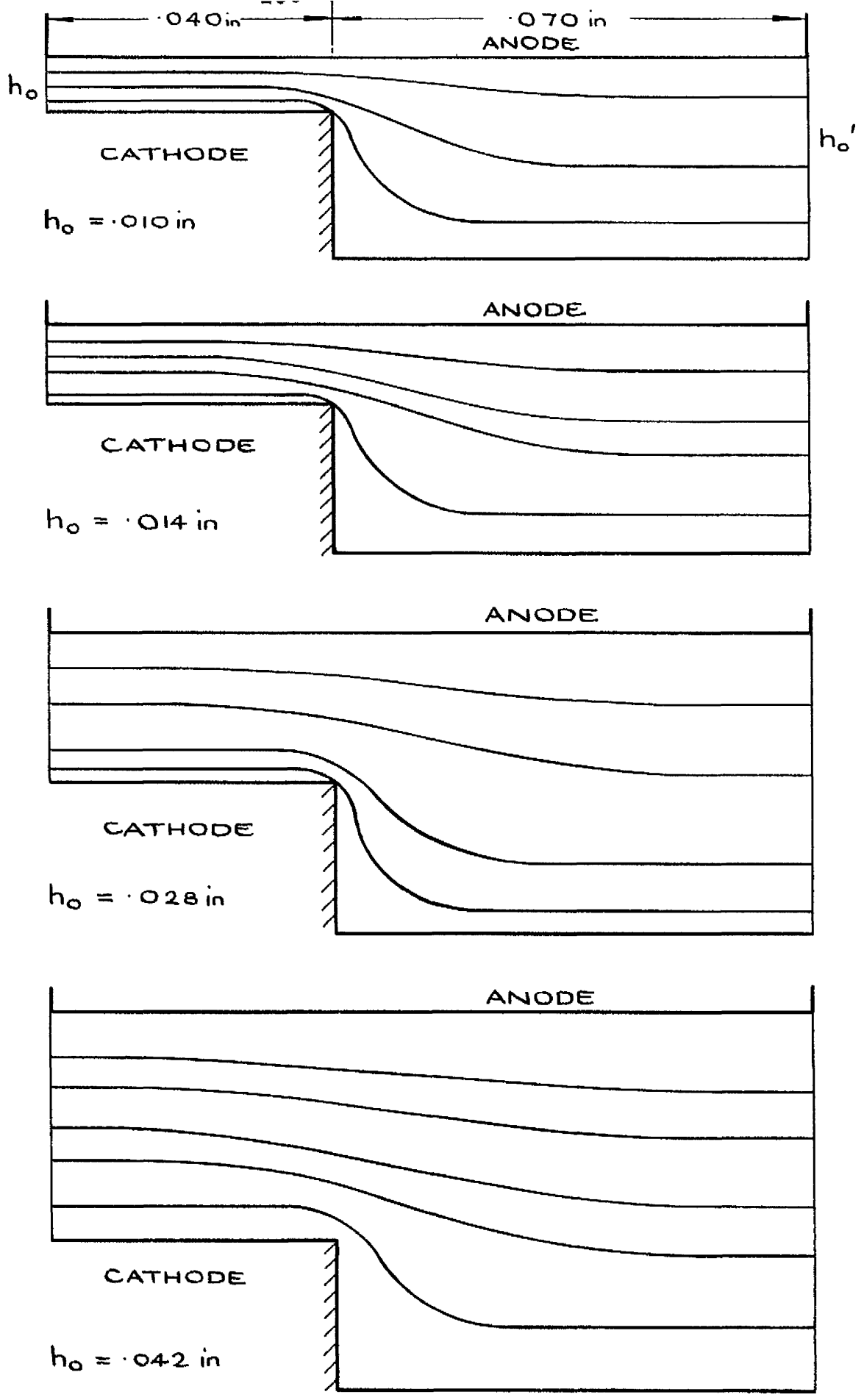

FIG. 6.7. INITIAL EQUIPOTENTIAL DISTRIBUTION FOR GAPS FROM ·010 in TO ·042 in (CATHODE STEP = ·028 in)

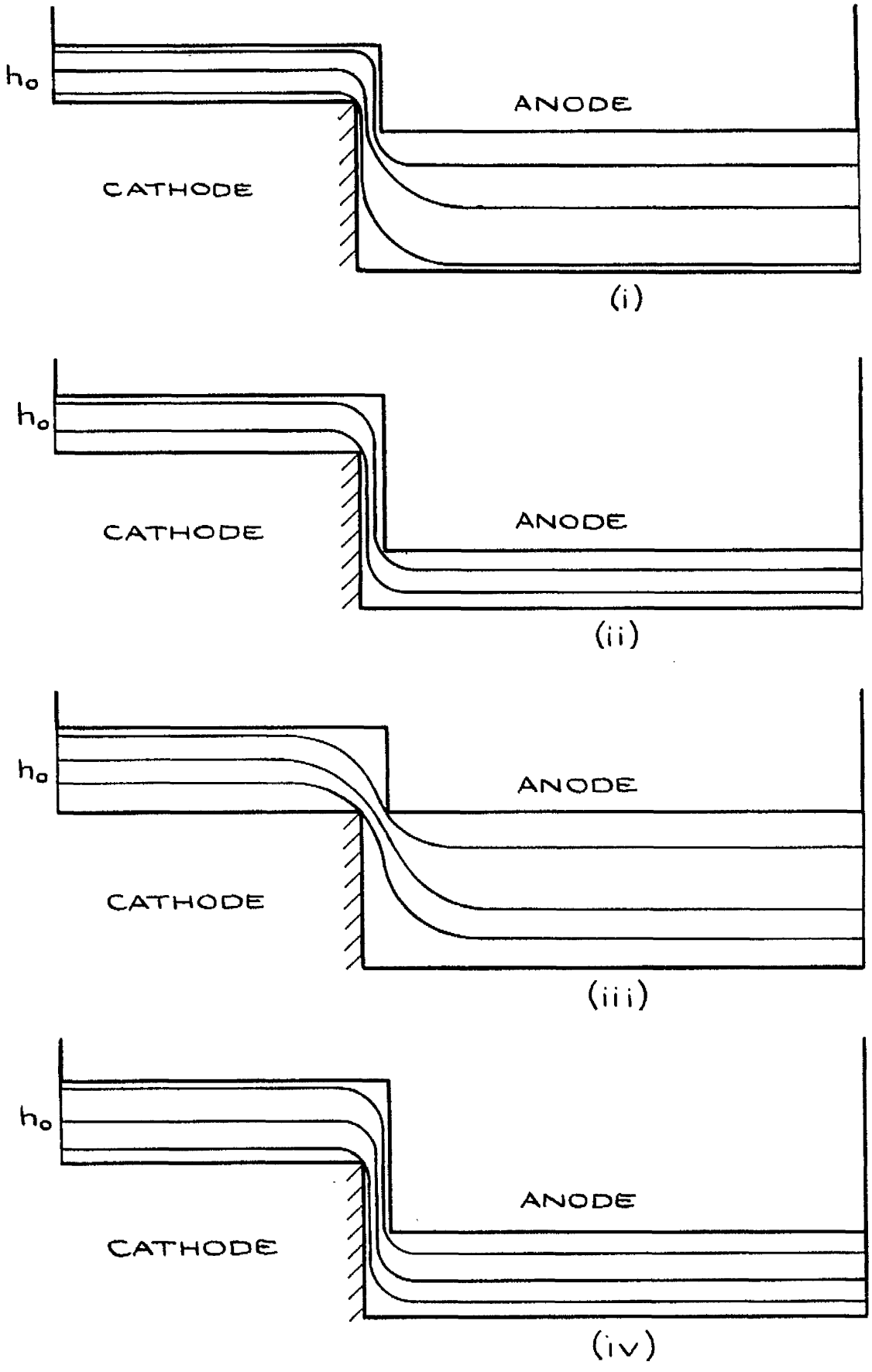

FIG. 6.8. EQUIPOTENTIAL DISTRIBUTION DURING MACHINING
(i) $S = \cdot 014$ in, (ii) $S = \cdot 028$ in ($h_o = \cdot 010$ in) (iii) $S = \cdot 014$ in, (iv) $S = \cdot 028$ in ($h_o = \cdot 014$ in)
(CATHODE STEP = $\cdot 028$ in)

of the cathode step. The reduced plots in Figs.6.7 and 6.8 indicate the equipotential for distances of 0.040 in and 0.070 in on either side of the line of cathode step. Beyond these limits the equipotentials were parallel).

6.6 Discussion

From Table 6.1, for a fixed cathode, the machining time required to achieve a given step decreases sharply as the initial gap is decreased. For the 0.125in stepped cathode the time for $s \to 0.9_0$ would be very long - 4560s. The machining times calculated for $s \to 0.9_c$ in equation (6.10) were substituted in equation (6.9) to calculate s. The fourth column shows that the exact values for s are smaller (about 0.7_c).

Fig.6.2 shows good agreement between experimental and theoretical anode step values as functions of machining time. However, sharp edges on the formed step were not obtained. The profile of the step became less distinct as the machining time (and hence gap width) increased. This was possibly due to a side current flow effect, not accounted for in the theory. It is discussed more fully below.

These observations indicate that to reduce the machining time and to increase the definition of the formed step gap control in forming is necessary.

Experiments to test the theory of the equilibrium gap were then performed. Fig.6.3 shows that for a flat cathode descending at a constant feed rate, and for the different initial gaps, the final gap always tends

to a limiting equilibrium value. The results also show that the nearer the initial gap width is to the equilibrium value, the shorter is the time required to achieve it. The experiments also prove that equation (6.19) is valid; i.e. for $h_o \neq h_e$, the subsequent gap initially varies linearly with time.

These observations were then used to investigate the relationship between feed rate and equilibrium gap. The results are shown in Fig.6.4: for a fixed applied voltage and for a range of equilibrium gaps, (0.010 in to 0.055 in) the feed rate varies inversely with the gap. There is good agreement between theory and experiment.

For such gaps, forming tests were done with the 0.028 in. and 0.125 in. stepped cathodes. The results, in Figs.6.5 and 6.6, show good agreement with theory: the larger gaps require a longer machining time to achieve a required step on the anode. In addition the definition of the steps, while more distinct than those obtained for the fixed cathode tests, still less well defined at the larger gaps (e.g. for the 0.045 in. gap, the step was defined over an anode length of about 0.15 in. whilst for the 0.010 in. gap, it was defined over a length of about 0.060 in.).

These effects were investigated using brass model electrodes placed on conducting paper.

From the equipotential plots at the start of machining (i.e. flat anode) shown in Fig.6.7 these observations can be made:

(i) parallel equipotentials are obtained only in regions away from the cathode step region.

(ii) in this area the equipotentials transcend not sharply but gradually from the smaller gap h_o to the larger gap h_o^1.

(iii) as the gap is increased the transition lines from gap h_o to gap h_o^1 are more gradual.

(iv) for this increase in gap the equipotentials become parallel at points further away from the cathode step region (comparison of similar equipotentials for gaps of 0.010 in. and 0.014 in. makes this clear).

These results can be applied to the experiments on forming:

(i) for regions where the equipotentials are parallel to the cathode surface, there will be an even current density distribution. Even machining will take place over such regions.

(ii) in the equipotential transition region from the smaller gap h_o to the larger gap h_o^1 the local current density will decrease gradually from the higher value at gap h_o to the smaller value at gap h_o^1. Thus the anode step will be smoothly and not sharply defined.

(iii) as the gap is increased, there will be a more gradual change in current density. The step profile will then be more gradually defined at larger gaps.

(iv) for the larger gaps, the step profile will be defined over a larger electrode length.

However, actual measurements of such lengths from the equipotential

plots is difficult. To do this requires knowledge of the shape of the anode as machining progresses.

The plots in Fig.6.8 were drawn to simulate typical conditions during machining. Even for ideal anode steps with sharp edges, smooth equipotential curves are still obtained. Thus in practice the anode step will not be sharply defined.

Comparison of similar equipotentials from (i) and (iii) shows that for the latter, the equipotentials become parallel to the electrode surface at further distances on either side of the cathode step line. This again indicates that for larger gaps, the anode step is defined over a wider electrode length, and its profile is more gradually defined than for smaller gaps.

6.7 Conclusions

1. In forming, gap control is necessary to reduce machining time and to improve the definition of the anode shape.

2. The smaller the controlled gap, the better is the definition of the anode profile.

Chapter 7

The effects on forming of temperature and hydrogen - theoretical considerations

7.1 Introduction

Two principal factors affect the forming process - electrolyte heating and hydrogen evolution.

The former effect is caused by the current as it crosses the gap. The temperature increase raises the electrolyte conductivity and hence raises the metal removal rate. Local machining rate increases in the direction of flow. Thus a configuration of plane, initially parallel electrodes will become wedge shaped.

An opposite effect is caused by the hydrogen evolved at the cathode. The gas reduces the conductivity and hence the machining rate. Due to the electrolyte flow, the volume of hydrogen increases towards the flow exit. The local machining rate then decreases along the electrode length developing a wedge profile in an opposite direction to that caused by temperature.

The magnitude of each effect is analysed seperately, in terms of flow rate and potential gradient. The variation in electrode profile along the electrode length is calculated; also, the machining time required to achieve steady state conditions is estimated.

7.2 The effect of temperature

The current crossing the gap causes the electrolyte temperature to rise. The temperature increase along the electrode length, $\frac{dT}{dx}$ can be

calculated from Joule's Law, if it assumed that all the heat remains in the electrolyte and that no other factors increase the temperature.

Assuming also Ohm's Law, the temperature rise is

$$\frac{dT}{dx} = \frac{K\ (V - V_o)^2}{h^2 \rho_e C v} \qquad (7.1)$$

where K, V, V_o, h, v have been previously defined, ρ_e = electrolyte density ($g/m\ell$), C is the electrolyte specific heat ($Jg^{-1}\,{}^oC^{-1}$).

Using the same assumptions, similar expressions have been deduced by Tipton[16] and by Merchant[33].

This temperature rise will cause the gap, conductivity and velocity to vary along the electrode length. Eqn. (7.1) should thus be written

$$\frac{dT(x)}{dx} = \frac{K\ (x)\ (V - V_o)^2}{h^2(x) \rho_e C v(x)} \qquad (7.2)$$

where K(x), h(x), v(x) are the local conductivity, gap width and velocity at point x along the electrode length.

The electrode profiles, initially and after machining time t are indicated in Figs.7.1.

7.2.2. Machining time required to achieve equilibrium

The final electrode profiles will be similar to those shown in Fig.7.2. In this figure the y axis gives the deviation of the profile at time t from the initial profile, for any x along the electrode length.

To find the machining time required to achieve the final profile, suppose that the system can be represented by a first order differential equation:

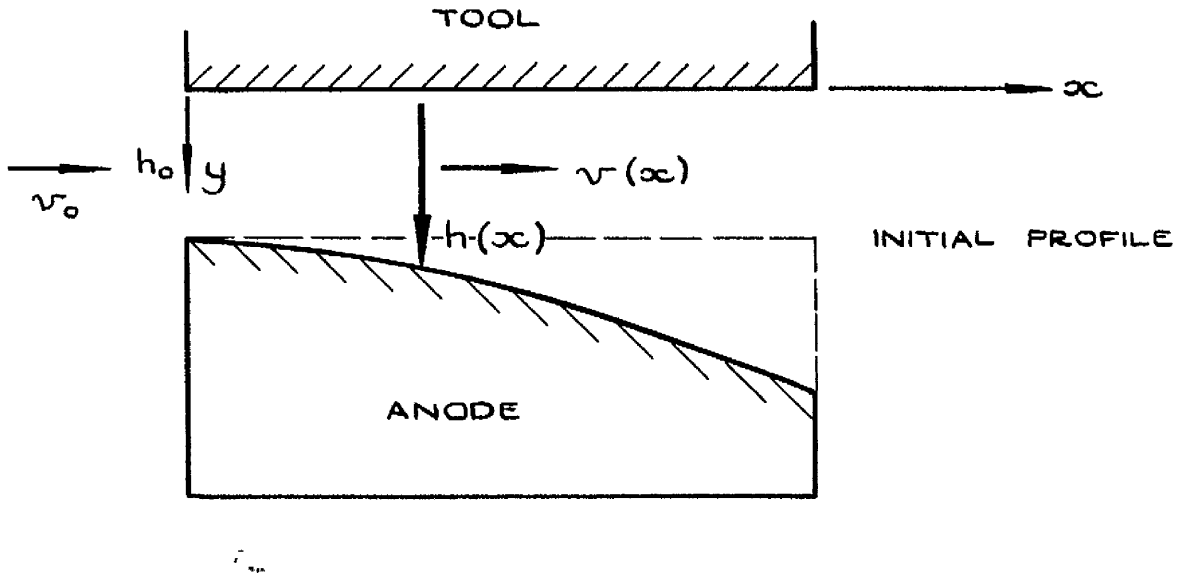

FIG. 7. 1. EFFECT OF TEMPERATURE ON EQUILIBRIUM GAP

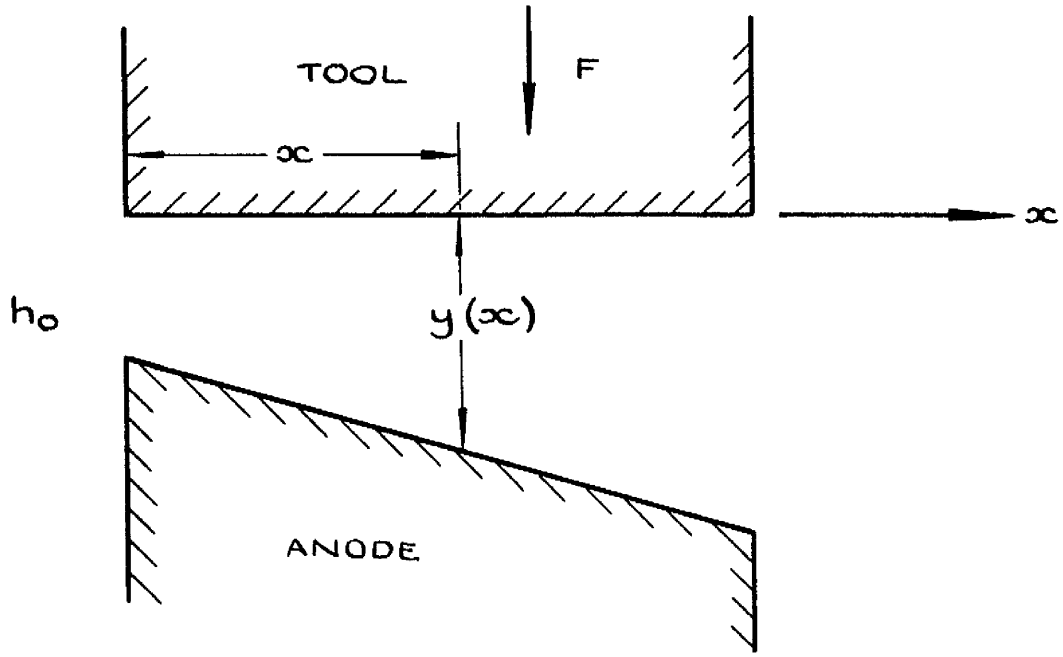

FIG. 7. 2. FINAL, STEADY STATE GAP POSITION

$$\tau \frac{dy}{dt} + y = y_f \qquad (7.3)$$

where τ is the time constant for the system and y_f is the final deviation at the point x.

The solution to equation (7.3) is

$$y = y_f (1 - e^{-t/\tau}) \qquad (7.4)$$

where $$\tau = y_f \Big/ \left(\frac{dy}{dt}\right)_{t=0} \qquad (7.5)$$

The general shape of the curve for equation (7.4) is shown in Fig.7.3.

7.2.3. Calculation of $y_f(x)$ Equilibrium condition

The steady state will be achieved when there is no further variation in gap along the electrode length. The local machining rates will then be constant, as will the local current density and the electrolyte volume flow rate.

For the last named condition, the velocity v(x) is

$$v(x) = \frac{v_o h_o}{h(x)} \qquad (7.6)$$

where v_o, h_o are the electrolyte velocity and gap width respectively at flow entry and are constant.

If the cathode descends vertically with feed rate U, the steady state gap (from Chapter 6) is given by:

$$h(x) = \frac{E\,(V - V_o)K(x)}{F\rho U} \qquad (7.7)$$

where ρ is the anode material density.

The current density is also constant along the electrode length:

$$\therefore \quad i(x) = \frac{(V - V_o)K(x)}{h(x)} = i_o \tag{7.8}$$

The temperature rise, $\frac{dT}{dx}$ will also then be constant. Using (7.8), $\frac{dT}{dx}$ becomes:

$$\frac{dT}{dx} = \frac{(V - V_o)K_o}{\rho_e C v h_o^2} = B, \text{ say} \tag{7.9}$$

The temperature difference between the temperature, T, at x, and the initial temperature, T_o, can be written

$$\Delta T = T - T_o \tag{7.10}$$

$$\therefore \quad \frac{d}{dx}(\Delta T) = \frac{dT}{dx} \tag{7.11}$$

$$\therefore \Delta T = \left(\frac{(V - V_o)^2 K_o}{\rho_e C v_o h_o^2}\right) x$$

$$= Bx \tag{7.12}$$

(Since at $x = 0$, $T = 0$ the constant of integration is zero).

If the conductivity K(x) is assumed to vary linearly with temperature:

$$K(x) = K_o(1 + \alpha \Delta T) \tag{7.13}$$

$$= K_o(1 + \alpha Bx) \tag{7.14}$$

where α is the temperature coefficient for conductivity.

$$\text{Now } h(x) = \frac{K(x)\ (V - V_o)}{i(x)} \tag{7.15}$$

$$= \frac{(V - V_o)K_o}{i_o} (1 + \alpha B x)$$

$$= h_o (1 + \alpha B x) \qquad (7.16)$$

$\therefore$ from Fig.(7.2)

$$y_f (x) = h(x) - h_o \qquad (7.17)$$

$$= B x$$

$$= \frac{(V - V_o)^2 K_o x}{\rho_e C v_o h_o^2} \qquad (7.18)$$

7.2.4. Calculation of $\left(\frac{dy}{dt}\right)_{t=0}$ - Initial State

If initially, the electrode surfaces are parallel, then y = 0. At any time, t, we have

$$y(x) = h(x) - h_o \qquad (7.19)$$

From Chapter 6, the rate of change of gap is

$$\frac{dh(x)}{dt} = \frac{E i(x)}{F \rho} - U \qquad (7.20)$$

$\therefore$ Using (7.19) and (7.20) the initial rate of change of y(x), $\left(\frac{dy(x)}{dt}\right)_{t=0}$ may be written:

$$\left(\frac{dy(x)}{dt}\right)_{t=0} = \frac{d}{dt} (h(x) - h_o)_{t=0} \qquad (7.21)$$

$$= \frac{E}{F\rho} (i(x) - i_o)_{t=0} \qquad (7.22)$$

The work of Tipton[16] is of use in finding an expression for $(i(x))_{t=0}$

He suggests that since that at the start of machining the gap has a constant value h_o at x=0, the velocity will also be constant. Eqn.(7.2) may then be written:

$$\frac{dT}{dx} = \frac{K(x)\ (V - V_o)^2}{h_o^2 \rho_e C v_o}$$

Assuming also that (7.13) applies and that

$$\frac{d}{dx}(\Delta T) = \frac{dT}{dx}$$

he obtains the expression

$$\frac{d}{dx}(\Delta T) - BK_o\ T = BK_o$$

For the boundary conditions $\Delta T = 0$ when $x = 0$ the solution is $\Delta T =$

$$\frac{1}{\alpha}\left[e^{\alpha B K_o x} - 1\right]$$

since the current density is $i(x) = \frac{(V - V_o)K(x)}{h_o}$,

Using (7.13) and the expression for (ΔT) gives

$$i(x) = \frac{(V - V_o)K_o}{h_o} e^{\alpha B K_o x}$$

$$= i_o e^{B K_o x} \qquad (7.23)$$

$$\therefore \left(\frac{dy(x)}{dt}\right)_{t=0} = \frac{E\, i_o}{F\rho}(1 - e^{\alpha B x}) \qquad (7.24)$$

$r(x)$ can also be found from (7.5) using (7.18) and (7.24).

The solution, equn.(7.4), can thus be written:

$$y(x) = \alpha\, h_o B x \left(1 - e^{-\frac{\alpha h_o B x\, t}{\frac{E\, i_o}{F\rho}(1 - e^{\alpha B x})}}\right) \qquad (7.25)$$

where $i_o = \dfrac{K_o(V - V_o)}{h_o}$

Thus for given values of the variables y(x) can be found as a function of time.

7.2.6 Theoretical Calculations

The effects of temperature have been calculated for an 8% NaCℓ electrolyte at initial temperature 18°C flowing between 1 in square electrodes (the anode being of mild steel) and for gap widths and electrolyte velocities in the ranges 0.010 to 0.040 in and 200 in/s to 2000 in/s respectively.

(For each gap the maximum velocity has been estimated for a pump pressure, p, of 250 lb/in^2, from the relationships

$$p = p_1 + p_2$$

where p_1 is the pressure required to overcome inertia, and p_2 is the pressure to overcome viscous forces.

For turbulent flow along rectangular channels of thickness h, p_1 may be written

$$p_1 = 0.5\rho_e v^2$$

and

$$p_2 = \frac{0.31\rho_e v^2 L}{4hRe^{0.25}} \qquad \text{(after Blasius)}$$

where $Re = \frac{2vh}{\nu}$

and L is the electrode length)

(The full data used are given in Appendix 4).

Fig.7.4 shows the dependence of the equilibrium temperature gradient (7.7) on electrolyte velocity and gap width.

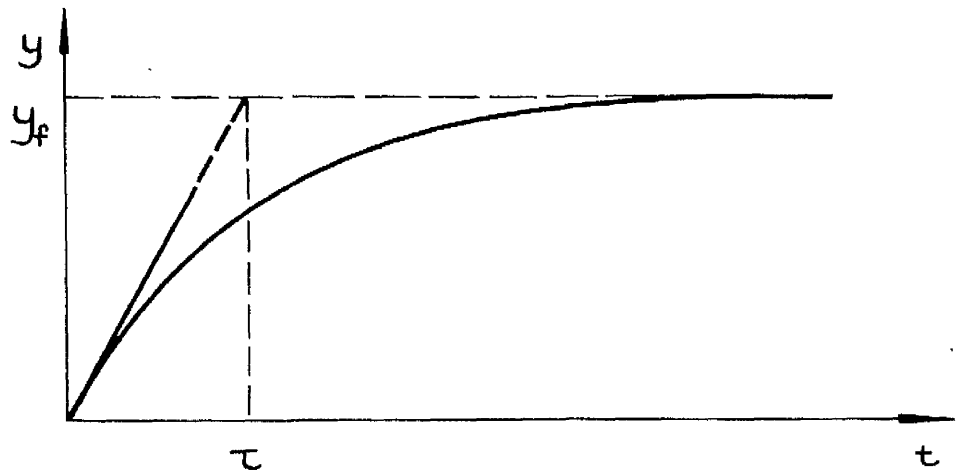

FIG. 7.3. TEMPERATURE EFFECT: SHAPE OF CURVE FOR EQUATION (7.4)

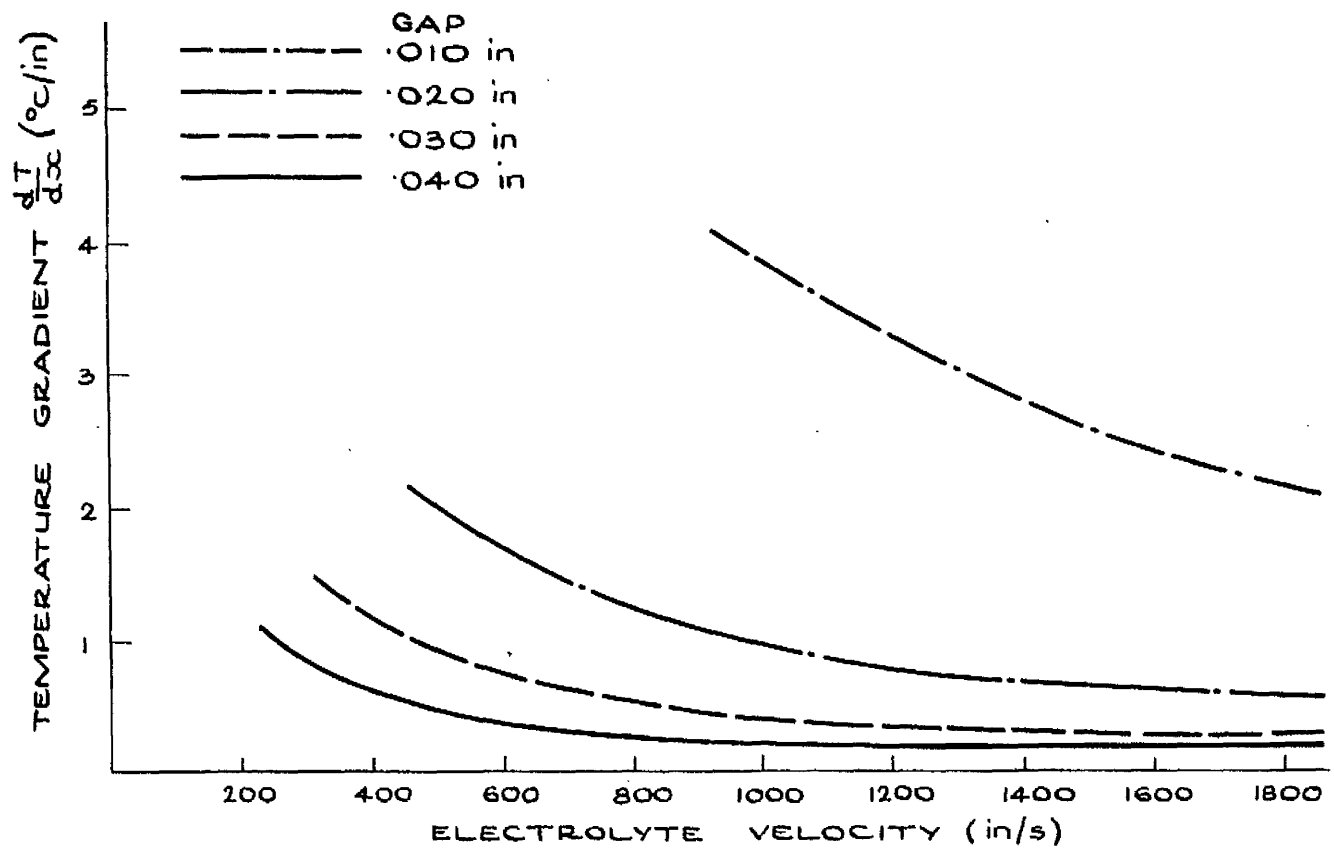

FIG. 7.4. EFFECT OF ELECTROLYTE VELOCITY AND GAP WIDTH ON TEMPERATURE GRADIENT ALONG THE GAP

Electrolyte velocity v (in/s)	Distance, x along electrode length (in)	0.1	0.2	0.3	0.4	0.5	0.6	0.7	0.8	0.9	1.0
230	Gap variation parameter $y_f(x)$ $(\times 10^{-3}$ in)	.09	.18	.28	.37	.47	.56	.66	.75	.85	.9
	Time for $y(x)=0.9y_f(x)$ t(s) (τ = 25%)	594	593	592.5	592	591	590	580	589	588	587.5
350	x	0.1	0.2	0.3	.4	.5	.6	.7	.8	.9	1.0
	$y_f(x)$ $(\times 10^{-3})$	.06	.12	.18	.25	.31	.37	.44	.50	.56	.62
	t (s) ($y(x)=0.9y_f(x)$) (τ = 258)	594	593.5	593	592.5	592	592.5	591.3	590	590	589.9
460	x	0.1	0.2	0.3	0.4	0.5	0.6	0.7	0.8	0.9	1.0
	$y_f(x)$ $(\times 10^{-3}$ in)	.04	.09	.14	.18	.23	.28	.33	.37	.42	.47
	t(s) (τ = 258)	594	5939	593.5	593	5928	592.5	592	5918	5915	591
580	x	0.1	0.2	0.3	0.4	0.5	0.6	0.7	0.8	0.9	1.0
	$y_f(x)$ $(\times 10^{-3}$ in)	.03	.07	.11	.15	.18	.22	.26	.30	.34	.37
	t (s) (τ = 258)	594	594	5937	593	593	592.9	592.6	5923	592	591.8

Table 7.1: Gap variation parameter $y_f(x)$ as a function of electrode distance x, and electrolyte velocity v, for a gap of 0.040 in. Time required for y(x) to approach $0.9y_f(x)$

h_o	Restraint on y_f(x=1 in)	y_f(x=1 in)	v (in/s)	t (s)
0.030	$.3 \times 10^{-3}$	.0003	690	592 (τ = 258)
.020	$.2 \times 10^{-3}$	.0002	1230	333 (τ = 145)
.010	$.1 \times 10^{-3}$	.0001	6000	36 (τ = 16)

Table 7.2: Effect of gap width on electrolyte velocity and time required to achieve 1% accuracy on $y_f(x)$, for x = 1 in.

h_o (in)	Restrain on $y_f(x)$ (x=1 in)	Accuracy	velocity v (in/s)	t (s)
0.040	$.2 \times 10^{-3}$	5%	230	587 (τ = 255)
.030	$.15 \times 10^{-3}$		310	329 (τ = 143)
.020	$.1 \times 10^{-3}$		460	145 (τ = 63)
.010	$.05 \times 10^{-3}$		1850	36 (τ = 16)
.040	$.08 \times 10^{-3}$	2%	350	590 (τ = 256)
.030	$.06 \times 10^{-3}$		460	330 (τ = 144)
.020	$.04 \times 10^{-3}$		1160	147 (τ = 64)
.010	$.02 \times 10^{-3}$		3700	36 (= 16)

Table 7.3: Dependence of accuracy of restraintimposed on $y_f(x)$ and machining time required upon electrolyte velocity, for gaps from 0.040 to 0.010 in.

Table 7.1 shows for $h_o = 0.040$ in the variation of the gap parameter $y(x)$ with electrolyte velocity v and distance x along the electrode length. The machining times required for equilibrium conditions to be approached (i.e. $y(x) = 0.9\, y_f(x)$) are also indicated. These have been calculated from (7.19), (using (7.28) to calculate the time constant τ). A mean value for τ has been used (although the factor only varies by 1s for x ranging from 0.1 in to 1 in).

Tables 7.2 and 7.3 give for some or all of the gaps $h_o = 0.040$ to 0.010, and for x = 1 in, the electrolyte velocities required to maintain an accuracy, $y_f(x) \leq 0.01\, h_o$, and $y_f(x) \leq 0.02\, h_o$, $0.05\, h_o$ respectively.

The machining times for $y(x) \rightarrow 0.9\, y_f(x)$ are also given.

7.2.7 Discussion

Fig.7.4 shows that for each of the gaps the temperature rise is small and will not cause electrolyte boiling.

The temperature increase will still affect the electrolyte conductivity. The gap will then vary from its equilibrium value. The magnitude of this variation is given by (7.22)

$$y_f(x) = h_o \alpha\, Bx$$

Note that B involves v (7.7). If an arbitrary restraint is imposed on $y_f(x)$, i.e. the electrode gap value must not vary by more than a fixed amount, say 1%, from its equilibrium value h_o then the electrolyte velocity required for this condition can be calculated from (7.22).

Obviously, and from (7.22), this effect is achieved more quickly for low x values (i.e. at the upstream end of the electrode length) than for high x values.

These effects have been investigated for a gap $h_o = 0.040$ in. The results are given in Tables 7.1 to 7.3.

For the gap to vary by only 1% or less, requires

$$y_f(x) \leq 0.4 \times 10^{-3} \text{in.}$$

Table 7.1 shows that a velocity v = 230 in/s brings $y_f(x)$ within the range for x = 0.1 to 0.4 in. For the whole length (x = 1 in) a velocity of 580 in/s is required. The approximate machining time required is 592 s).

Clearly, equilibrium is not achieved until the $y_f(x)$ value for the largest x (i.e. x = 1 in) is below the imposed limit. For the gaps h_o = 0.030 to 0.010 in, table 7.2 gives the velocities required for

$$y_f \ (x = 1 \text{ in}) \leq 0.01 \ h_o$$

and the machining times required.

From the table the observations are made that:

(i) as the gap is decreased, higher velocities are required to achieve the restraint on $y_f(x)$.

(ii) for these velocities the machining time for equilibrium decreases.

For the gap h_o = 0.010 in, the required velocity, v = 6000 in/s is greater than possible for a pump pressure of 250 lb/in^2. Thus an

accuracy of 1% is not obtainable.

Table 7.3 shows that for these conditions a 2% accuracy is not possible, but that an accuracy of 5% is attainable.

Comparison of the results from Tables 7.2 and 7.3 also shows that if the accuracy required for the gap is lowered, a lower electrolyte velocity and a smaller machining time are required to achieve it.

7.2. Conclusions

1. For an 8% NaCℓ solution flowing at velocities ranging from 200 to 1850 in/s between 1 in square electrodes with initial gaps of 0.040 to 0.010 in, the equilibrium temperature increase along the gap is small.

2. If a restraint is imposed on the amount by which the gap may increase along the electrode length, then the electrolyte velocity required to achieve it increases as the initial gap is decreased. However, as the velocity is increased, the machining time is decreased.

3. For any gap h_o, if the accuracy required is lowered, a lower velocity and a smaller machining time are required to achieve it.

7.3 The effect of hydrogen

Suppose that the plane, initially parallel electrodes have width b and length ℓ, and that the electrolyte at temperature T_o, flows between the electrodes with constant volume flow rate Q. For a constant voltage V, and constant cathode feed rate U, suppose that machining commences when the gap is initially h_o. Assume also that h_o is the equilibrium gap for a system undisturbed by hydrogen.

The initial configuration is shown in Fig.7.5. The wedge-shaped profiles caused by the hydrogen are shown in Fig.7.6.

In Fig.7.5, for any point x along the electrode length, the y axis gives the deviation of the anode profile from the initial profile.

As in 7.2, for an Ohmic relationship at point x we have:

$$i(x) = \frac{K(x)\ (V - V_o)}{h(x)} \qquad (7.26)$$

Kennedy[34] has done some calculations on the pressure change along the gap due to hydrogen. From his analysis and from the equation given by De La Rue and Tobias[35] (see below (7.27)) he has derived an expression for the change in conductivity along the electrode length. The method of using the results of De La Rue and Tobias has again been employed. However, in this expression the term involving pressure has only a second order effect on conductivity. Thus instead of using a complex expression for pressure in this term, an average equivalent quantity has been substituted. This involves only standard temperature

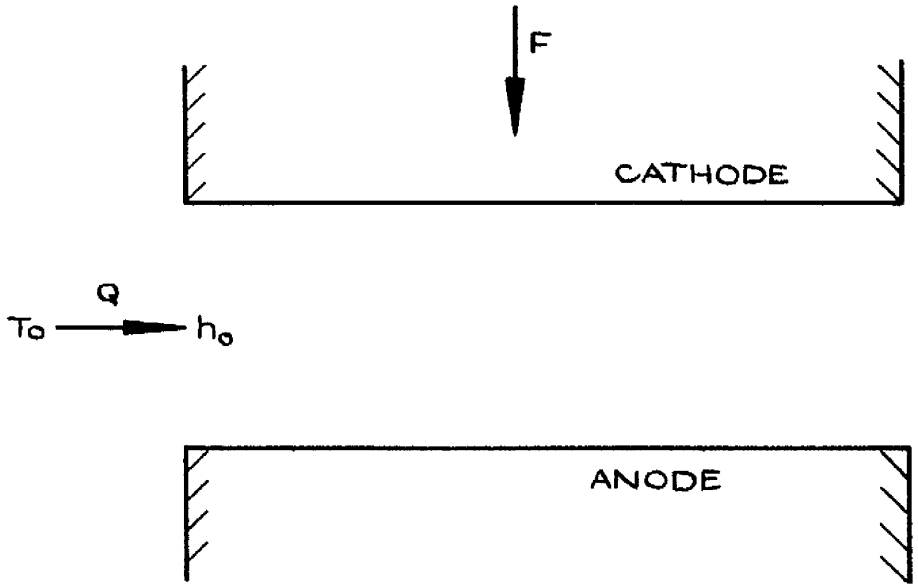

FIG. 7.5. INITIAL PROFILES OF PLANE PARALLEL ELECTRODE

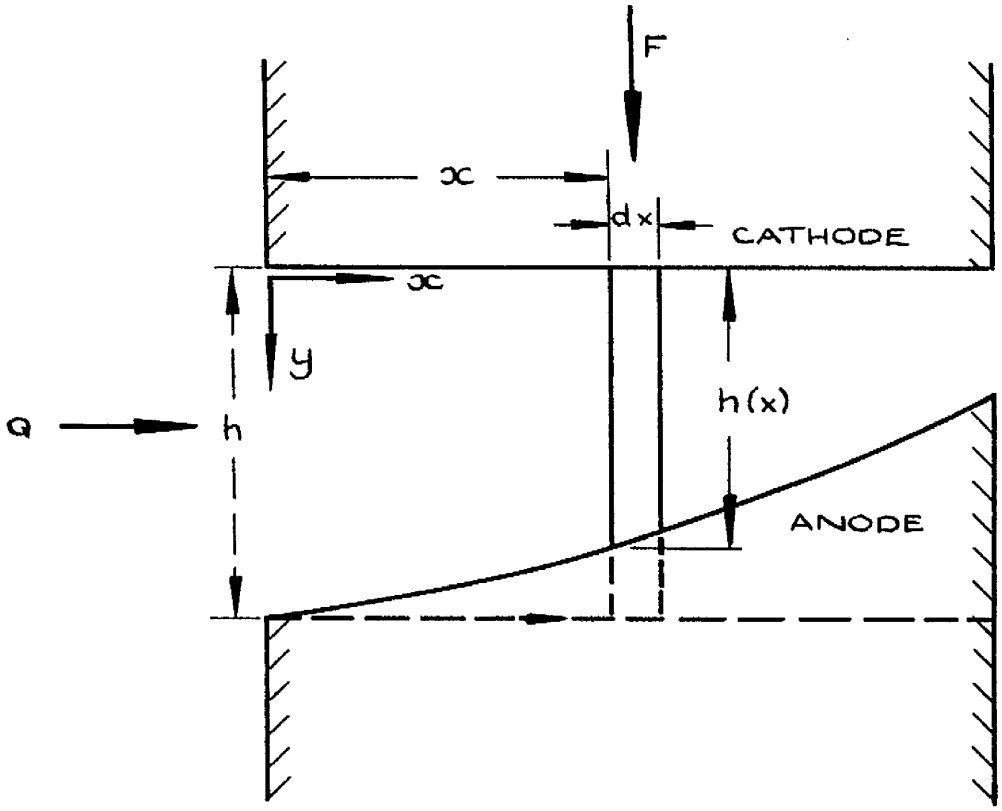

FIG. 7.6. EFFECT OF HYDROGEN ON ANODE PROFILE

and pressure values.

From the work of De La Rue and Tobias[35], K(x) can be expressed as a function of the ratio f(x), of hydrogen volume rate V_H to the electrolyte volume flow rate $\mathcal{Q}$:

$$K(x) = K_o\ (1 - f(x))^{3/2} \qquad (7.27)$$

K_o being the conductivity at flow entry.

$$f(x) = \frac{V_H(x)}{\mathcal{Q}}$$

7.3.2 Determination of f(x)

In Fig.7.5, consider the element dx, of depth h(x) and width b (electro width). Current produced at the element = $i(x)\,dx\,b$ (7.28)

where i(x) is the current density at x

$\therefore$ total current produced from x = 0 to x = x, $= \int_0^x i(x)\,b\,dx$

$\therefore$ total mass/s of gas produced $= \frac{E_H I}{F}$

$$= \frac{E_H}{F}\int_0^x i(x)\,b\,dx \qquad (7.30)$$

where E_H is the chemical equivalent (g) for hydrogen,

Also, from the Gas Law

$$P(x)\ V_H\ (x) = \frac{m(x)\ R\,T\,(x)}{W} \qquad (7.31)$$

where P(x), $V_H(x)$, m(x), T(x) are the pressure, volume and mass

production rates, and temperature at the point x, R is the Gas Constant and W the molecular weight for hydrogen.

Using eqns. (7.30) and (7.31) gives:

$$V_H(x) = \frac{E_H R T(x)}{F W P(x)} \int_0^x i(x)\, b\, dx \qquad (7.32)$$

If the gas is assumed to obtain instantaneously the electrolyte velocity at point x, v(x), then the fraction $\frac{dx}{v(x)}$, of it is in the volume element at any given time,

i.e. the volume of gas in the element is

$$\frac{dx}{v(x)} \cdot \frac{E_H R T(x)}{F W P(x)} \int_0^x i(x)\, b\, dx \qquad (7.33)$$

Volume of electrolyte in the element = $b\, h(x)\, dx$ (7.35)

$$\therefore \text{ using (7.27), } f(x) = \frac{E_H R T(x)}{F W P(x) v(x) h(x)} \int_0^x i(x)\, dx \qquad (7.36)$$

Now f(x) has only a second order effect on K(x). Then, put

$\int_0^x i(x)\, dx = i_o x$, (7.37), as an approximation and since P(x) and T(x) are not known along the gap, put

$$\frac{E_H R T(x)}{F W P(x)} = G \qquad (7.38),$$ an average equivalent quantity.

In the subsequent calculations, standard temperature (273°K) and pressure (1 Atmos) values have been used in calculating this expression. (Recently, Hopenfeld and Cole[36] have shown that this assumption is valid).

Since $\mathcal{Q}$ is constant, put

$$v(x) = \frac{\mathcal{Q}}{bh(x)} \tag{7.39}$$

$\therefore$ (7.36) becomes

$$f(x) = \frac{\mathcal{C} i_o b x}{\mathcal{Q}} \tag{7.40}$$

7.3.3 Machining time required to achieve equilibrium

Similar to the method for electrolyte heating (7.2.2), the system may be represented by a first order differential equation:

$$\tau_1 \frac{dy}{dt} + y = y_f \tag{7.41}$$

where τ_1 is the time constant.

The solution is

$$y = y_f (1 - e^{-t/\tau_1}) \tag{7.42}$$

where $\tau_1 = y_f \Big/ \left(\frac{dy}{dt}\right)_{t=0}$ (7.43)

7.3.4 Calculation of $y_f(x)$ - Equilibrium condition

As before, for equilibrium conditions the current density is constant along the gap:

$$\therefore \quad i_o = \frac{K_o(V - V_o)}{h_o} = i(x)$$

$$= \frac{K(x)(V - V_o)}{h(x)} \tag{7.44}$$

and $$h(x) = \frac{E(V - V_o)K(x)}{F\rho U} \qquad (7.45)$$

Using eqns. (7.27), (7.40) and (7.45) gives

$$h(x) = \frac{E(V - V_o)K_o}{F\rho U}\left(1 - \frac{G i_o b x}{Q}\right)^{3/2} \qquad (7.46)$$

Noting that $h_o = \frac{E(V - V_o)K_o}{F\rho U}$, and assuming that $\frac{G i_o b x}{Q} \ll 1$ (also proven to be valid by Hopenfeld and Cole[36]), gives

$$h(x) = h_o\left(1 - \frac{3}{2}\frac{G i_o b x}{Q}\right) \qquad (7.47)$$

As before, $y_f(x) = h_o - h(x)$

$$= \frac{3}{2}\frac{G i_o b h_o x}{Q} \qquad (7.48)$$

(Note that since $i_o = \frac{K_o(V - V_o)}{h_o}$, $y_f(x)$ is independent of h_o).

7.3.5 Calculation of $\left(\frac{dy}{dt}\right)_{t=0}$ - Initial State

As before, suppose that, initially, $y = 0$

$$\therefore \left(\frac{dy(x)}{dt}\right)_{t=0} = \frac{E}{F\rho}\left(i_o - i(x)\right)_{t=0} \qquad (7.49)$$

Using (7.26), (7.27) and (7.40), and assuming that initially, $h(x) = h_o$ gives

$$i(x) = \frac{K_o(V - V_o)}{h_o}\left(1 - \frac{3}{2}\frac{G K_o (V - V_o) b x}{h_o Q}\right) \qquad (7.50)$$

$$\therefore \left(\frac{dy(x)}{dt}\right)_{t=0} = \frac{EK_o(V - V_o)}{F\rho\, h_o}\left(\frac{3}{2}\frac{GK_o(V - V_o)\, bx}{h_o\, Q}\right) \qquad (7.51)$$

Thus, from (7.43), using (7.48) and (7.51)

$$\tau_1 = \frac{+\ h_o^2}{\frac{EK_o(V - V_o)}{F\rho}} \qquad (7.52)$$

(Note that τ_1 is independent of f(x))

The expression for y(x) (eqn. 7.42) becomes:

$$y(x) = \frac{3}{2}\frac{Gi_o bx}{Q}\left(1 - e^{-\frac{th_o^2 F\rho}{EK_o(V - V_o)}}\right) \qquad (7.53)$$

y(x) can thus be found in terms of t and x, for given values of the process variables.

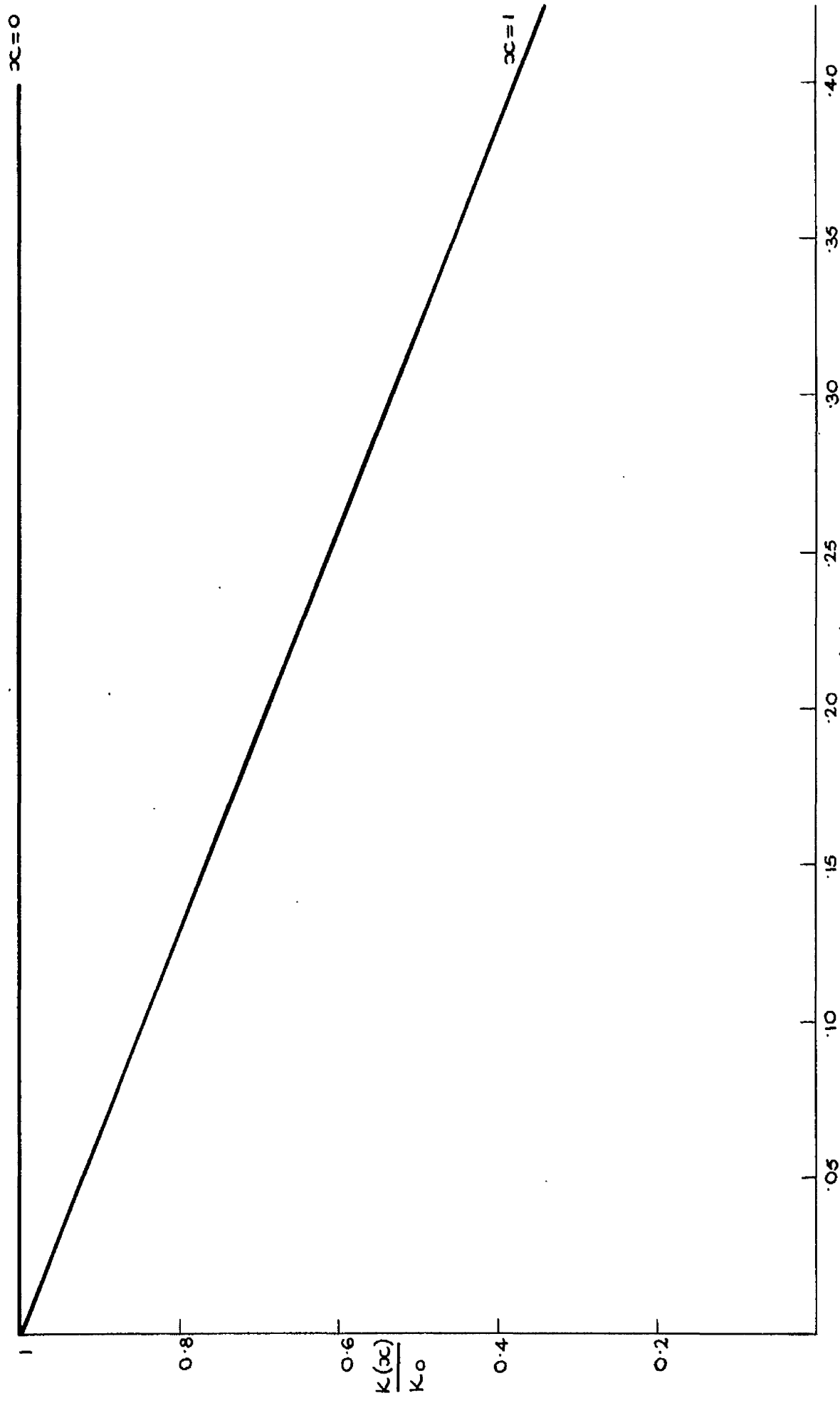

FIG. 7.7. CONDUCTIVITY RATIO $K(x)/K_0$ AS A FUNCTION OF RATIO $f(x)$, (HYDROGEN EVOLUTION RATE/VOLUME FLOW RATE) AT $x = 0$ AND $x = 1$ in.

Electrolyte volume flow rate Q (in^3/s) (cm³/min)	Electrolyte velocity v (in/s)	Distance x along electrode length (in)	0.1	0.2	0.3	0.4	0.5	0.6	0.7	0.8	0.9	1.
9.0 (2)	230	Gap variation parameter $y_f(x)$ (in x 10^3)	.3	.6	0.9	1.2	1.5	1.8	2.1	2.4	2.7	3.
14 (3)	350		.2	.4	.6	.8	1.0	1.2	1.4	1.6	1.8	2.
18 (4)	460	$y_f(x)$	.15	.3	.4	.6	.7	.9	1.0	1.2	1.3	1.
23 (5)	580		.12	.2	.3	.4	.6	.7	.8	0.93	1.1	1.
32 (7)	800		.08	.17	.26	.35	.4	.5	.6	.7	.79	0.
42 (9)	1050		.06	.13	.20	.27	.3	.4	.4	.54	.61	0.
51 (11)	1280		.05	.11	.16	.22	.27	.3	.35	.44	.50	0.
60 (13)	1500		.04	.09	.14	.19	.23	.28	.3	.37	.42	0.
69 (15)	1730		.04	.08	.12	.16	.2	.24	.28	.32	.36	0.
79 (17)	1980		.03	.07	.1	.14	.18	.2	.25	.28	.32	0.

Table 7.4: Hydrogen effect: gap variation parameter as a function of elect distance x, and electrolyte flow rate Q for a gap of 0.040 in.

h_o (in)	Restraint on $y_f(x = 1 \text{ in})$	Q (in^3/s)	v (in/s)	t(s) ($y(x) = 0.9y_f(x)$)
.040	$\leq .4 \times 10^{-3}$	69	1730	595
.030	$\leq .3 \times 10^{-3}$	83	2770	334
.020	$\leq .2 \times 10^{-3}$	> 83	-	-
.010	$\leq .1 \times 10^{-3}$	> 83	-	-

Table 7.5: Flow rate, velocity, and time required to achieve 1% accuracy for $y_f(x)$ (For x = 1 in). (Gaps h_o = 0.040 to 0.010 in)

Accuracy	h_o	Restraint on $y_f(x=1\,in)$	Q (in^3/s)	Velocity v (in/s)	t
2%	.040	$.8 \times 10^{-3}$	37	920	880
	0.030	$.6 \times 10^{-3}$	46	1540	890
	0.020	0.4×10^{-3}	65 (not attainable)	3230	900
	0.010	$.2 \times 10^{-3}$	83 (not attainable)		-
5%	0.040	2×10^{-3}	14	350	890
	.030	1.5×10^{-3}	18.0	620	890
	.020	1×10^{-3}	23.0	1160	895
	.010	$.5 \times 10^{-3}$	55 (not attainable)	5540	895
10%	.040	4×10^{-3}	9	230	890
	.030	3×10^{-3}	9	310	890
	.020	2×10^{-3}	14	690	892
	.010	1×10^{-3}	28 (not attainable)	2770	822
20%	.040	8×10^{-3}	4.6	120	895
	.030	6×10^{-3}	4.6	150	895
	.020	4×10^{-3}	9.0	460	890
	.010	2×10^{-3}	14	1380	890

Table 7.6: Dependence of accuracy of restraint imposed on $y_f(x)$, on electrolyte velocity and time, for gaps from .040 to 0.010 in.

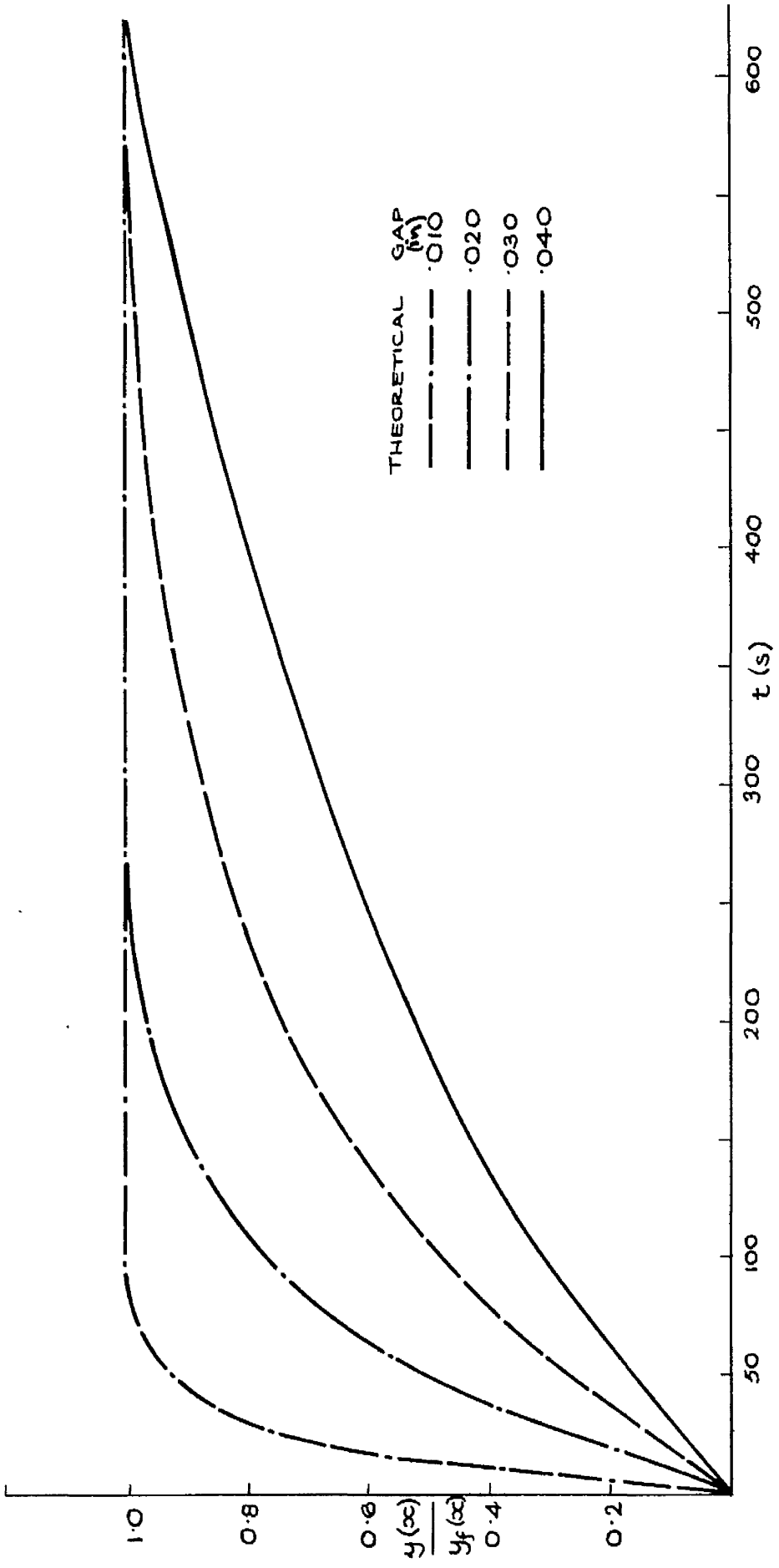

FIG. 7.8. RATIO $y(\infty)/y_{f(\infty)}$ AS A FUNCTION OF GAP WIDTH h_0 AND TIME OF MACHINING t.

7.3.7 Theoretical calculations

The effects of hydrogen on an electrode-electrolyte system, similar to that described in (7.2), have been investigated.

Fig.7.7 shows the relationship between the ratio of conductivities, $K(x)/K_o$, and the ratio of hydrogen evolution rate to electrolyte volume flow rate, $f(x)$, for $x = 1$ in (i.e. for the flow exit point).

Table 7.4 shows, for a gap $h_o = 0.040$ in, the gap variation parameter $y(x)$ as a function of electrode distance x and volume flow rate Q, for x and Q ranging from 0.1 in to 1 in, and from 9 in^3/s to 79 in^3/s respectively.

Tables 7.5 and 7.6 show for gaps from 0.040 to 0.010 in, the dependence of the restraint imposed on $y(x)$ on electrolyte flow rate Q and machining time t, for restraints of 1% , and 2, 5, 10 and 20% respectively.

In Fig.7.8, for $x = 1$ in, the ratio $y(x)/y_f(x)$ is plotted as a function of gap h_o and machining time t, for h_o values ranging from 0.040 to 0.010 in.

Note: In the tables, for each Q and h_o value, the corresponding value for electrolyte velocity is also given.

7.3.8 Discussion

Fig.7.7, shows that, for any given flow rate, the conductivity is reduced more for smaller gaps, than for larger ones: e.g. for a flow rate of 4.6 in^3/s, for $h_o = 0.010$, $K(x)/K_o = 0.4$, but for $h_o = 0.040$, $K(x)/K_o = 0.84$.

This reduction in conductivity will reduce the gap along the electrode length, (c.f. the effect of temperature on conductivity is to increase the gap).

Comparison of equivalent $y_f(x)$ values from Tables 7.4 and 7.2 shows that the hydrogen has a greater effect than temperature; e.g. for $Q = 9.0\,in^3/s$ (i.e. $v = 230\,in/s$), and for $x = 0.1\,in.$

$y_f(x = 0.1)$ for hydrogen $= 0.3 \times 10^{-3}\,in$

and $y_f(x = 0.1)$ for temperature $= 0.09 \times 10^{-3}\,in$

and for $Q = 18\ in^3/s$ $(v = 460\,in/s)$

$y_f(x = 1\,in)$ for hydrogen $= 1.5 \times 10^{-3}\,in$

and $y_f(x = 1\,in)$, for temperature $= .47 \times 10^{-3}\,in.$

Thus the overall effect is a decrease in gap along the electrode length.

Also from Table 7.4, flow rates higher than those for temperature effect are needed if the gap is not to vary by more than a certain amount.

e.g. for a variation along the length of not more than 1%, a minimum flow of $69\,in^3/s$ is required (c.f. temperature effect: $9\,in^3/s$).

From Table 7.5, for the gaps 0.030 to 0.010 in, the flow rates required for the maintenance of a 1% accuracy in gap exceed those possible from a pump whose capacity is 250 lb/in.

Lesser accuracies can be obtained for more practical flow rates. Table 7.6 shows that for accuracies from 2% to 20% imposed on $y_f(x)$,

for x = 1 in, the flow rates for each gap, diminish considerably on reduction of the accuracy required. e.g. for a gap h_o = 040 in a 2% accuracy requires a flow rate of 37 in^3/s but a 20% accuracy requires a flow rate of less than 4.6 in^3/s.

A 0.010 in gap still requires high flow rates. For a 2% accuracy, a flow rate exceeding 83.0 in^3/s is required, for a 20% accuracy, 14 in^3/s (1380 in/s).

The machining times required for y(x) to approach $y_f(x)$ ($y(x) = 0.9y_f($ are also given in Table 7.5. (These have been calculated from equation (7.53)). They show that for each gap and flow rate, the machining time required is almost constant at about 890 s.

Conclusions

1. The effect of hydrogen on the gap is much greater than that of temperature. Thus the overall effect is a decrease in the gap in the direction of flow along the electrode length.

2. To maintain a required accuracy of gap requires high flow rates (e.g. 37 in^3/s to maintain a 2% accuracy on a gap of .040 in). The smaller the gap, the greater is the flow rate required.

3. For small gaps, e.g. .010 in, the normal flow rates for E.C.M. conditions may not be sufficient to maintain a high accuracy (e.g. a flow rate of 55 in^3/s would be required to maintain a 5% accuracy on a gap of 0.010 in).

Chapter 8

General Conclusions and Suggestions for Further Research

In Chapters 2 to 7 possible solutions have been presented to some of the problems encountered by users of the E.C.M. process.

In Chapter 2 it has been shown that the current density may be calculated from Ohm's Law if the electrolyte velocity is sufficiently high.

In Chapter 3, the anodic products of machining have been shown to have negligible effect on the properties of the bulk electrolyte.

Favourable results may be obtained when the electrolyte velocity is high, e.g. the surface roughness of mild steel decreases as the flow rate is increased, (Chapter 4). Increasing the flow rate also reduces the effects of temperature and hydrogen on forming, (Chapter 7).

In the work on forming reported in Chapter 6, high flow rates have been used for this purpose. For such conditions it has been indicated that the anode shapes have best definition when the electrode gap is small.

Problems concerning the electrochemistry of the process have also been investigated. Methods for calculating electrochemical equivalents for alloys have been presented in Chapter 4. The use of the potentiostat for selecting electrolytes for different metals has also been established. For suitable electrolytes the current efficiency of the machined metal is generally high.

From these observations, further work can be suggested:

Experiments must be done on the effects on forming of temperature and hydrogen. Measurement of the variation of the electrolyte temperature along the length of the gap would be necessary. Insertion of thermocouples at the flow entry and exit points to the machining area should be simple enough. However, the thermocouple wires would have to be chosen so that they would not be attacked by the solution, and so that their junction would not be fractured by the flowing electrolyte. As the gap is so small, temperature measurement in the machining area may be more difficult. Since the anode is dissolved during machining, insertion of the thermocouples into the electrolyte from the cathode surface would probably be more practical.

For the hydrogen effect, pressure measurement is a similar problem. In addition a theoretical analysis has yet to be published of the pressure distribution along the gap length. Such an investigation would possibly involve the effects of two and/or three phase fluid flow. Some industrial users have reduced the effect of hydrogen on the conductivity by imposing a back pressure at the flow exit point. This effect could be investigated both theoretically and experimentally.

Such work is necessary before design studies are commenced of cathode tools to machine certain shapes. In this work an investigation of the electric field distribution in the gap would help. This could be done either by solution of Laplace's Equation or by direct plotting using electrode models on conducting paper, (see Chapter 7).

On the electrochemical side, further investigations with the potentiostat can be done. In Chapter 5, the effects on the polarization curves of additives to the electrolytes have not been investigated. Useful work in this direction is possible, e.g. for cast iron, it would help if an electrolyte agent were found which would prevent the formation of the passive layer on the electrode surface. Also the problems associated with forming would be lessened if an agent could be found which would dissolve the hydrogen evolved at the cathode. This would possibly eliminate the effect of the gas on the electrolyte conductivity.

While the current densities and flow rates reported in Chapter 5 are much higher than other typical values from potentiostat studies, they are still less than those encountered in E.C.M. Interesting development work could be done to see if pertinent results from the potentiostat are possible for E.C.M. conditions. Such information would be invaluable. It would give knowledge of the anode potential and electrolyte velocity required at a given current density to achieve a certain surface finish.

Two other problems are obvious:

A technique for actual gap measurement during machining has yet to be reported. Such a method would be greatly helpful to investigations of the process.

No estimates appear to have been made of the energy efficiency. This involves knowledge of the current and voltage efficiency. The former is easily calculable (see Chapter 4). For the latter the decomposition

potential required to achieve machining must be known. Any applied potential above this value simply helps to heat the electrolyte. Whilst certain values may be obtained from the literature, there is no apparent knowledge of the effects of flow rate and current density on the decomposition potential. An investigation of these effects would also be very useful.

Research based on the above suggestions would greatly clarify many of the problems in E.C.M.

Appendix 1

The Barmax Machine Installation

1.1 Introduction

A Crow, Hamilton and Co. Ltd. "Barmax" electrochemical machine, manufactured under licence from Rolls Royce Ltd., was used for the experiments described in Chapters 2, 4 and 6.

The machine was originally designed to give constant current control. The work discussed in Chapter 4 was performed using this system. Later the control system was changed to allow constant gap machining. At the same time the electrolyte flow system was simplified. The re-designed equipment was used for the investigations described in Chapters 2 and 6.

The former system, the associated flow system, and experimental apparatus and procedure are first described.

1.2 Constant current apparatus (see Chapter 4)

The Barmax machine is shown in Fig. A.1. The perspex work jig used with the machine has been previously described. (See Fig.2.1 and section 2.1).

The anode electrodes were held by a fixing screw in the jig, which was mounted on a brass support. This was secured by tee bolts on the stainless steel machine table.

Two jigs have been used:

(a) Current densities to 500 A/in^2.

The electrodes were cylindrical with a diameter of 1.3 in.

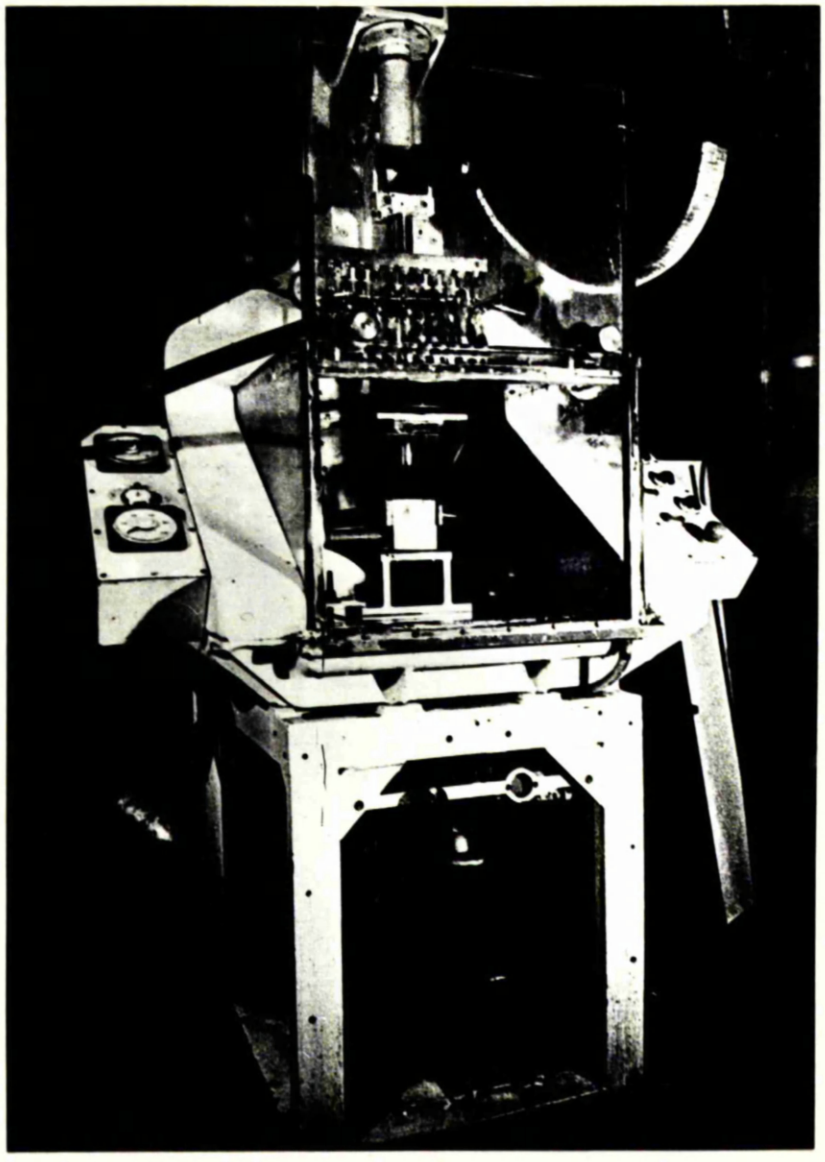

Fig A.1 The Barmax Experimental Machine

The cathode was moved vertically along the axis of the anode. For current densities up to 100 A/in^2, this was done by a servomotor, part of a system, described by Wilkinson and Stuart[37], designed to keep the gap constant. For a constant temperature, the current density is also held constant.

For higher current densities, the cathode was driven manually.

(b) current densities from 300 to 1200 A/in^2

The electrodes were square, with side 0.45 in. The vertical movement of the cathode was controlled manually.

In (a) monel was chosen for the cathode material, because of its resistance to corrosion by sodium chloride solution. In (b) brass was used, as it was more easily machined than monel. There was no difference in the experimental results obtained, but the electrolyte did have a corrosive effect on the brass.

1.2.1 Electrolyte Flow System

A schematic diagram of the flow system is given in Fig.A.2.

A Saunders six stage centrifugal pump delivered electrolyte from a 100 gallon (27000 in^3) storage tank to the jig at pressures up to 250 lbf/in^2 and at flow rates up to 92 in^3/s. The electrolyte discharged from the jig to a sump tank beneath the machine and was returned to the storage tank by a sump tank, activated by a level switch in the sump tank.

After about 20 hours machining the electrolyte was pumped to the

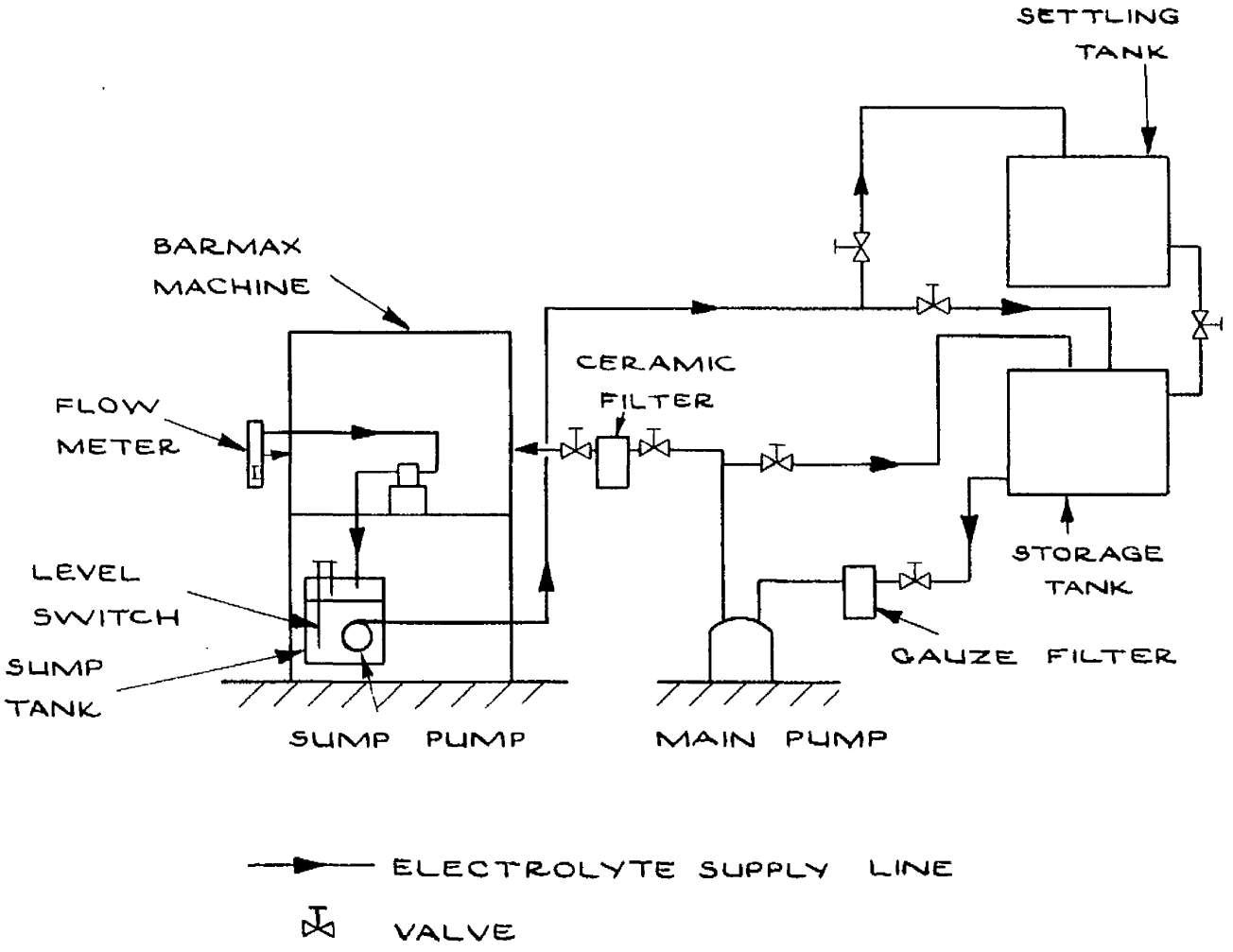

FIG. A.2. SCHEMATIC DIAGRAM OF ORIGINAL FLOW SYSTEM FOR BARMAX MACHINE.

settling tank and left for about 24 hours to allow the metal hydroxides to settle. Clear electrolyte was then drawn off and returned to the storage tank. The settling tank was also used for the preparation of fresh electrolyte.

Three filters were used:

(a) a brass gauze filter, in the pump suction line, which retained particles greater than 0.040 in.

(b) a ceramic filter, in the delivery line, which retained particles greater than 0.001 in.

(c) a cylindrical, perforated, stainless steel filter, in the entry line to the jig, which retained particles greater than 0.020 in.

Flow rate was measured by a Platon "Gapmeter" flowmeter of the rotometer type, graduated up to 20 gallons/min. (92 in^3/s) and fitted in the pump delivery line. The flow rate was varied by a hand valve in the by-pass line.

Electrolyte temperature was measured at the exit from the jig with a mercury thermometer, graduated in $0.1^{\circ}C$ divisions.

Machining times were taken with a stop watch.

1.2.3 Electrical system

A Dynamo and Electrical Services Ltd. silicon rectifier capable of 1000A at 9 to 15V was used to supply power to the Barmax machine.

Automatically controlled constant currents could be obtained by connecting the appropriate resistors and by adjusting the control amplifier settings. At current densities above $100 A/in^2$ this became a

prolonged operation requiring about 2½ hours to make the necessary changes. For this reason the equipment was modified to allow constant current machining by manual adjustment of the cathode.

Anode measurements

The anode weight was measured to 0.001g with a Gallenkamp electric balance.

Surface roughness (to 200 microinches) was measured with a Rank Taylor Hobson Talysurf '105' instrument.

1.2.4 Procedure

A weighed specimen was fitted in the jig. The pump was switched on and the valves adjusted to give the required flow rate. The electrolyte temperature was noted.

Further procedure is related to:

(i) Current densities to 100A/in^2 : automatic current control

Before the experiments at each current density, machining tests were carried out to allow the setting of the resistors and amplifiers to the appropriate values for that current density.

For the experiments, the machining cycle was started by push button. The cathode advanced automatically to the position for the required current density. The current density built up to this value in about 10s. After 10 minutes machining the cathode was retracted and the electric power and flow switched off.

(ii) Current densities above 100A/in^2: manual current control

The electric power was switched on and the cathode position

adjusted to give the required current density. The flow rate was checked as above. During machining the cathode was advanced manually to keep the current density constant. After 5 minutes machining, the electric power and flow were switched off.

For each procedure, at the end of machining the specimen was removed for observation and reweighing.

The tests were repeated for different flow rates and current densities.

1.3 Constant gap apparatus

The current feedback control system was unsuitable for experimental work because of the time required to change from one current setting to another. An offer by Rolls Royce Ltd. to change the control system was accepted.

The new system allows adjustments to be made in less than 10 minutes. It is based on the concept of the equilibrium gap, discussed in Chapter 6: for a constant applied voltage, and for any one electrolyte/metal combination, the cathode feed rate is inversely proportional to the equilibrium gap width. By empirical machining tests a potentiometer, the settings of which control the feed rate, was initially calibrated for a range of gaps. Changes in conductivity were monitored with a conductivity cell, the A.C. voltage from which is rectified and fed into a summing junction. The other signal for the junction comes from the voltage proportional to the speed of the motor driving the cathode. The resultant error signal adjusts the cathode drive rate to maintain the constant gap.

Thus after the initial calibration, any gap could be obtained by simply readjusting the potentiometer setting. By adjusting the cathode drive position, the equilibrium gap could be achieved after only about 5 s machining.

1.3.2 Electrolyte flow system

During these alterations, the flow system was modified. The main electrolyte tank was moved under the machine and the main pump sited alongside. This dispensed with the need for a sump tank and a scavenge pump. This pump was now used for draining the tank. To obtain the low flows (up to 23 in^3/s) described in Chapter 2, the pipe system was altered further and the auxiliary pump used to give these flows. As before, the flow rates could be varied by hand valve.

The fully modified flow system has been shown in Fig.2.2.

1.3.4 Electrode system

A similar system to that described in section 1.2 of the Appendix was used. The electrodes were square, of side 1 in., the cathode of brass and the anodes of mild steel, were used.

The modified Barnam equipment was used for the work described in Chapters 2 and 6. The appropriate procedures are given in each chapter.

Appendix 2

Solution of Equation (6.11). See Chapter 6

Eqn.(6.11) is

$$t = \frac{1}{U}\left[(h_o - h) + \frac{\beta}{U} \ln\left(\frac{\beta - Uh_o}{\beta - Uh}\right)\right]$$

This equation is solvable by iteration

Let $F(h)$ = R.H.S. of (6.11)

Let $F(h) = 0$

If h_o is a solution of $F(h) = 0$, then $h_o + \Delta h$ is a better solution, where

$$\Delta h = -\frac{F(h)}{F^1(h)}$$

where $F^1(h) = -\frac{1}{U} + \frac{\beta}{U} \cdot \frac{1}{(\beta - Uh)}$

Write $h_1 = h_o + \Delta h$

More exact solutions can then be found:

$$h_2 = h_1 + \Delta h$$

$$\vdots = \vdots \quad \vdots$$

$$h_r = h_{r-1} + \Delta h_{r-1}.$$

where $(h_r - h_{r-1}) < \epsilon$, where ϵ is specified.

Appendix 3

Composition of metals used.

Element (%) / metal	Bi	Cr	Ti	Al	Ni	Cu	Fe	C	Mg	Si	Mn	S
Nickel				-	99 (min)	.25 max	0.4 max	0.15 max	0.2 max	0.15 max	0.35 max	0. m.
Cast Iron				-	.098	-	Balance	3.03	-	2.22	0.53	0.
Mild steel				0.007	0.138	-	Balance	.244	-	0.046	0.752	0.
Nimonic 75		18 to 21	0.2 to 0.6 max	-	Balance	0.5 max	5 max	.08 to 0.15	-	1.0 max	1.0 max	
Nimonic 75 (assumed)		19.5	0.4	-	72.5	0.5	5.0	0.1	-	1.0	1.0	
Monel					63 (min)	28-34	2.5 max	0.3		0.5 max	2 max	
Monel (assumed)					63	31.7	2.5	0.3		0.5	2	
Al-Cu Alloy	0.5			94.0		5.0						
Copper	0.05				99.9							C
Aluminium				99		0.1	0.7				0.1	

Note: for the experiments the metals used : nickel, copper, aluminium, and cast iron and mild steel were assumed to consist of 100% Ni, Cu, Al and Fe respectively.

Appendix 4

Data used in Calculations

For sources see Kaye and Laby's Tables and International Critical Tables.

Chapters 2, 6, 7 : (5% NaOH solution)

$\sigma_0 = 1.3$ g mole/ℓ ; $\theta = 3.0 \times 10^{-2}$ deg^{-1} ; $D = 1.25 \times 10^{-5}$ cm^2/s ;

$E = 27.92$; $E_H = 1$; $\mathcal{E} = 0.0071$ in^3/C ; $\mu_0 = 0.105\,\Omega^{-1}$cm^{-1};

$V = 12V$; $V_c = 2V$; $M = 2$; $z = 2$;

$\alpha = 0.0215$ deg^{-1} ; $\beta = 0.62 \times 10^{-5}$ in^2/s ; $\rho = 7.6$ g/mℓ ;

$\rho_e = 1.055$ g/mℓ ; $\nu = 1.1 \times 10^{-2}$ in^2/s

Chapters 3,4 (20% NaOH solution)

$\mu_0 = 0.195\,\Omega^{-1}$cm^{-1} ; $\rho_e = 1.149$ g/mℓ ; $\nu = 0.97$ cP

From the relationships described in Chapter 7, the following maximum electrolyte velocities for a pump pressure $p = 250$ lb/in^2 were computed:

(Note: $p = p_1 + p_2$: See Section 7.2.6)

h_0 in	p_1 lb/in^2	v in/s
0.010	104	1450
0.020	160	1800
0.030	188	1940
0.040	204	2050

REFERENCES

1. [illegible], W.B. — Electrochemical machining, Technical Proceedings, American Electroplaters Society, 1963, 6, 147.

2. MOUNTFORD, N.D.G. — Electrochemical machining, Trans. Institute of Metal Finishing, 40, 171, 1963.

3. BOOTHROYD, G. — Fundamentals of metal machining, First edition 1965 (Edward Arnold, London).

4. HOAR, T.P. and ROTHWELL, G.P. — The influence of flow on anodic polishing - I Electrochemica Acta, 9, 135, 1964.

5. HOAR, T.P. and ROTHWELL, G.P. — The influence of flow on anodic polishing - I Electrochemica Acta, 10, 405, 1965.

6. HIGGINS, J.K. — The anodic dissolution and electrolytic polishing of metals, Journal Electrochemical Society, 106, 999, 195

7. ORD, J.L. and BARTLETT, J.H. — Electrical behaviour of passive iron, Journal Electrochemical Society, 112, 160, 19

8. JACQUET, P.A. — The principles and scientific applications of the electrolytic polishing of metals, Sheet Metal Industry, 24, 2015, 1947.

9. EDWARDS, J. — The mechanism of electropolishing of copper in phosphoric acid solution, Journal Electrochemical Society, 100, 189 and 2230, 1953.

10. [illegible], W.G. — Electrolytic polishing, I and II. Journal Applied Physics, 10, 724, 1939 and 11, 797, 1940.

11. COLE, R.R. — Basic research in electrochemical machining - present status and future directions, Int. Jnl. Production Research, 1965, Vol.4 2, 75.

12. COLE, R.R. — An experimental investigation of the electrolytic grinding process, American Soc. Mech. Engineers, Journal Engineering for Industry Series B, 83, 194, 1961.

13. FINCH, J. and COLE, R.R. — Surface effects and residual stresses in electrolytica ly ground steel, American Soc. Mech. Engineers. Journal Engineering for Industry, Paper No. 61 - WA- 1962.

14. COLE, R.R. and HOPENFELD, H. — An investigation of electrolytic jet polishing at high current densities, American Soc. Mech. Engineers, Journal Engineering for Industry, Series B, 85, 395, 1963.

15. CUMBERBATCH, J.W. and TURNER, D.S. — Electrochemical Machining - study of the effects of some variables, Production Engineer, 1966 May 270.

16. TIPTON, H. — The dynamics of electrochemical machining, International Machine Tool Design and Reseer Conference, University of Birmingham, 1964.

17. [illegible], C.L. — Electrochemical machining of metals, Trans. Inst. Metal Finishing 41, 1, 1964.

18. LEVICH, V.G. — Physicochemical Hydrodynamics, First English Edition Prentice-Hall, Englewood Cliffs, N.J. 1962.

19. SCHLICHTING, H. — Boundary Layer Theory, McGraw-Hill, London 1960, 509.

20. [illegible], N.H. — Physical Chemistry Oxford Clarendon Press 1956.

21. KAYE, G.W.C., and LABY, T.H. — Physical and Chemical Constants, Twelfth Edition, Longmans, London, 1959.

22. INTERNATIONAL CRITICAL TABLES.

23. BAYER, J. — Final Report on electrolytic machining development, G.E. Company, Cincinnati 1964.

24. MELLOR, J.W., — Modern Inorganic Chemistry Longmans London 1947.

25. Encyclopedia of electrochemistry, (Editor: C.A. Hampel) 1st Edition, Chapman and Hall, New York, 1964, p.47.

26. HURLEN, T. — Acta Chem. Scand. 1961, 15, 1231.

27. EVANS, V.R. — Introduction to metallic corrosion, Edward Arnold, London 1963, p.134.

28. UHLIG, H.H. — Corrosion and corrosion control, New York, John Wiley, 1965, p.68.

29. KLEINER, V.B. — Personal Communication, June 1966, Kleiner Electrochemical, Dunellen, N.J.

30. LARSSON, C.N. — B.S.A. Group Research Centre, Birmingham. Private communication.

31. TEGART, W.J. — The electrolytic and chemical polishing of metals. Pergamon Press, London, 1959.

32. FORTNEYER, C.E. — Electrochemical machining - the versatile metal removal process. American Soc. Tool and Manufacturing Engineers, 1964, Paper No. 643.

33. MERCHANT, M.E. — Newer methods for the precision working of metals - research and present status. Machine Tool Design and Research Conference, University of Birmingham, 1962.

34. KENNEDY, A.B. — Formerly Department of Mechanical Engineering University of Glasgow, Personal Communication

35. De La RUE, R.E. and TOBIAS, C.W. — On the conductivity of Dispersions, J. Electrochem. Soc. September 1959, 827.

36. HOPENFELD, J. and COLE, R.R. — Electrochemical machining - prediction and correlation of process variables. American Soc. Mech. Engineers Paper No.66, Prod.-5.

37. WILLIAMSON, B.H. and STUART, G.R. Development of electrochemical machining techniques.
Electronics and Power, December 1964, 420.